POLITECNICO DI TORINO

Master's degree in Engineering and Management

Development of a Metrological Digital Twin for a Focus-Variation Coordinate Measurement System

Supervisors

Prof. Galetto Maurizio

Dr. Giacomo Maculotti

Candidate

Ludovica Garavaglia

332838

March 2026

Abstract

This thesis is developed within the framework of the European project ADAM, which aims to establish metrological traceability for Digital Twins of coordinate measurement systems. The characterization of three-dimensional surfaces is essential for assessing the form and topography of components.

Coordinate measuring systems extend traditional Coordinate Measuring Machines (CMMs) by integrating optical measurement methods and non-Cartesian carriers.

Among these, innovative measurement approaches enable the acquisition of surface topographies using focus variation microscopes mounted on collaborative robotic arms (cobots).

The objective of this thesis is to develop a Digital-Metrological Twin of a focus variation system by analyzing the sensitivity of measurements and systematic measurement errors with respect to key measurement parameters, such as wavelength, light intensity, and the geometry of the measured object.

Summary

List of Figures

List of Tables

List of Formulas

Introduction

In the past, the primary purpose of traditional manufacturing processes was to develop components characterized by a specific nominal geometry, without paying particular attention to their surface roughness.

All those micro- and nano-scale features of the topography were considered, in practice, simply a by-product of the processing technique, meaning that there was no intent to define and control them, other than keeping them below a certain level.

Recently there has been a shift from the production of stochastic surfaces to the production of structured surfaces, because of the increasing diffusion of advanced components.

In relation to these advanced components, surface characteristics and properties have become of fundamental importance in defining their function.

As a result, the objective became the definition and design of surfaces whose features are optimized for improving the functions related to the surface itself.

Since the performance of the part depends on these complex microstructures, there is an urge to develop a method to measure them with extreme precision to ensure that the final product works properly.

During the initial stages of the industrial production process, the assessment of the surface texture was performed uniquely through the evaluative ability of the operator, who compared the roughness values of the sample under test with those of tactile comparison samples.

The development of technology and equipment over time brought the advent of the first stylus profilometers. This entails a diamond stylus moved along a linear path on the surface of the object, used to translate asperities from physical to electronic form.

At the beginning, the result of this process was not numerical but rather a chart or audio signal, which aimed to simply distinguish between a smooth surface and a rough surface.

It was only after the development of digital electronics that output became a numerical value.

For a long time, the standard remained profile measurement (2D), meaning that the surface was characterized by a single cross-section, mathematically represented as a function z(x).

However, this method involved a number of drawbacks, which led to the switch to areal topography (3D) from profilometry. The surface is now described by a function z(x,y), with the purpose of extending measurement to the third dimension.

The main goal was no more testing surface smoothness but rather the evaluation of the interaction between the micro-geometry of the surface with the surrounding environment.

To ensure product quality, measurement traceability and calibration infrastructure have been introduced [1,2].

Traceability is defined as the property of the result of a measurement whereby it can be related to stated references, usually national or international standards, through a documented unbroken chain of comparisons all having stated uncertainties.

Calibration, by contrast, is the operation that, under specified conditions, in a first step establishes a correspondence between the quantity values with measurement uncertainties provided by measurement standards and corresponding indications with associated measurement uncertainties and, in a second step, uses this information to establish a relation for obtaining a measurement result from an indication [2].

It was around 1947 that Rolt was pressing for surface texture measurement to produce a unique number, which could be used to define surfaces and enable comparisons.

The first parameter used was Rq, but it was quickly substituted by the Ra parameter, obtained using a planimeter.

A relevant contribution was made by the work carried out in the EU project called 'CALISURF', which was completed in 2000. The goal of this project was to define the artefacts for calibration of profile measuring instruments, leading to the type A-D artefacts in ISO 5436 part 1 [3].

All these works though, were paying attention to surface profile measurement. The first work on areal surface texture characterization, instead, was performed by a consortium as part of a European project led by Ken Stout from the University of Birmingham, ending with

the publication of the ‘‘Blue Book’’. This project led ISO to start the standardization work on areal surface texture.

Traceability has a dual nature. In order to achieve a traceable surface texture measurement result, two different components must be taken into consideration.

These are:

- the impact on traceability of the measurement process (Hardware) representing the physical interaction between the instrument and the surface
- the impact of the analysis algorithms and parameter calculations (Software) representing the algorithms used to process raw data and calculate roughness parameters

The process that leads to the calibration of the instrument, which is fundamental to ensure hardware traceability, consists of:

- The Axes of Operation which ensures the accuracy of X, Y, and Z scales
- The Spatial Frequency Response to understand how the instrument responds to different surface frequencies

Traceability, overall, is obtained through a hierarchical structure, this being either a pyramid or a chain, which is needed to transfer traceability in surface texture measurement from the national laboratory to the industry.

Various kinds of instruments can be categorized for this purpose.

Primary instrumentations are maintained by the National Metrology Institutes. They are highly accurate instruments, usually based on laser interferometry directly traceable to the definition of the metre. They are used to calibrate material measures with remarkably low standard of uncertainty.

Secondary/Industrial Instruments, on the other hand, are the ones present at industrial level. Instead of being calibrated with a laser as primary instrumentations, they are calibrated by measuring material measures. Material measures, in turn, have been certified by the primary instruments.

The relevant issue is that, while a solid infrastructure exists for two-dimensional stylus instruments, an adequate system for three-dimensional areal instruments has not yet been defined.

To the end of finding a solution for the above gap, the concept of Traceability Chain has been proposed. This idea, shown in Figure 1 below, represents an ideal chain of actions in a series of steps.

At the top, the definition of the SI unit, the metre, can be found, acquired using stabilized lasers at National Metrology Institutes.

Starting from there, various steps are needed to reach measurements in industry. The instruments involved in this process are:

- A Primary Instrument employed to measure or realize 3D surface topography
- Material Measures, which are calibrated using the primary instrument. They are then used for calibrating the industrial/secondary instruments

While this chain mainly addresses hardware traceability, software-related effects must be controlled through standardized algorithms and parameter definitions.

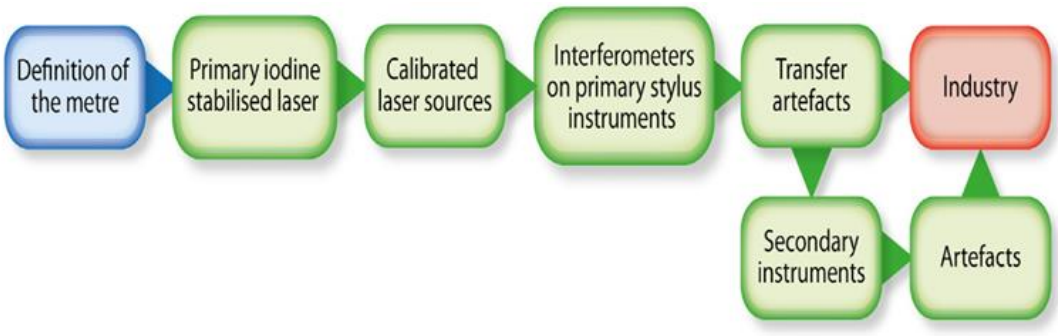

Figure 1: Graphical representation of the Traceability Chain [3].

Despite these advancements, defining a physical Traceability Chain for areal 3D measurements remains a challenging activity because of the large diversity of industrial surface topographies and the complicated interaction between the instrument and the sample.

The greatest complication when calculating uncertainties in surface texture measurement is the contribution of the surface itself.

In such cases, indeed, the production of Material Measures could be impracticable, since the production of certified artefacts able to simulate ultra-complex geometries would be a time and cost-consuming process [3].

The concept of a Virtual Measurement System has been introduced with the aim of finding a solution to this situation.

The idea is to build a Digital-Metrological Twin of the physical instrument, capable of simulating the entire measuring process of the complex workpiece. This Digital-Metrological Twin can measure a virtual surface, acting as the virtual environment in which it is possible to test the instrument's response to any geometry without having to physically produce the sample each time.

This digital approach is directly related to the concept of Traceability Chain, since it provides a solid method for estimating measurement uncertainty, in cases where physical certified workpieces are not accessible.

This guarantees traceability even in difficult industrial situations, thereby achieving the fundamental prerequisite according to which a measurement's result is meaningful only if reported with its uncertainty.

This research is a contribution to the European Project for the Analysis and Design of Advanced Metrology, named ADAM, aimed at developing metrological traceability for Digital-Metrological Twins of coordinate measuring systems.

As pointed out beforehand, the examination of areal topography is relevant to the definition and study of complex artifacts.

Differently from traditional Coordinate Measuring Machines, which move along cartesian coordinates of X, Y, and Z axes, and measure discrete points of an object, modern Coordinate Measuring Systems introduced optical measurement techniques and are not restricted to pure cartesian movements only.

Among other innovative optical measurement methods, it is important to remark the contribution played by Focus Variation microscopes, which are capable to acquire high-resolution 3D topographies.

Such microscopes are not fixed, but rather built on “cobots”, collaborative robotic arms, that guarantee automated scanning of extensive surfaces.

This thesis focuses on the development of a Digital-Metrological Twin for a Focus Variation system, by analyzing sensitivity of measurements and identification of systematic measurement errors in relation to specific physical parameters.

Chapter 1. Surface Metrology and Coordinate Measuring Systems

1.1 Metrological Characteristics of Measuring Instruments

The definition of “metrology” according to the International Vocabulary of Metrology (VIM) is “the science of measurement and its application” [2].

Dimensional Measurement is defined as the measurement procedure of obtaining one or more numerical results that can be attributed to a geometric characteristic of an artefact.

Measurement is not to be considered as the simple outcome of a device, but the overall result of a complex process, defined "Measurement Complex".

This system comprehends different interacting elements, such as the instrument, the operator, the environmental conditions and the measurand itself [1].

Measurements must be performed under well-specified conditions to obtain trustworthy output, i.e. results that include a reliable statement of uncertainty.

The VIM definition of the principal metrological properties of a measuring instrument is:

- resolution: the least change in the quantity being measured, that will produce an observable change in the measured indication.
  In the scenario of optical areal instruments, resolution is further split into Lateral Resolution and Vertical Resolution.
- sensitivity: ratio of the change in an indication of a measuring system and the corresponding change in a value of a quantity being measured.
- stability: feature that ensures that the metrological properties of a measurement instrument do not change over time.
- precision: closeness of agreement between indications or measured quantity values obtained by replicate measurements under identical conditions on the same or similar objects.

Generally, precision is associated with the variance (σ^2) of the repeated measurements and is typically evaluated through Repeatability and Reproducibility studies.

The concept of Repeatability represents an ideal condition, according to which measurements are performed adopting the same measurement procedure, same operators, same measuring system, same operating conditions and same location, and replicate measurements on the same or similar objects over a short period of time.

On the other hand, Reproducibility better reflects the actual working conditions under which measurements are carried out. This specific case entails the replication of measurements on the same or similar objects, involving different locations, operators and measuring systems.

- trueness: closeness of agreement between the average of an infinite number of replicated measured quantity values and a reference quantity value. It is inversely related to systematic measurement error, and it is not related to random measurement error.
- accuracy: ability of the instrument to provide responses close to the true value, characterized by low measurement error.
- uncertainty: non-negative parameter characterizing the dispersion of the quantity values being attributed to a measurand, based on the information used. It enables comparison between the measurement result with references and specifications. Each measurement result is affected by errors of some kinds, making it differ from the real value of the measurand [2].

Chapter 2. Metrological Framework

2.1 Traceability

Traceability and calibration are two basic principles on which the credibility of any measurement outcome is based. The result of a measurement, indeed, is meaningless on its own, since its significance is linked to the possibility of being compared and trusted.

To ensure that the measurement output is verifiable and comparable, the measuring instruments must be calibrated on precise standards at both national and international levels. The various calibration levels form a chain of traceable calibrations.

VIM has defined the concept of traceability as the “property of a measurement result whereby the result can be related to a reference through an unbroken chain of calibrations, each contributing to the measurement uncertainty” [2].

Traceability in general has immense relevance because it ensures that measured results are reliable, repeatable, reproducible, compatible, and comparable, regardless of the method and instrument used for the measurement, as well as the location and time.

This is possible because each measurement output is connected to references at higher levels, culminating with the definition of the SI unit, the metre, defined as a primary standard according to the directives of the “Bureau Internationale des Poids et Mesures“, BIPM.

As illustrated in Figure 2, international standards are at the top of the traceability pyramid and are characterized by the highest level of accuracy and lowest level of measurement uncertainty.

Moving from the top to the bottom of the pyramid, the number of instruments increases exponentially, as well as the degrees of uncertainty that characterized measurements; less precision has been registered in the lower levels of the pyramid.

The major purpose of the traceability chain is to assign values of uncertainty to measure outputs, to better define whether the measurement performed can be trusted or not [3].

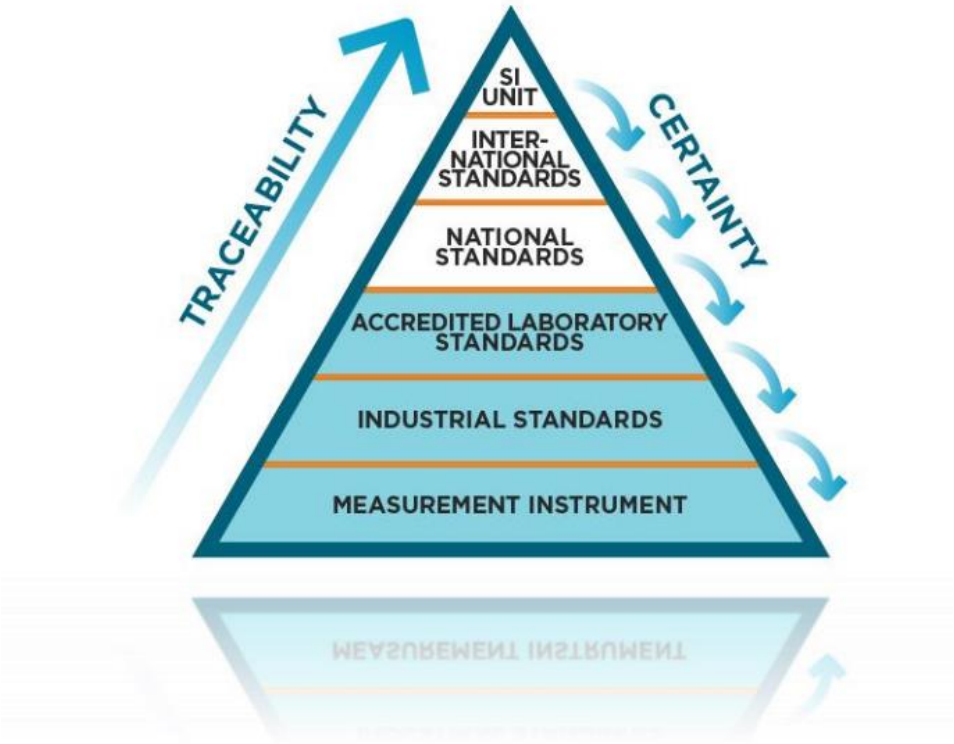

Figure 2: Traceability pyramid [77].

At the top of the pyramid lies the International Definition of SI System, which is considered an abstract representation of complete accuracy, since it corresponds to zero uncertainty [4].

In the SI System, the base unit of length is the metre, which has been introduced in 1983 and has been defined as the distance traveled by light in a vacuum in exactly 1/299,792,458 of a second, fixing the speed of light as a universal constant [6].

Moving to the second level of the traceability chain, the National Metrology Institutes (NMIs) plays a crucial role. Here, primary measurement standards are created and maintained.

The concept of the primary standards of measurement corresponds to the starting physical point of the traceability chain, being characterized by the highest level of metrological features and is independent of other standards related to the same quantity.

The degree of uncertainty at this stage is still very little, in the order of nanometers (10^{-9} m).

The next step is critical in ensuring the spread of traceability information from the national level to industrial level.

National Laboratories are not always easily accessible. In cases where this is not feasible, a relevant role is covered by Accredited Calibration Centres, which possess accurate reference standards that have been in the past be calibrated by National Metrology Institutes (NMIs).

Since this step is reached by descending along the pyramid, it is characterized by higher levels of uncertainty, but still low enough to produce high-quality standards.

At the bottom of this hierarchy the Industrial Level is located. This level contains most of the working instruments.

These devices are commonly used to test real objects and compare their performances with requirements. Being located at the bottom level, those instruments are characterized by the highest degree of uncertainty, of the order of microns, but still within defined margins [7].

2.2 Calibration

To preserve the traceability chain, an operation must be performed on the instrument, for maintaining its accuracy: calibration.

Calibration determines the performance characteristics of an instrument, system or reference material.

One of the main purposes of instrumentation design is the elimination of elements that bring measurement errors. To keep obtaining measurement outputs within a specified tolerable range, the measurement must be calibrated [3].

According to VIM, calibration is an operation composed of two subsequent steps:

1. establishes a relation between the quantity values with measurement uncertainties provided by measurement standards and corresponding indications with associated measurement uncertainties.
   This leads to the determination of the error:

$$\text{Error} = Y_{ind} - Y_{ref} \qquad [1]$$

2. uses this information to establish a relation for obtaining a measurement result from an indication [2].

The term “calibration artefacts” refers to specific samples, characterized by know and calibrated values, measured by an instrument to test its accuracy and used to improve the measurement process of samples of unknown values. The results give some insight into the relationship between the instrument's measurement method and the measured values.

Differently from the procedure of adjustment, which physically changes some parameters of the metrological tool, the operation of calibration does not alter in any way the features of the instrument, but it simply generates a representation of its performance errors and uncertainties at a specific point in time [3].

2.2.1 Limits of Calibration

The traditional procedure of calibration exhibits some limits, specifically in relation to the calibration of 3D geometries of complex artefacts.

Line profiling method is the procedure that leads to the creation of two-dimensional graphs, aimed at defining surface irregularities. This method captures the height variations of the surface along a single scan line, mathematically defined as $z(x)$, where z represents the height of the artefact and x the coordinate along the measurement direction.

However, 2D profiles present some limitations, since they are not able to give information about the surface features in the transverse direction, y.

To overcome this problem, areal topography methods have been introduced, consisting in the representation of topographical images of the surfaces, mathematically expressed as $z(x, y)$, with y being the axis perpendicular to x [3,8].

Among the different ways to conduct line profiling, for sure particular attention must be given to tactile stylus instruments, which physically cross the surface along a linear path, with a constant applied load.

Stylus instruments can also be used to measure areal surface topography by moving the stylus across the surface in a raster fashion and generating an areal map [9].

To perform areal topography analysis, it is not convenient to use stylus instruments because of their slowness. It would be better instead to imply optical instruments, which can capture information over a full field of view in just one time. In this context, the properties of the surface are particularly relevant, since the interaction between the surface and the optical instrument is carried out through electromagnetic principles, such as reflection, diffraction, scattering [10].

For profile traceability, indeed, the majority of NMIs dispose of either primary or secondary instrumentations. The latest ones are calibrated via material measures, which have been in turn calibrated using primary instrumentation at another NMI.

Instead, areal traceability is still quite new and needs to be further studied. In figure 3 a primary instrument that uses laser interferometry with a linear ball-screw bearing and stylus and optical probes is showed.

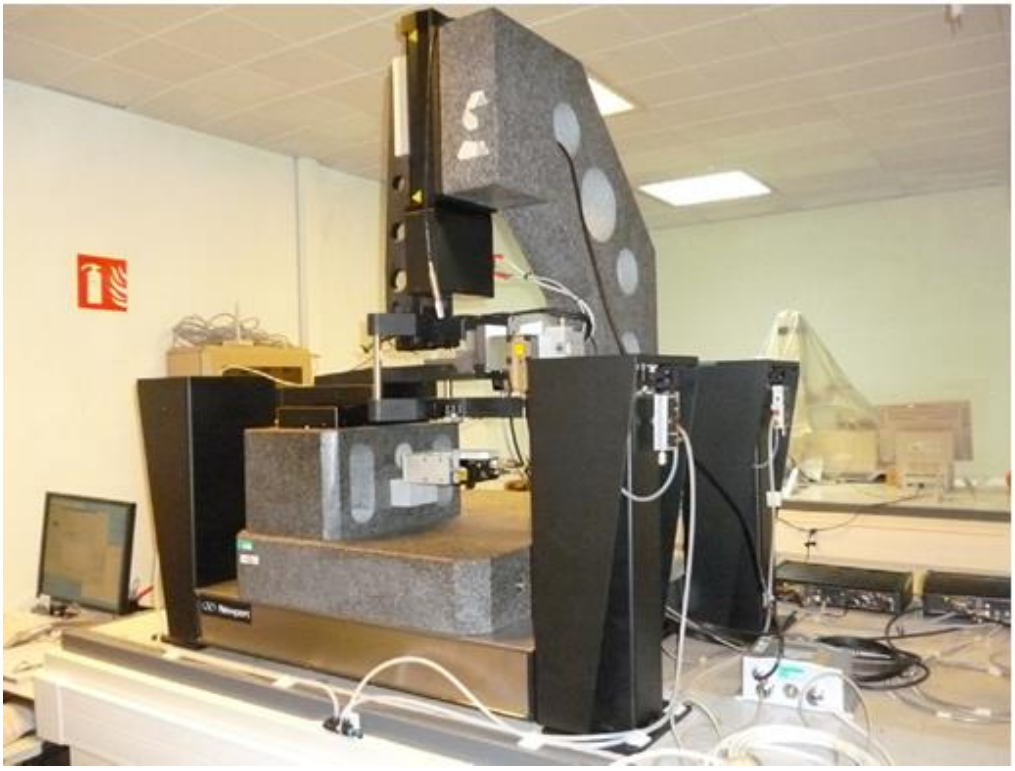

Figure 3: The primary areal surface instrument at LNE [3].

While the calibration process is relatively simple in the case of traditional stylus profilometry, more difficulties arise in the case of areal calibration, due to the complex interaction between the instrument's features and the surface's topography.

2.2.2 Overcome the Limits of Calibration. Metrological Characteristics

To overcome the limits of calibration for areal surface topography instruments, the concept of Metrological Characteristics (MCs) has been defined and standardized under ISO 25178-600. Metrological characteristics are introduced to capture all the features that influence measurement results and are useful to generate common standardized calibration routines.

It became common knowledge, indeed, that the process of instruments calibration should follow simple measurement frameworks, in which input quantities are able to define the errors along the measurement axes and an evaluation of the measurement uncertainty.

The measurement result obtained using optical instruments is influenced by the complex interaction between the surface topography and the optical instrument itself. In this case, the elimination of every error source is infeasible; instead, metrological characteristics can offer support by capturing the overall effect of these errors on the measurement output, providing an evaluation of the instrument's performance.

However, a limitation is present: current analytical models are used to treat MCs as independent quantities, even if an important role is played by their interaction. For such reasons, they are not useful when designers require precise knowledge of the features of the instruments [3, 10, 11,23]

Metrological characteristics are the ones shown below table 1:

Metrological characteristic	Symbol	Main potential error along
Amplification coefficient	α_x, α_y, α_z	x, y, z
Linearity deviation	l_x, l_y, l_z	x, y, z
Flatness deviation	z_{FLT}	Z
Measurement noise	N_{M}	Z
Topographic spatial resolution	W_{R}	Z
x-y mapping deviations	$\Delta_x(x, y)$, $\Delta_y(x, y)$	x, y
Topography fidelity	T_{Fi}	x, y, z

Table 1: list of metrological characteristics [10].

- amplification coefficient: slope of the linear regression line obtained from the response function.
- linearity deviation: maximum local deviation of the instrument's response curve from a straight line.
- flatness deviation: deviation of the measured topography from an ideal plane.
- measurement noise: noise added to the output signal occurring during the normal use of the instrument.
- topographic spatial resolution: ability of a surface topography measuring instrument to distinguish closely spaced surface features.
- x-y mapping deviation: gridded image of x- and y deviations of actual coordinate positions on a surface from their nominal positions.
- topography fidelity: closeness of agreement between a measured surface profile or measured topography and one whose uncertainties are insignificant by comparison.

2.3 Measurement Uncertainty

Metrological Characteristics (MCs) have been defined also in order to fulfill the fundamental requirement of Measurement Uncertainty estimation, which is helpful in enhancing the comparison of the results acquired using different measuring instruments.

Some of the MCs previously described are properties of the instrument or environment and can be used for uncertainty estimation independent of the specific topography being measured. These characteristics include the amplification coefficient, linearity deviation, flatness deviation, x-y mapping and topographic spatial resolution.

On the other hand, measurement noise and topography fidelity are dependent on the physical properties of the surface being measured [1, 10].

A single measured quantity is not sufficient for expressing the result of measurement. A complete result must be described by the value obtained from the measurement process, the measured quantity value, and its measurement uncertainty, which quantifies the doubt associated with the measurement process due to inevitable systematic and random errors.

The most problematic issue in the measurement uncertainty calculation in the measurement of surface textures lies in the part played by the surface itself.

There are numerous approaches to estimating measurement uncertainty, as well as different types of uncertainty, as highlighted in Figure 4 below.

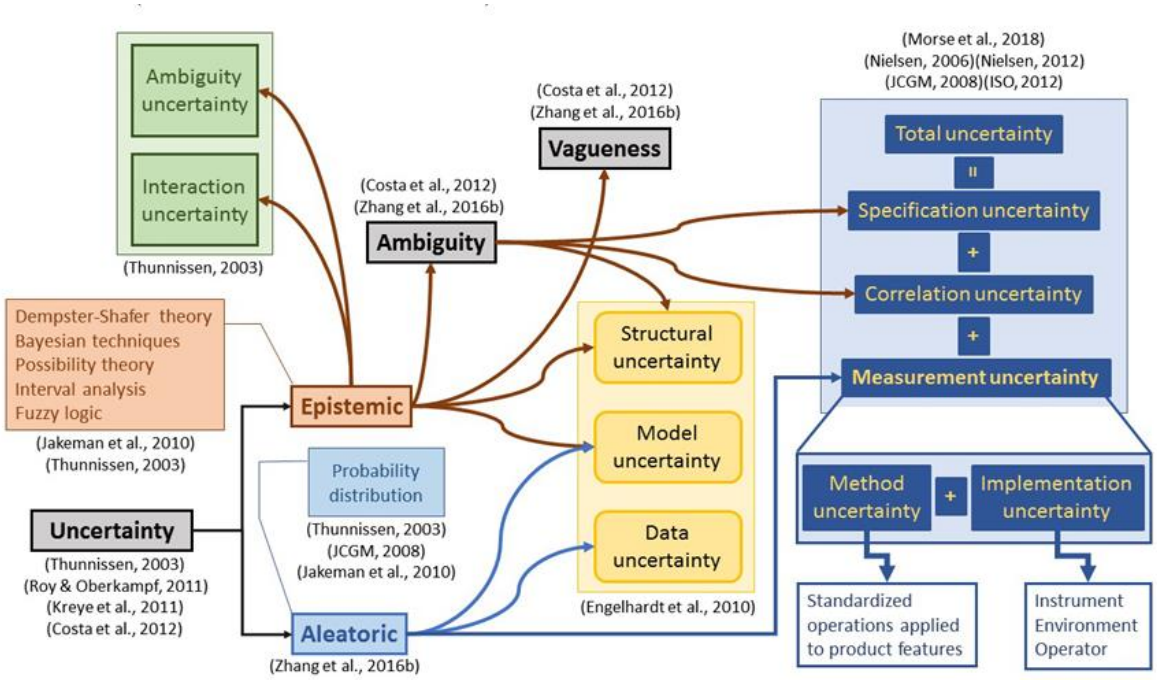

Figure 4: Summary of the uncertainty types and their possible estimation methods [37]

For the moment, most research has been concentrated on the estimation of uncertainty for 2D profile metrology, and therefore further research is still needed to better define measurement uncertainty for areal surface texture measurements.

One of the several methods available for determining uncertainty is the ISO recommended GUM method, described in the “Guide to the expression of uncertainty in measurement”, which follows either an analytical method, based on the law of propagation of uncertainty, or a numerical approach, utilizing the Monte Carlo technique, to combine standard uncertainties from various sources.

Thie GUM method is composed of different steps:

- identify all the sources that contribute to measurement uncertainty
- compute the standard uncertainty of each component of measurement uncertainty

- compute the combined standard uncertainty by aggregating the individual uncertainty components according to the law of propagation
- calculate the expanded uncertainty (U) by multiplying the combined uncertainty with the coverage factor k
- define the final result of the measurement in the form: [2]

$$Y = y \pm U$$

where U is the value of uncertainty and y is the quantity measured

While the GUM method is excellent in the determination of uncertainty of simple dimensional quantities, it is not well established for areal surface texture uncertainty [4, 12].

Measurement uncertainty associated with surface texture depends on how much variability exists across different areas of a part and is typically found by performing multiple measurements across the inhomogeneous areas of a given surface.

When surface texture parameters are calculated, the procedure to estimate uncertainty is usually divided into two components: the contributions to the uncertainty due to the measuring device and the uncertainty resulting from the calculation of the surface texture parameter itself.

A rigorous uncertainty analysis has been carried out by the National Physical Laboratory (NPL) for primary areal surface topography instruments adopting Monte Carlo techniques.

Despite these advancements, analysis for general industrial areal surface texture measurements need to be further developed [13,14].

The distinction between influence quantities and metrological characteristics is illustrated in Figure 5.

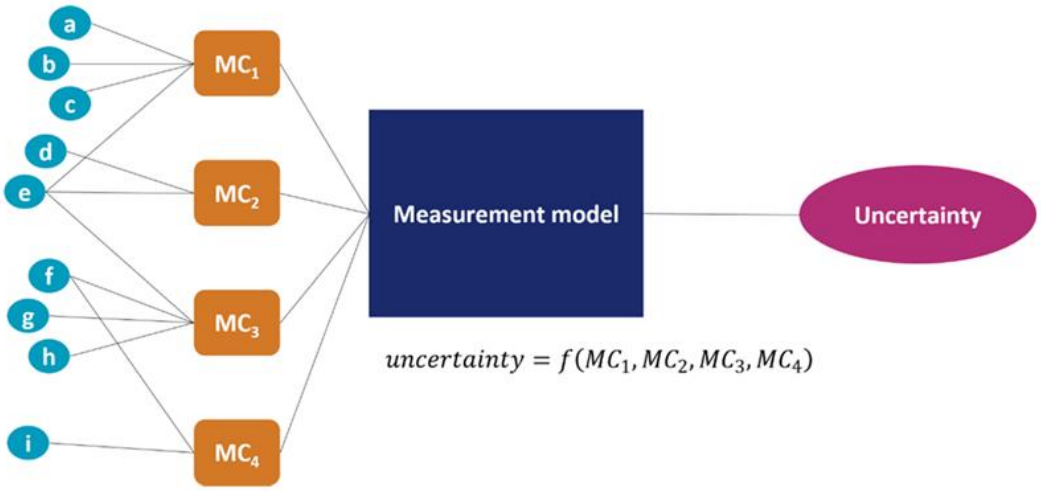

Figure 5: Illustration of the metrological characteristics framework to estimate measurement uncertainty [10].

However, metrological characteristics are only one of the possible approaches to uncertainty estimation.

An alternative and more advanced approach, widely used in the coordinate metrology world, e.g., for coordinate measurement machines (CMMs), is the use of a Virtual instrument. In this process, a virtual measurement system considers various influence factors and simulates the measurement using an accurate model that mimics the real measurement process, performing a virtual experiment by:

- generating a virtual surface
- simulating the interaction between the surface and the sensor
- computing the result and comparing it with the reference to define statistically the value of the uncertainty

At present, virtual instruments for contact stylus surface measurement are well established; on the other hand, Virtual Instruments for optical surface metrology are not yet defined due to the complexity of optical measurement and the large variety of surface types [3].

2.4 Measurement Errors

The definition of measurement error according to VIM is the following: “measured quantity value minus a reference quantity value”. The concept of measurement error can be applied in two cases:

1. when there is a single reference quantity value to refer to, which occurs if a calibration is made by means of a measurement standard with a measured quantity value having a negligible measurement uncertainty or if a conventional quantity value is given, in which case the measurement error is known
2. the object being measured is a quantity that is to be expressed in a unique true value or in a set of true values within a negligible range, in which case the measurement error is unknown [2].

Measurement errors can be distinguished in systematic or random.

Systematic measurement error refers to the component of measurement error that in replicate measurements remains constant or varies in a predictable manner. In this context, it is possible to define the relationship that links the specific error whit its cause. There are various techniques that can be employed to reduce the effects of such kinds of measurement errors:

- correction: calculation of the measurement error and its distance from the measured value
- compensation: physical phenomenon which compensates for the variation of the result is associated to the measurement
- elimination: identification and remotion of what causes the measurement error

Random measurement error refers to the component of measurement error that in replicate measurements varies in an unpredictable manner, being characterized by a random nature. These types of errors correspond to the residuals of the systematic errors and of the other influencing factors and are managed with statistical methods based on the normal distribution.

The term “measurement accidents” refer to those random errors that are rare and higher with respect to the cloud of normal random errors and are reduced by exclusion principles.

The concept of uncertainty in measurement is what is left after removing systematic errors, as well as those related to measurement accidents and random errors [1,4].

2.4.1 Physical Sources of Errors

The measurement result is always dependent on specific factors interacting together.

Under this paradigm, the major error sources that can be grouped into four major categories are: Environment, Instrument, Measurand (Workpiece), and Procedure/Strategy.

- environmental factors: among these, one of the most important factors is temperature, given that many materials expand or contract with temperature changes.

  Systematic errors occur when the measurement temperature is different from the reference temperature.

  Another factor that needs consideration is vibrations, which can cause relative motion between the sensor and the surface. For optical measurement systems, lighting conditions can also affect the sensor.
- instrument factors: characteristics of the device have a large impact on the errors linked to its kinematics and sensing technology.

  Misalignments in axes can lead to considerable errors in measurements.
- workpiece factors: the features of the object that is being measured produce a relevant influence on the measurement errors.

  In specific cases of surface metrology, the sample surface is often the major source of uncertainty, since some of the properties of that surface, such as roughness, hardness, and cleanliness, are factors in the interaction between the sample surface and the sensor.
- measurement strategy: the approach used to undertake the measurement, which impacts the total outcome of the measurement [15,16,17,20].

2.5 Form and Surface Topography Parameters

Surface topography is defined as the feature on a component that separates it from the surrounding environment and through which all interaction between the component and the surroundings take place. The need to control and measure it is becoming of fundamental importance.

Surface texture instead represents the characteristics that remain once the form has been removed [5,18].

According to the ISOO terminology, the concept of surface texture encompasses roughness, waviness and unfiltered profile.

The raw data gathered by a Coordinate Measuring System contains a superposition of different wavelengths, which represent the Form, the intermediate undulations that correspond to the Waviness, and ultimately the Roughness.

In order to perform a study of the surface texture, the nominal form must be eliminated through the application of the F-operator. Then, to separate roughness from waviness, some filters must be applied.

The S-filter removes small-scale noise, and L-filter eliminates long-wavelength components. The output surface is defined as S-L surface, on which roughness parameters are computed [9,18,19].

2.5.1 Profile Standards

There are nine ISO specification standards that describe the measurement and characterization of surface profile, all determined using stylus instruments.

In a typical stylus instrument, represented in Figure 6, a diamond tip is dragged across the surface being measured and the vertical motion of the tip in response to surface topography is measured. The vertical motion of the stylus tip and the displacement of the instrument parallel to the surface are used to determine a profile of the surface.

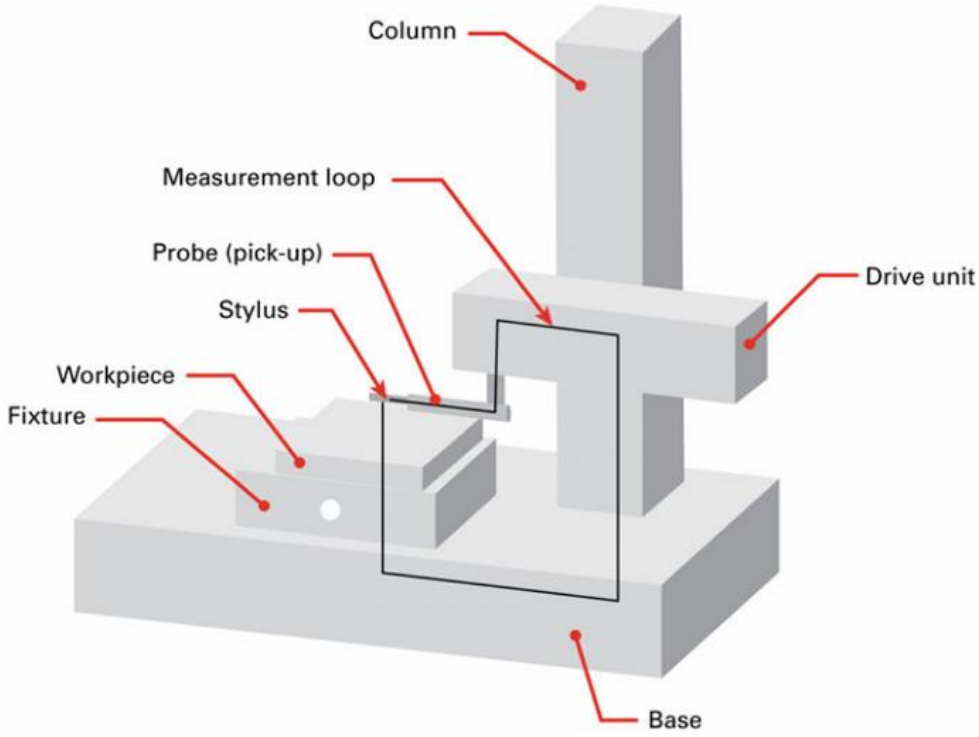

Figure 6: representation of a typical stylus instrument [11].

Specific standards for surface profiles have already been well defined, through the determination of two-dimensional parameters, standardized by ISO 4287:1997, which have been calculated considering single profiles characterized by information in the horizontal and vertical direction.

Surface profile measurements are obtained by moving a stylus across a line on the surface and representing that line mathematically as a height function with lateral displacement, z(x).

ISO 4287:1997 defines three series of 14 parameters each (P-parameters, R- parameters and W-parameters) as reported in Table 2 below; instead, the ranges the values can assume are defined in ISO 4288:1996.

P-parameters describe the unfiltered profile, R- parameters the roughness profile and W-parameters the waviness profile.

Parameters defined in ISO 4287:1997			
Pp	Rp	Wp	Maximum profile peak height
Pv	Rv	Wv	Maximum profile valley depth
Pz	Rz	Wz	Maximum height of profile
Pc	Rc	Wc	Mean height of profile elements
Pt	Rt	Wt	Total height of profile
Pa	Ra	Wa	Arithmetical mean deviation of the assessed profile
Pq	Rq	Wq	Root mean square deviation of the assessed profile
Psk	Rsk	Wsk	Skewness of the assessed profile
Pku	Rku	Wku	Kurtosis of the assessed profile
PSm	RSm	WSm	Mean width of the profile elements
Pdq	Rdq	Wdq	Root mean square slope of the assessed profile
Pmr(c)	Rmr(c)	Wmr(c)	Material ratio of the profile
Pdc	Rdc	Wdc	Profile section height differences
Pmr	Rmr	Wmr	Relative material ratio

Table 2: representation of 2D parameters, defined in ISO 4287:1997 [18].

To describe surfaces characterized by different properties at different depths, ISO 13565 defined parameters derived from the bearing curve [3,9,13,18].

2.5.2 Areal Standards

To better analyze surface texture, it is fundamental to develop three-dimensional parameters.

For sure, one of the major contributions in this context concerns the improvement of visualization techniques and image analysis able to generate trustful representations of the surface.

Standards for areal characterization are progressively being published through ISO 25178, but they need to be further analyzed.

Table 3 shows a set of fourteen three-dimensional parameters, most of which are obtained starting from 2D parameters, and are denoted by “S” instead of “R” to demonstrate that they are calculated over the entire measured surface.

To determine these parameters, a reference surface to which compare the measured heights is necessary.

Amplitude parameters	
Sq	Root mean square deviation
Sz	Ten point height
Ssq	Skewness of height distribution
Sku	Kurtosis of height distribution
Spatial parameters	
Sds	Density of summits
Str	Texture aspect ratio
Sal	Fastest decay autocorrelation length
Std	Texture direction
Hybrid parameters	
SΔq	Root mean square slope
Ssc	Arithmetic mean summit curvature
Sdr	Developed surface area ratio
Functional parameters	
Sbi	Surface bearing index
Sci	Core fluid retention index
Svi	Valley fluid retention index

Table 3: Representation of 3D parameters, defined in ISO 25178 [18].

S-parameters can be categorized into height/amplitude, spatial, hybrid, and functional parameters.

Height parameters are used to quantify the statistical distribution of height values z(x,y) along the Z-axis.

Amplitude parameters are characterized by:

- Root Mean Square Height, Sq: it is computed as the standard deviation of the surface heights, and it is useful for the validation of optical devices, by analyzing the spread of peaks and valleys from a mean plane. [3]

$$Sq = \sqrt{\frac{1}{A}\iint_A z^2(x,y)dxdy}$$

- Arithmetic Mean Height, Sa: defined as the arithmetic mean of the absolute value of the height within a sampling area. [4]

$$Sa = \frac{1}{A}\iint_A |z(x,y)|dxdy$$

- Maximum Height, Sz: corresponds to the total vertical distance between the highest peak Sp and the lowest valley Sv, across the entire measured surface area, calculated as the sum of the absolute values of Sp and Sv. This parameter is very sensitive to isolated peaks and pits which may not be significant. [5]

$$S_z = S_p - S_v$$

  This parameter is highly sensitive to outliers. In optical metrology, the presence of spikes, which correspond to false peaks due to reflection errors, drastically increases the value of Sz.

- Skewness (Ssk) and Kurtosis (Sku) parameters represent respectively the symmetry and deviation of a histogram of the heights of all measured points, from an ideal Normal curve.

  In particular, Ssk parameter describes the shape of the topography height distribution, and Sku is a measure of the sharpness of the surface height distribution. [6][7]

$$Ssk = \frac{1}{Sq^3}\frac{1}{A}\iint_A z^3(x,y)dxdy$$

$$Sku = \frac{1}{Sq^4}\frac{1}{A}\iint_A z^4(x,y)dxdy$$

Among the hybrid parameters, it is relevant:

- Root Mean Square Gradient, Sdq: it is used to measure the steepness or inclination of a surface, computed as the root mean square of all slope components across the entire measurement area. [8]

$$Sdq = \sqrt{\frac{1}{A}\iint_A \left[\left(\frac{\partial z}{\partial x}\right)^2 + \left(\frac{\partial z}{\partial y}\right)^2\right] dxdy}$$

  Optical instruments are characterized by specific limit values for the maximum detectable slope, defined by the objective's Numerical Aperture (NA). When the value of Sdq is too high, there is the possibility that some points will not be measured, since the light reflected does not return to the sensor.

Instead, an important spatial parameter is the following:

- Autocorrelation Length, Sal: horizontal distance of the ACF(tx,ty) which has the fastest decay to a specified value s, with s being greater or equal to zero, and lower than 1. [9]

$$Sal = \min \sqrt{tx^2 + ty^2}$$

  ACF is the autocorrelation function, and it evaluates the correlation of a part of an image with respect to the image in its totality. The ACF is defined as a convolution of the surface with itself, shifted by (tx, ty): [10]

$$ACF\ (tx, ty) = \frac{\iint z(x,y)z(x-t_x, y-t_y)dxdy}{\iint z(x,y)^2 dxdy}$$

[9, 18, 20]

2.6 Coordinate Measuring Machines (CMMs)

2.6.1 Operating Principles of CMMs

Coordinate Measuring Machines (CMMs) have been introduced in the late 1950s and are generally adopted to verify the dimensional and geometrical tolerances of a manufactured product.

As defined in ISO 10360-1, CMM is an electromechanical system composed of a set of three bodies that move linearly within a Cartesian volume, and able to generate the three orthogonal axes (X, Y, Z) of the machine reference system.

The fundamental operating principle relies on the physical acquisition of discrete points on the workpiece surface.

Each CMM is composed of different systems, each one aimed at fulfilling different functions:

- Machine system: it is responsible for the relative movement between the probe and the workpiece. Its primary function is to guarantee a rigid, stable, and repeatable Cartesian reference frame.

  The system usually consists of a base, leaning on the floor and supporting the carriages, used for moving along three orthogonal directions and different reading scales, applied to the carriages for identifying their positions along their single direction of movement.
- Probing system: through the production of a signal, the reading of the scale is enabled. When the stylus tip touches the workpiece, the CMM memorizes the contact point coordinates.
- Software system: by analyzing the gathered coordinates using calculation algorithms, it defines the dimensional and geometrical features of the product.
- Control system: electronic component responsible for motion, data synchronization and error map correction [21, 22, 23].

There are different types of CMMs. The most common ones are shown in figures 7, 8, 9, 10 below.

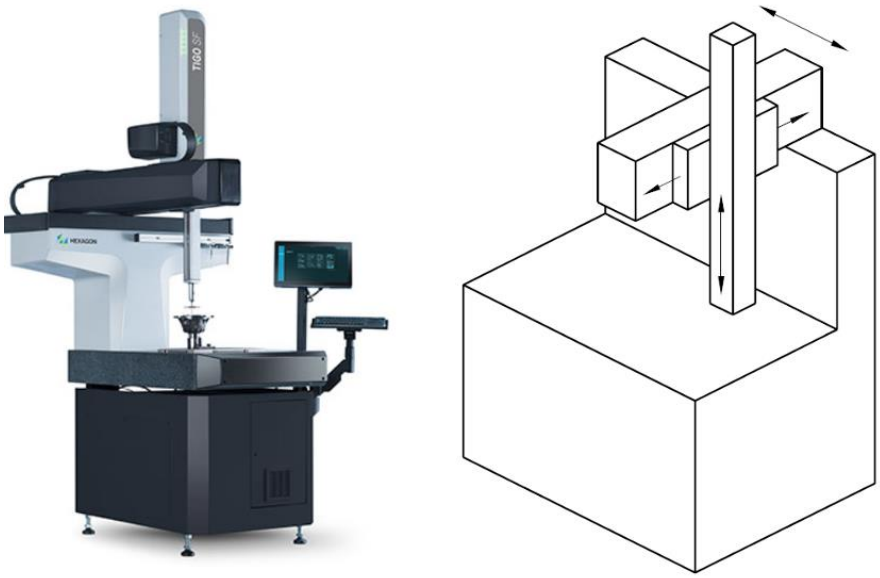

Figure 7: Fixed table cantilever CMM [78].

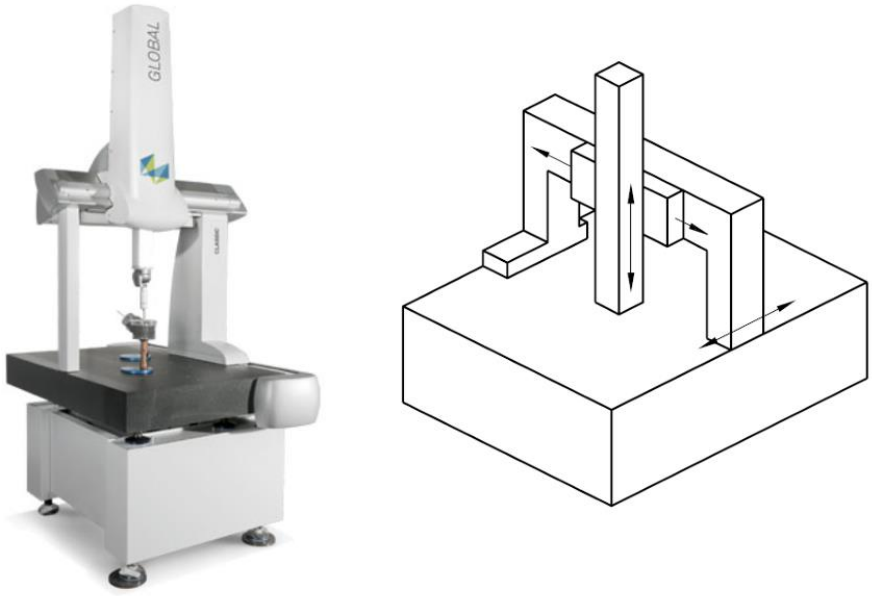

Figure 8: Moving bridge CMM [78].

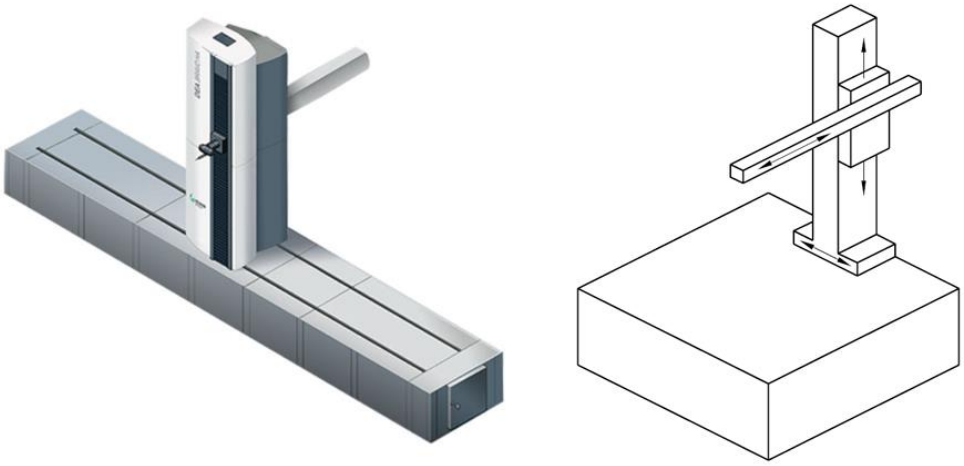

Figure 9: Moving ram horizontal-arm CMM [78].

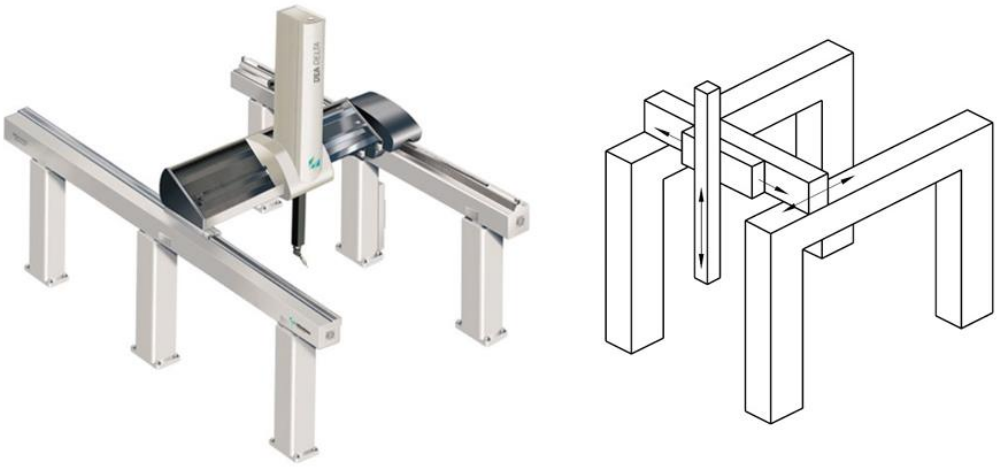

Figure 10: Gantry CMM [78].

2.6.2 Limits of CMMs

Traditional Coordinate Measuring Machines (CMMs), which have been considered for a very long time as the standard devices for coordinate metrology in industrial scenarios, are characterized by physical and operational limits.

The measurement output generated by CMMs is related to different factors interacting together, such as probe characteristics, probing strategy, measurement speed, environmental conditions, and data processing algorithms.

Each measuring device has certain geometrical defects that have an impact on the measurement results, and hence it becomes important to detect and resolve them.

The Mechanical Filtering Effect, as shown in Figure 11, has been recognized as one of the most significant metrological limitations, caused as a result of the finite dimensions of the stylus tip, thereby resulting in distortion of the measured object's surface.

The stylus tip traverses over the object's surface, and in so doing, it aims at determining the coordinates of its center point, as well as providing a representation of the object's surface.

The surface scanning of the product under test through a tactile probe is a widely used practice to obtain the object's measured surface, although it also results in dilation of the object's surface as a result of the stylus tip.

Considering that the radius of the CMM probe tip is generally between 0.5 mm and 3 mm, the stylus is not able to penetrate valleys greater than its diameter. Consequently, the high frequencies are lost.

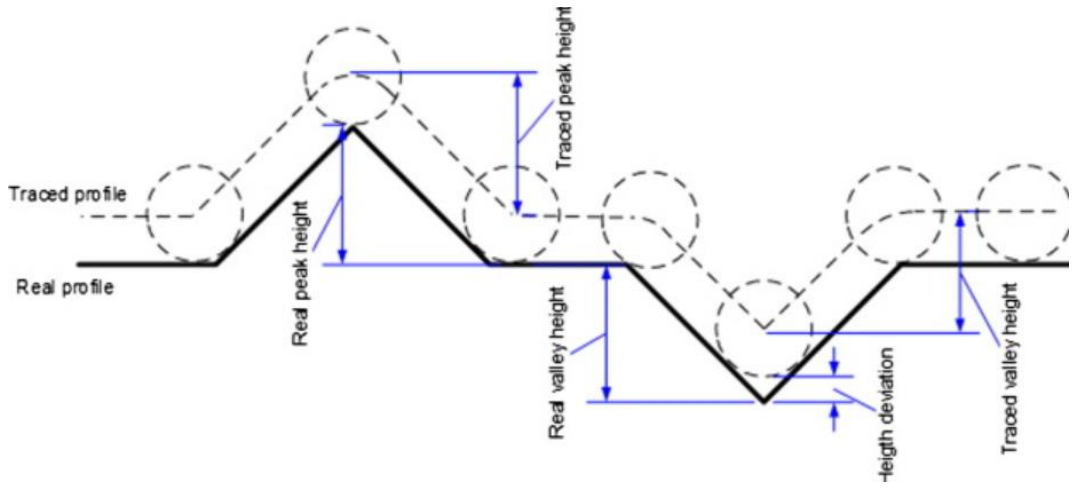

Figure 11: Tip mechanical filtering effects [24].

By analyzing the differences between the real workpiece profile and the profile traced by the stylus, it is clear that the stylus tip, due to its geometrical limitations, tends to round off the peaks making them greater, although the peak height remains constant.

On the other hand, the valleys are smoothed and their height is decreased.

Even if the morphological operations are performed on the traced surface, the real surface is not attainable because of the nonlinearity of the functional methods applied for traced surface correction.

Morphological operations can help in redefining the original surface only for those surface areas where the curvatures are larger than that of the stylus tip.

As represented in Figure 12 below, large stylus tips reduce the surface irregularities, whereas small tips enable the reconstructed surface to better approximate the real surface.

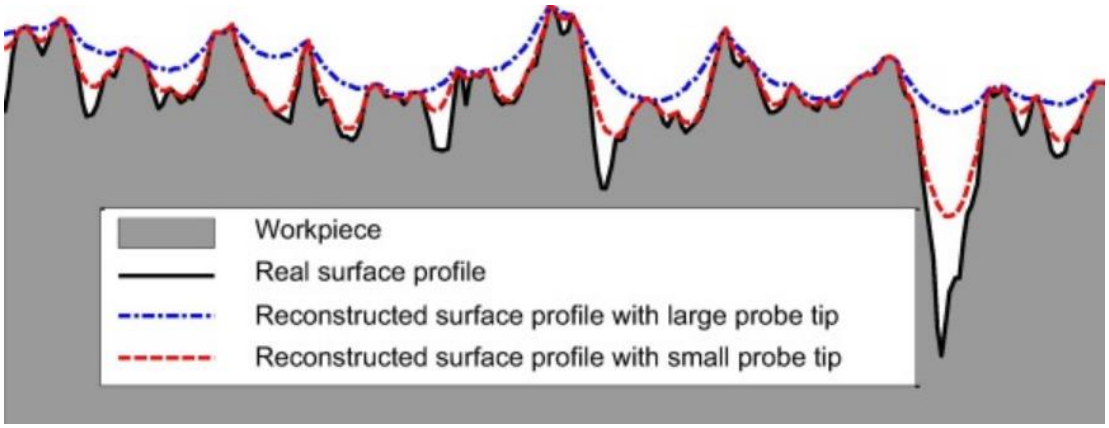

Figure 12: Reconstructed real mechanical surfaces vary with the tip size [24].

Moreover, another weakness of CMMs is related to their strong dependence on the conditions of the environment in which they are located.

The performance of coordinate measuring machines is greatly affected by temperature values, which are not at the reference value.

Even if CMMs are in large part automated, a human component is still necessary, in particular for the step of definition of the measurement process. This aspect, in turn, plays a crucial role in terms of measurement accuracy as well as repeatability [18, 24].

Chapter 3. Extension of CMMs with Optical Methods

The increasing complexity of modern manufacturing environments highlights the limitations of traditional Coordinate Measuring Machines (CMMs), which result from the complex relationship between the tactile probe of the CMM and the surface of the part.

Additionally, another disadvantage of CMMs relates to the time required to scan and collect by contact a high number of surface points.

To overcome the limits of CMMs, a technologically advanced method to perform surface topography evaluation has been introduced, which involves the adoption of optical measuring instruments.

Optical instruments have an advantage with respect to stylus instruments, in which the motion of the stylus can lead to damage of the surface being measured [11, 25].

3.1 Optical Measuring Instruments

Optical measuring instruments are employed in the measurement of optical surfaces through non-contact measurement techniques, which rely on the interaction between the incident light beam and the surface itself.

The electromagnetic surface has been defined by ISO 25178-2 as the “surface obtained by the electromagnetic interaction with the skin model of a workpiece”.

Optical metrology has witnessed relevant expansion with the increasing adoption of Industry 4.0, since well-developed non-contact measuring devices that guarantee a reduction of inspection time and continuous monitoring of process quality, apart from the ability to capture dense datasets, became fundamental in the context of measurements and metrological analyses to be performed in real-time.

Optical sensors typically perform measurements along the x-y plane, while the measurement of height, defined by z, is accomplished with the use of auto-focusing by moving the sensor up and down in the machine Z-axis.

Measurement of the surface is not done through contact, unlike the use of contact probes, which reduces the possibility of deforming the surface under investigation.

Due to the lack of physical contact between the two parts, Optical Measurement Instruments extract surface information by employing electromagnetic radiation in the visible or near-visible spectrum.

The performance of such instruments is strictly related to how light is generated and managed.

These types of devices illuminate the surface of the product under test by emitting a beam of light, such as light-emitting diode (LED), laser, or broadband white light.

The illuminated surface modifies the incident light through reflection, scattering, or refraction, depending on the specific surface features.

The light reflected by the surface will be collected and transformed into digital data by optical sensors like cameras or photodetectors, which will then be processed through specific algorithms for enabling the extraction of high-quality surface geometric information [3, 11, 26, 27, 28].

Different types of optical measuring instruments can be identified, related to the measuring principle undertaken.

Some optical devices are designed for measuring the real surface topography by either scanning a beam or using the field of view, others instrument instead proceed by measuring a statistical parameter of the surface, usually by analyzing the distribution of scattered light.

Among the most widely used optical instruments, Machine Vision System (MVS), shown in Figure 13 below, can be found, which employ calibrated optical lenses and high-resolution cameras to capture 2D images of the object, which are useful for identifying edges and contours, but less effective for surface topography measurement.

The images created are then analyzed using specific techniques that make it possible to localize surface geometrical characteristics such as edges, contours, or corners. These devices are particularly useful when there is the need to inspect large production runs on small parts [29, 30].

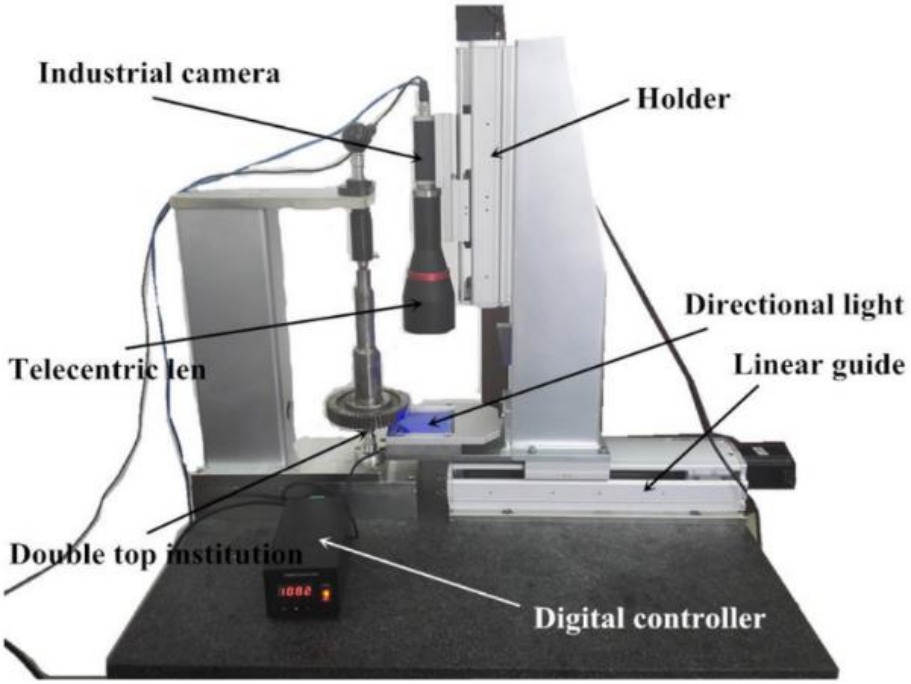

Figure 13: Machine Vision System [79].

Another important type of optical device is represented by optical three-dimensional scanning systems, visible in Figure 14, which are employed to generate virtual three-dimensional model of the real object analyzed. These instruments make it possible to transfer all details of the scanned object to a computer environment, in a very short time frame.

To do so, the optical sensor projects different fringe patterns onto the scanned objects. However, only the points that are visible from both cameras are recorded, meaning that different measurements must be performed to generate the digitalization of the entire object [31].

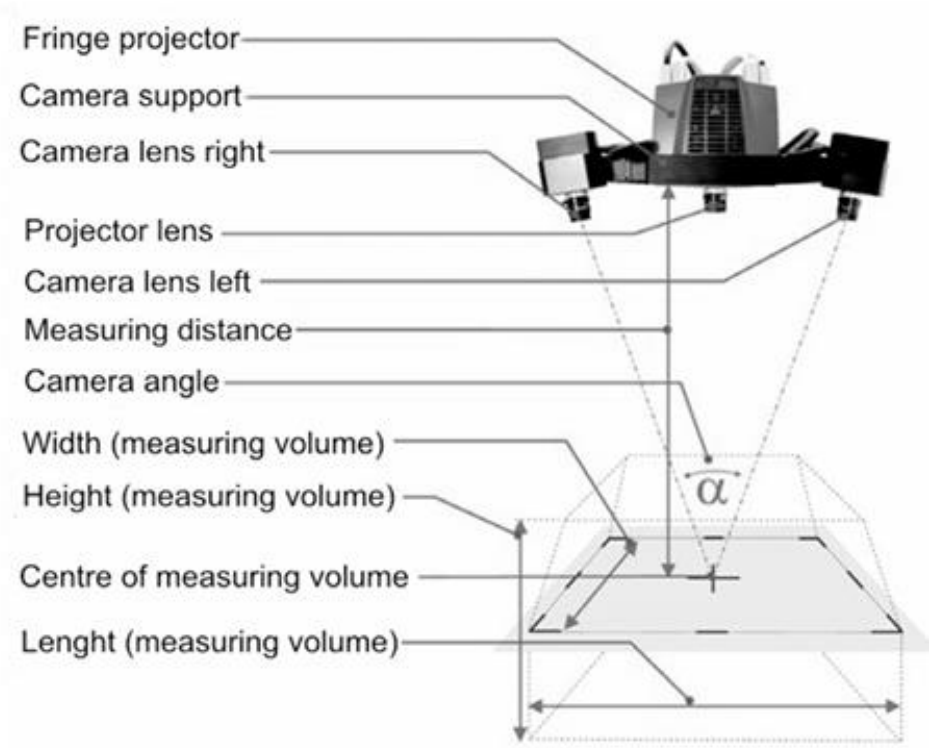

Figure 14: Optical three-dimensional scanner [31].

Another relevant type of optical instrument is represented by laser-based distance and displacement measuring instrument, such as Laser triangulation sensor.

These devices compute the distance of an object from the surface by analyzing the features of reflected laser light.

In the case of Laser triangulation sensor, represented in Figures 15 and 16, the sensor projects a laser beam onto the surface of the object to be measured, and the reflected light hits with a specific angle, a receiving element.

The change in the angle of the light allows the computation of the distance from the measuring sample, with precision in the micrometer order [32, 33, 34, 35].

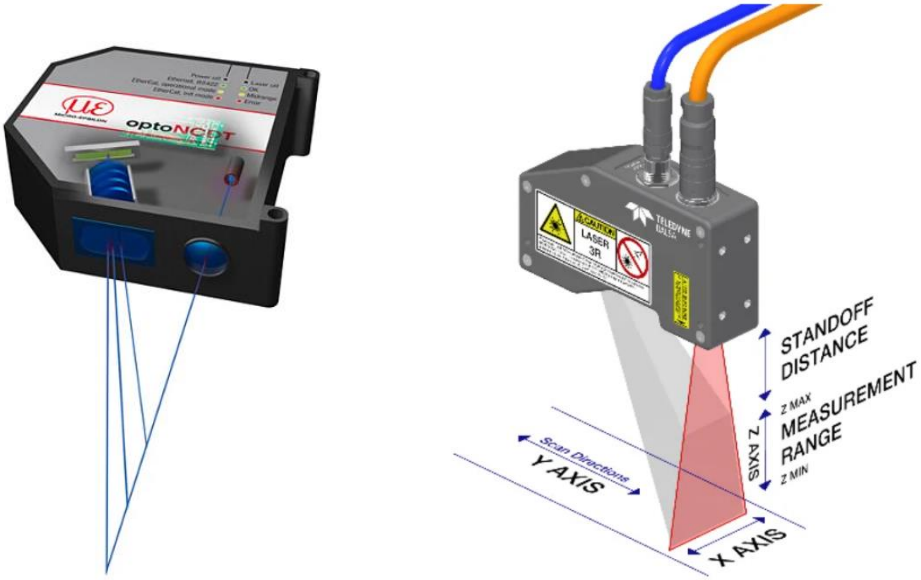

Figure 15, 16: Representation of laser triangulation sensors [34, 35].

To conclude, another relevant type of optical instrument is represented by Surface topography measuring systems, introduced by ISO 25178-6, to measure small-scale geometrical features on surfaces and generate high-quality three-dimensional measurements of surface characteristics [36].

In this context, to acquire information related to surface height, the following working principles can be adopted: coherence scanning interferometry CSI, confocal microscopy CM and focus variation FV. These methods are all able to provide areal surface topography measurement.

Focus variation is a technology able to acquire information about form, wear and roughness of the surface, employing a small depth of focus of an optical system with vertical scanning to gather topographical and color information from the variation of focus.

Precision optics, containing different lens systems equipped with different objectives, as shown in Figure 17, are moved vertically with respect to the object, bringing small parts of the surface in and out of focus with a stream of data being continuously registered at different resolutions. This vertical motion is necessary to generate a full detection of the product, which would not be possible otherwise due to the shallow depth of field of the optics.

The light goes through the optical path from a light source, reaching the product via the objective and it is reflected in multiple directions.

For every pixel position (x, y), a Focus Curve is generated by computing a sharpness metric, usually standard deviation or variance of grey values within a small neighbor kernel (n x n) across the captured z-planes. The exact surface height z (x, y) is not just the position of the image with the highest contrast, instead it is calculated by applying a curve fitting algorithm, rather a polynomial regression or Gaussian, to the top of the focus curve. This interpolation enables the achievement of a vertical resolution significantly better than the physical vertical step size.

Algorithms are then used to transform the collected data into three-dimensional information and a true color image with full depth of field, by analyzing the focus variation along the vertical axis.

Focus variation overcomes some of the limitations of general optical methods, since this technique is not restricted to special illumination, such as coaxial illumination, meaning that the maximum measurable slope angle is not only dependent on the numerical aperture of the product, and it can guarantee true color information for each measured point.

Focus variation can also be employed for the measurement of steep surface flanks, which instead are complicated to be assessed by other 3D measurement technologies.

Otherwise, the maximum measurable slope will be defined by: [11]

$$\alpha_{max} = \sin^{-1}(NA) .$$

However, this technique can be adopted only for surfaces characterized by a relevant variation of focus in the vertical direction, and a precise illumination type, such as Coaxial light, optimal for reflective surfaces, and Ring light, used for scatter light into the lens in case of inclined surfaces.

Figure 17: Precision optics for focus variation technique [37].

Focus variation is less precise in case of transparent surfaces, since light goes through the surface without being sufficiently reflected, or highly reflective surfaces, which can cause over saturation of the sensor. For smooth surfaces, the focus curve is flat, and the algorithm cannot detect the peak, incurring in Non-Measured Points.

Focus variation is largely employed in the evaluation of surface roughness, upstaging traditional contact stylus, due to their generation of smoothing effect and eventually alteration of the spaceman's surface. A new set of roughness standards has been defined, which highlights the similarity in the results obtained from focus variation and traditional tactile techniques.

Focus variation is also capable of assessing a wider range of different surface texture parameters such as amplitude parameters, volume parameters, fractal dimension of the surface, with respect to classical tactile stylus [11, 26, 37, 38, 39].

Confocal microscopy can be adopted for analyzing surface texture and can measure both rough and smooth surfaces, providing the highest possible lateral resolutions and excellent contrast. It is considered a high-quality technique capable of eliminating out of focus light, enhancing contrast and enabling three-dimensional specimens' replications, though the combination of two-dimensional images collected at different heights of the product.

Confocal microscopy operating principles are illustrated in Figure 18 below:

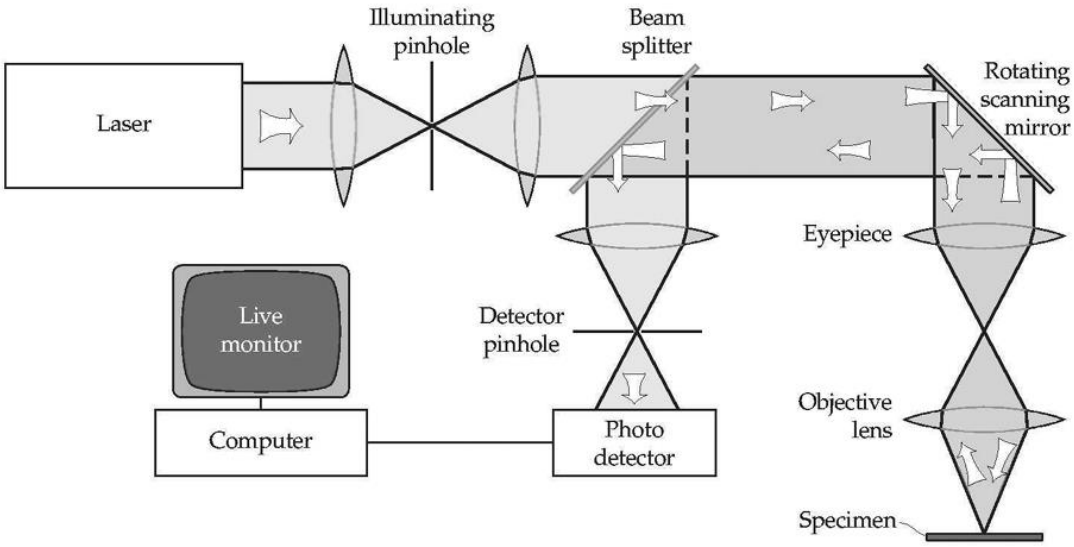

Figure 18: Surface roughness measurements by confocal microscopy [40].

This method consists in focusing a light from a semiconductor laser, restricted by a pinhole, on the surface measured, generating on it an incident spot.

The reflected light passes through another pinhole and reaches a photo multiplier, where the image is generated. This second pinhole is important because acting like a filter, it ensures that the light which is out of focus will be excluded [11, 27, 40].

Lastly, coherence scanning interferometry, represented in Figure 19 below, is a measurement technique that employs the wave interference of light to measure the topography of surfaces which are complex in terms of roughness, steps, discontinuities, and structure.

The broadband light source is divided into two paths: the measurement beam that reaches the surface of the product, which is moved vertically, and the reference beam, which instead is sent to an internal reference mirror.

The light reflected by the two surfaces will be combined at a detector, where the reflections interfering with each other generate patterns of light and dark intensities, whose peak corresponds to zero optical path difference.

This enables to detect the absolute height z, which is defined by the vertical position of the objective where the peak verifies.

CSI is generally employed to generate full three-dimensional datasets, useful for surface texture analysis and precise areal surface measurement at nanometer scale [41, 42].

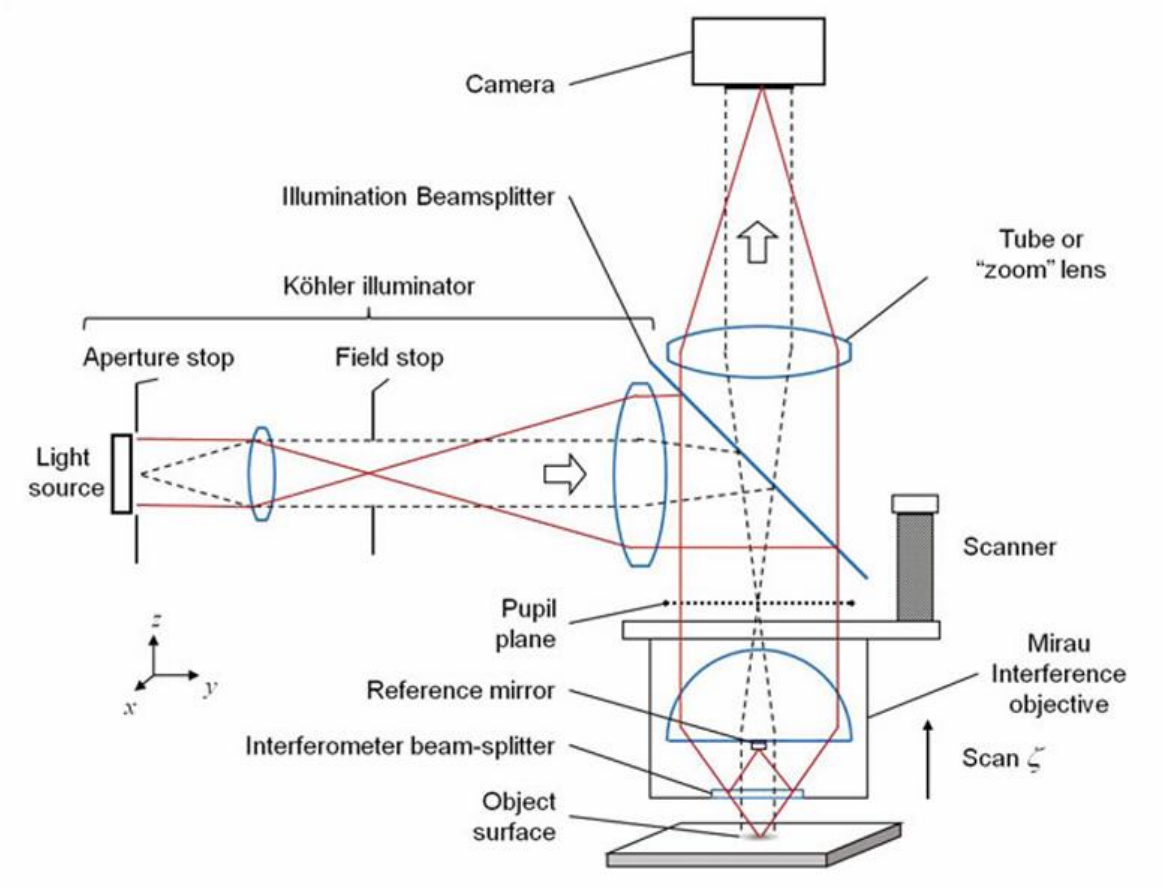

Figure 19: Geometry of an interference microscope suitable for CSI [11].

3.2 Limitations of Optical Measuring Instruments

Although optical measurement instruments offer key benefits, including reduction of the inspection time and non-contact related advantages, they are subject to significant limitations as well.

For example, the precision of measurement result performed employing optical techniques is low compared to the ones conducted using tactile devices.

The operation of optical measurement devices is greatly dependent on the complex relationship that exists between the object of interest and electromagnetic waves.

From a broader perspective, the measurement's accuracy depends on the optical properties of the surface, such as reflectivity, color, transparency, and roughness.

Those surfaces characterized by high reflectivity could result in sensor saturation and several reflections, leading to measurement errors or data loss.

On the other hand, dark surfaces tend to worsen the output signal quality by reflecting insufficient light.

In case of transparent or semi-transparent materials, light may penetrate the material and instead of reflecting on the actual product's surface, it will scatter from sub-surface layers.

The micro-scale topography of the object's surface is critical in determining the quality of results obtained from optical measurement devices. The relationship between the incident light and the roughness amplitude differentiates optically smooth surfaces from optically rough surfaces.

A surface is characterized as smooth if the surface height variation within the diffraction limited lateral resolution of the observation is smaller than $\frac{\lambda}{4}$ and it generates flat focus curves leading to data loss.

Instead, it is defined as optically rough if the surface height variation is larger than $\frac{\lambda}{4}$ and light is scattered in multiple directions, improving measurement results quality [11].

The quality of results obtained from optical measurement devices is greatly dependent on external environmental conditions, among which the most relevant ones are ambient light,

that affects controlled illumination, vibrations, causing phase errors, and temperature changes.

Another factor that plays a crucial role in this context is the type of illumination used, which is defined according to the interaction between the incident light and the object's atoms. This is coherent when the scattered light is in phase with the exciting light field, leading to speckle noise, and incoherent when the scattered light does not preserve a fixed phase relationship with the incident optical field, limiting speckle phenomena.

Occlusions and shadows represent another criticality for the proper functioning of optical devices, since a clear optical path between the optical sensor and the surface is needed.

Elements like deep cavities, undercuts, sharp edges, or complex internal geometries risk being left unmeasured.

In addition, optical instruments need to be calibrated to ensure precise and repeatable measurements.

Overall, optical devices are subject to two different types of outliers. The first type is called Non-Measured Points (NMP) and happens when a valid height z cannot be due to a very flat focus curve or the reflected intensity is too low, and the second type is spikes, which are isolated points characterized by particular height values [11, 39, 43, 44].

Chapter 4. Multisensor Integration and Hybrid Systems

The limitations of optical instruments led to the introduction of new hybrid measurement devices, called so because they combine innovative optical sensors, such as laser triangulation sensors and structured light sensors, mounted on CNC's or CMM's heads, creating a contact-optical measuring system, as Figure 20 shows.

Figure 20: Representation of a hybrid system [45].

This introduction has been significant since it incorporates the strengths of both measuring techniques: the accuracy of conventional contact probes regarding the identification of measurement points and the high rates of data capture and speed of optical methods.

Different optical sensors are located around the working volume to measure the full object's surface, and in addition to that, the CMM's contact head has the task of re-measuring those portions of the object that have not been captured by the sensors or require better precision.

The results obtained from the use of the optical sensors and the CMMs are unified to form a single dataset due to the unification of the different coordinate systems of the optical scanner and the CMMs.

This provides a cloud of points that is analyzed by special algorithms to determine the potential error and the areas that require further measurement by the CMMs.

Only after these two measurements are completed and the data from both systems combined, a virtual 3D representation of object is generated [45, 46].

Chapter 5. Automated Optical Inspection in Industry 4.0

Although contact measurement instruments have been largely employed in the past, the advent and diffusion of Industry 4.0 have highlighted the importance of optical measurement methods, even for their ability to effectively adapt to the production line, reducing capital costs and human error, increasing automation, and limiting scrap and rework.

In-process monitoring can produce the highest profit gains, in terms of reduced capital costs, increased automation, reduced human error and, most importantly, less scrap and rework

In any case, the metrological environment has become more demanding in terms of accuracy, speed and quality of measurements, becoming less tolerant toward errors, generating the need for optical measurement instruments rather than contact measurement instruments [27].

5.1 Focus Variation on Robotic Platforms

Focus Variation is an optical three-dimensional technique employed in areal surface topography analysis, which has the capability of measuring quantitatively the surface roughness, wear, and form at the same time.

This is a relatively new method, that has addressed the limitations of traditional three-dimensional surface topography measurements, which are often carried out using a contact stylus method and coordinate measuring machines.

Although these systems are capable of measuring with high precision, they are unable to be integrated into in-line processing systems due to the limitations of traditional three-dimensional surface topography measurement.

A key advantage of focus variation is indeed its low level of sensitivity to environmental vibrations with respect to coherence scanning interferometry, which is highly impacted by environmental noises that cause phase errors during the measurements.

Apart from that, focus variation is widely used because it can capture a cloud of points through just a single vertical scanning and determine their local contrast, instead of simply highlighting the peak intensity or phase interference of a single point, as is done by respectively CM and CSI [11, 39].

For these reasons, Focus Variation has been declared, among the different areal topography methods available, the most suitable one for robotic integration.

A relevant role in the measurement of micro-geometries features on large high precision parts is played by a three-dimensional optical sensor based on the focus variation technique mounted on a collaborative six-axis robot, as illustrated in Figure 21 [47, 48].

Since focus variation is not restricted to just one type of illumination, the use of ring light illumination can help get over a particular constraint resulting from cobots' geometry, consisting in the impossibility to align the sensor perfectly perpendicular to the surface normal.

Furthermore, the vertical scan range depends on the working distance of the objective, which could range between 3.2 and 22 mm, space useful to avoid impact between the cobot and the specimen.

This system helps to find automatic solutions that can be employed directly in the production line, contributing to decreasing the time needed to analyze extended objects, reducing the reliance on human operators and enabling the measurement of geometry and roughness of the cutting edges of the tool, with correlated detection of eventual edge defects.

In contrast, if assessment of cutting edges is carried out using conventional measurement equipment, this will be a much longer process, involving the removal of the cutting insert from the cutter, positioning it within the equipment, carrying out the assessment, and finally replacing it within the cutter. [11, 39, 47, 49].

Figure 21: Collaborative robot, equipped with a high-resolution 3D sensor [47].

5.2 The Limit of Accuracy of Robots

ISO 9283:1998 is the International Standard that defines performance criteria and test methods for the manipulation of industrial robots.

Differently from coordinate measuring machines, which are characterized by a high degree of precision, industrial robots are mainly designed for speed and repeatability, at the expense of lower accuracy.

According to the standards, pose accuracy and pose repeatability are two fundamental metrics for the evaluation of robots' performance.

Pose accuracy is the performance criteria that define the distance between the commanded coordinate and the average of the real positions, instead pose repeatability is the characterization of the robot's ability to reach the same point multiple times, coming from the same direction.

The positioning and orientation errors of industrial robots are generated by different factors, that can be categorized into geometric and non-geometric ones.

Despite geometric errors, caused by manufacturing and assembly activities, constitute most of robots' errors, also non-geometric factors must be taken into consideration, such as flexible and thermal deformation of joints and links. The difference between the actual features of the robot manufactured and its theoretical specifications contributes to the definition of robot accuracy.

Calibration can be used to improve robot positioning accuracy through the determination of kinematic parameters using software, instead of physically altering the design or the structure of the robot itself.

However, physical calibration is unable to completely eliminate geometric and non-geometric errors.

Therefore, the impossibility to determine the relationship between the positioning error caused by the robotic arm and the output of the optic sensor, has emphasized the benefits of off-line definition and simulation of robot tasks.

This link between optical performance and kinematic uncertainty is at the base of Digital-Metrological Twin development [50, 51, 52, 53].

Chapter 6. Digital-Metrological Twin

The increasing importance of areal surface topography measurements has led to a significant higher level of measurement uncertainty, particularly evident in optical measurement systems, caused by the interaction between the measuring device, the product's surface topography and the algorithms used for data processing.

The increasing trend towards the use of robotic platforms further negatively influences the measurement output due to vibrations and kinematic errors.

Since it is impractical to apply classic calibration techniques to such systems, state-of-the-art methods have been introduced, capable of performing uncertainty evaluation virtually though modelling, simulation, and analysis of measurement systems.

The key to achieving these advances is by transforming physical processes into computer simulations that allow for the creation of a Digital-Metrological Twin [10,11,54].

6.1 From Virtual Instruments to Digital-Metrological Twin

The first step towards a digitalized measurement process was achieved through Virtual Coordinate Measuring Machines (VCMMs), which were developed to overcome the limitations of contact measurement approaches to access uncertainty estimation.

In order to estimate the measurement uncertainty, it is necessary to model the measurement process though different Monte Carlo methods, helpful to identify the relevant variables and the range of possible measurement results.

As illustrated in Figure 22 below, a cloud of points is created through the interaction of the virtual probe and the surface of the object; the Monte Carlo simulation is then carried out to randomly sample the probability density function of the possible variables affecting the uncertainty and the measurement results [55,56,57].

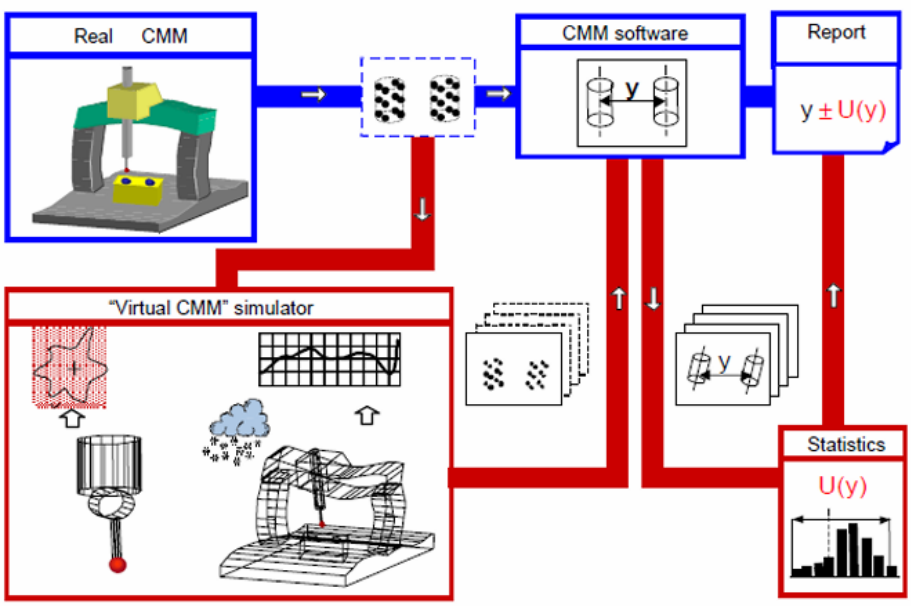

Figure 22: Data flow of the integrated VCMM [80].

Instead of focusing on macroscopic geometric errors, VCMMs model residual and random errors, which are not eliminated by Computer-Aided Accuracy (CAA) corrections [58,59].

However, VCMMs have some limitations, including the need to operate under specific environmental conditions and the need for frequent calibration. In addition, it is difficult to simulate the interaction of the probe and the surface of the object and the changes over time [59].

VCMMs, along with other virtual measuring devices, are an offline type of measurement system, characterized by several differences from the real measurement process. This is a relevant problem, since the same level of accuracy and reliability should be covered by physical and virtual devices.

The impossibility of dynamically simulating changes in the physical system, along with the lack of a real-time link between the real measurement and its digital replication, emphasizes the need for measurement techniques that exceed static simulation.

The next major discovery is indeed covered by Digital-Metrological Twins, capable of synchronizing virtual and physical systems thought mathematical models and real-time data processing [60,61,62].

The key difference between virtual experiments and digital twins is that in digital twins, dynamically modifications in the virtual world are made to accurately determine the similarity between the physical world and the virtual world. Instead, in virtual experiments, the system is considered to be in a static state with no time-dependent modifications [63].

6.2 Architecture of a Digital-Metrological Twin

Although the concept of digital twins appeared for the first time at the beginning of the 21st century in Grieves' work related to virtual-real-driven product life management (PLM), the idea of a virtual duplication was first employed by NASA, detailing it in NASA's integrated technology roadmap.

The scope was to build a reliable duplication of a space vehicle, able to replicate on earth the behavior of a vehicle operating in space [63,64,65,66,67]

A digital twin is described as a virtual instance that accurately replicates a physical system, capable of reflecting the current state of the object through automated dynamic updates of the digital model thanks to data acquired from sensors and processed in real time.

Unlike a digital model, which is a virtual version of a physical object with which there is no automatic exchange of data, and a digital shadow, in which data are only shared from the physical entity to the digital one, a digital twin instead is distinguished by a two-way twinning.

This bidirectional flow of information, as shown in Figure 23 below, is achieved through a physical-to-virtual (P2V) connection, that employs sensors able to capture the current state of the physical entity, which will be then transferred to the virtual replication, and a virtual to-physical (V2P) connection, used to supervise the physical entity and sending to it specific commands to achieve target results in the physical system.

The digital twin concept connects two environments: a physical environment, which hosts the object to be simulated, and which is equipped with sensors, and a virtual environment which hosts virtual entities that are replicas of a physical object.

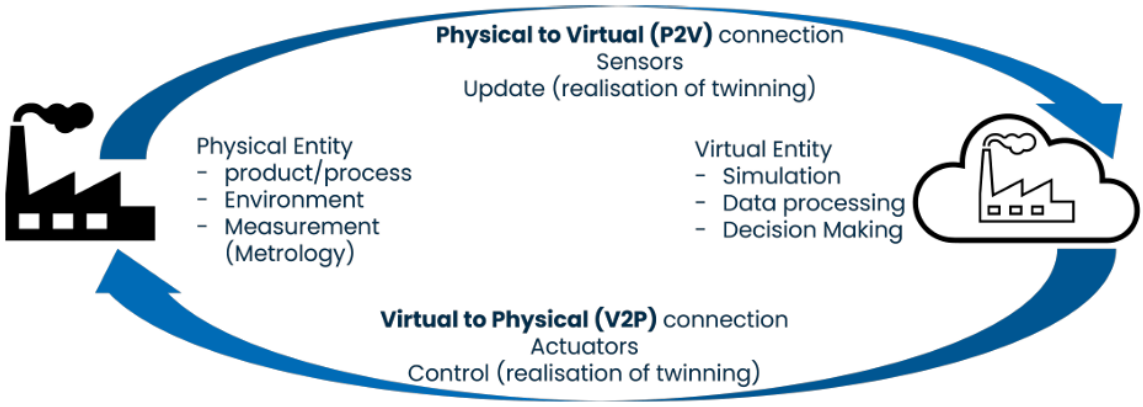

Figure 23: DT main components and scope [63].

Thanks to the automatic exchange of data between the physical and the digital entity, the virtual replica is always kept up-to-date to accurately reflect the changes in the physical object.

The physical entity's condition may change due to internal factors such as the effects of wear, damage, and fatigue, which result in the degradation of the overall performance of the physical object.

On the other hand, the physical entity's condition may also change due to external factors such as the loading or usage of the object.

The data sent from the physical system to the virtual one, including information related to environmental characteristics, engines and battery condition, are of particular importance. This information has the capability of being employed by the digital twin to accurately predict the system's health and calculate the useful lifespan of the system, hence improving the physical object's performance.

Most digital twins have been developed with the aim of being incorporated into decision-making processes, due to their capability of predicting the system's responses to safety critical events and the ability to highlight problems before they arise, managed by scheduled preventive maintenance.

In this context, the relationship between the two entities can proceed even after the sale of the physical product, guaranteeing full supervision of the performance and maintenance.

The diffusion of digital twins can support the transition from mass production towards individualized production, while simultaneously reducing costs and test duration [57,63,65,68].

The concept of measurement uncertainty in relation to digital twins' role, became relevant only recently.

However, the results of a given digital twin, to be integrated into a traceability chain, must be metrologically traced, thus making it a Digital-Metrological Twin (D-MT).

Digital-Metrological Twin (D-MT) has been defined as a numerical model aimed at describing a complete measurement process characterized by an associated measurement uncertainty for a specific measured value, which is traceable to the units of the international system of units, having all parameters traceably determined and including traceable and validated measurement uncertainty.

So, D-MT requires additional features with respect to generic digital twins, since they do not simply mimic a physical product, but they also ensure that the output of the virtual entity is reliable, traceable and accurate [63,65].

6.3 Digital-Metrological Twin for a Measurement Uncertainty Evaluation

The role of metrology in digital twins is to ensure the accuracy of the output of the virtual replica through the application of SI units, traceability to national standards, and uncertainty assessment.

To obtain a traced simulation result, indeed, uncertainty evaluation must be performed, which consists in achieving for each value of a measurand, a corresponding value of uncertainty.

It is possible to classify the uncertainty into Epistemic uncertainty, which is due to insufficient knowledge and wrong assumptions, and Aleatoric uncertainty, generated by the variability of the physical process.

In the context of digital twins, the types of uncertainty are as follows: Uncertainty of the diagnosis, which is due to errors in the sensors employed to capture the current state of the physical system, Uncertainty of the prognosis, which is generated by errors in the

simulation, and lastly Epistemic errors, due to the modeling strategy and the exchange of data.

All these types of uncertainty must then be combined to obtain a single value of the uncertainty of the measurement.

All sources of uncertainty related to the physical measurement device and process must be identified and taken into consideration in the simulation process. Therefore, the information that flows from the physical entity into the virtual one through a digital thread must comprehend both the data computed on the physical object, together with their corresponding uncertainty values.

In the context of the Digital-Metrological Twin, uncertainty evaluation is performed by associating probability distributions to all the relevant input quantities, which are then propagated through the digital model in order to produce an estimation of the associated output uncertainty in real-time.

In this context, the evaluation of the associated uncertainties can be performed before and during the measurement process due to the close and continuous connection between the physical and the digital environments.

This allows the results of the associated uncertainties to be as close as possible to the real world, as the results of the measurements performed on the physical object are continuously updated in the digital simulation in real-time.

On the other hand, the traditional approaches are mostly used as a tool for post-processing the results of the measurements and cannot be considered as part of the continuously updated digital model of the measurement system.

To ensure reliability of both virtual and physical entities, it is necessary to establish the traceability of the Digital Twin through the calibration of the measurement system.

To this end, artifacts have been employed, which are physical objects characterized by high level of accuracy, used as standards for calibration activities in both digital and physical systems.

In conclusion, Digital-Metrological Twins have enabled the transition from static uncertainty estimation to dynamic uncertainty evaluation, through real-time data acquisition, probabilistic transmission of uncertainty, and the use of SI traceable calibration [57,63,65,69,70].

Chapter 7. Methodology

7.1 Instrument

The instrument used to perform the measurement activities of the analysis is the Alicona IF-SensorR25, as illustrated in Figure 24 below.

The device allows the automatic evaluation of shape and roughness parameters, thereby guaranteeing high accuracy and traceability of the measurements obtained. It can be used to obtain repeatable results during the evaluation of the characteristics of the surface at the micrometric or submicrometric scale.

Alicona is a non-contact instrument, whose working principle is Focus Variation, which is an optical measurement method for three-dimensional measurement of the surface by utilizing multiple lenses with different objectives during a single vertical scan.

It is a three-dimensional optical measurement device that can be employed both in the production line and in laboratory environment, thanks to its standardized interfaces. It can also be combined with a 6-axis collaborative robot, to enable higher flexibility [71,72].

Figure 24: Alicona IF-SensorR25 [71].

Some of Alicona's features are shown in Table 4 below:

GENERAL SPECIFICATIONS

Positioning volume (Z)	25 mm (mot.)

OBJECTIVE SPECIFIC FEATURES

Objective magnification (*)		**10x**	**20x**	**50x**	**2xSX**	**5xAX**	**10xAX**	**20xAX**	**50xSX**
Working distance	mm	17.5	16	10.1	34	34	33.5	20	13
Lateral measurement area (X,Y) **(X x Y)**	mm mm^2	2 4	1 1	0.4 0.16	10 100	3.6 13.03	2 4	1 1	0.4 0.16
Measurement point distance	µm	1	0.5	0.2	5	2	1	0.5	0.2
Finest lateral topographic resolution	µm	2	1	0.64	10	4	2	1	0.64
Measurement noise	nm	40	20	10	1240	165	45	25	15
Vertical resolution	nm	100	50	20	3500	460	130	70	45
Vertical measurement range	mm	16	15	9	25	25	25	19	12
Measurement speed		≤ 1.7 million measurement points/sec.							
Accessibility	°	31	29	19	40	51	51	39	26

(*) Objectives with longer working distance available upon request

RESOLUTION AND APPLICATION SPECIFICATIONS

Objective magnification		**10x**	**20x**	**50x**	**2xSX**	**5xAX**	**10xAX**	**20xAX**	**50xSX**
Min. measurable height	nm	100	50	20	3500	460	130	70	45
Max. measurable height	mm	16	15	9	25	25	25	19	12
Height step accuracy (1 mm)	%	0.1							
Min. measurable roughness (Ra)	µm	0.3	0.15	0.08	n.a.	n.a.	0.45	0.25	0.15
Min. measurable roughness (Sa)	µm	0.15	0.075	0.05	n.a.	n.a.	0.25	0.1	0.08
Min. measurable radius	µm	5	3	2	20	10	5	3	2
Min. measurable wedge angle	°	20							
Max. measurable slope angle	°	87							

ACCURACY

Flatness deviation	2 mm x 2 mm with 10x objective	U = 0.1 µm
Max. deviation of a height step measurement	height step 1000 µm height step 100 µm height step 10 µm height step 1 µm	$E_{Uni:St:ODS,MPE}$ = 1 µm, σ = 0.1 µm $E_{Uni:St:ODS,MPE}$ = 0.4 µm, σ = 0.05 µm $E_{Uni:St:ODS,MPE}$ = 0.3 µm, σ = 0.025 µm $E_{Uni:St:ODS,MPE}$ = 0.15 µm, σ = 0.01 µm
Profile roughness	Ra = 0.5 µm	U = 0.04 µm, σ = 0.002 µm
Area roughness	Sa = 0.5 µm	U = 0.03 µm, σ = 0.002 µm
Distance measurement	XY up to 2 mm	$E_{Bi:Tr:ODS,MPE}$ = 0.8 µm
Wedge angle	β = 70 ° - 110 °	U = 0.15 °, σ = 0.02 °
Edge radius	R = 5 µm - 20 µm R > 20 µm	U = 1.5 µm, σ = 0.15 µm U = 2 µm, σ = 0.3 µm

$E_{Uni:St:ODS,MPE}$ & $E_{Bi:Tr:ODS,MPE}$ conform toISO 10360-8

SOFTWARE

Interface	integrated scripting language; LabVIEW framework; .NET remoting interface; Alicona Inspect Professional (enables GD&T measurement)

Table 4: Alicona's characteristics [71].

The purpose of the study is to develop a digital twin of a Focus Variation system by considering the sensitivity of the measurement obtained on a specific artefact and the systematic measurement errors by analyzing the measurement factors of the device.

The factors that need to be examined are objective, intensity, contrast, polarizer, illumination type and lateral resolution; they are listed in Table 5 below, along with their corresponding levels.

Source	Factor	Levels
Instrument (ALICONA IF-SensorR25)	Objective	10x, 20x
	Intensity	0.2, 0.3, 1
	Contrast	0.5; 2.5; 4
	Polarizer	Y-N
	Illumination Type	Ring (POLITO)
	Lateral Resolution	10x: 2; 5; 12.58 20x: 1.3; 3.2; 8.39
Measurand		Sensofar flt (POLITO)

Table 5: Relevant factors for the measurement

The objective is used to define magnification, field of view, and numerical aperture, which define both lateral and vertical resolution as well as the maximum depth of field achievable.

In this experiment, measurements are repeated with two objectives: a 10x objective with a larger field of view but lower lateral resolution, and a 20x objective used to measure smaller surface areas with higher lateral resolution.

Three intensity levels are used, which define how much light is reflected from the surface and measured by the sensor. Due to the possible features characterizing different surfaces, such as reflectivity, roughness, darkness, it is fundamental to choose the right level of intensity.

Contrast is used to define how much a peak in contrast must be to define a valid point for a three-dimensional reconstruction. In cases in which contrast is set too low, there is the possibility of mistakenly assuming noises as valid surface features, on the contrary, for too high contrast, some valid areas may not be taken into consideration.

The polarizer is set to either Yes or No, depending on whether a polarizer is used in the measurement.

The function of the disc is to make the reflected light opaquer, thereby reducing or eliminating unwanted reflections and increasing image saturation and contrast, thus increasing reliability on the reflective surface.

When set to Yes, glare is reduced, unwanted reflections from metallic or polished surfaces are minimized and contrast distribution becomes more uniform, albeit at the expense of reduced light intensity.

In the experiment, the type of illumination used is the Ring type, which reduces shadows on the surface under test by lighting the surface from multiple angles.

This type of illumination is characterized by uniform circumferential lighting not reflecting directly into the camera, as instead coax illumination does.

With regard to the lateral resolution, this is defined as the capacity of the optical device to distinguish two adjacent points on the x-y horizontal plane of the surface under test.

A higher lateral resolution implies longer measurement time and better small surface's features representation. The system implements a lateral filter with gaussian kernel to preprocess measured data and reduce noise content, possibly due to scattering. The set lateral resolution, while maintaining the pixel size, modifies the kernel dimension.

The full factorial experimental design requires that a total of 108 measurements be made, obtained from multiplying the total number of levels for each factor: 2 x 3 x 3 x 2 x 1 x 3.

Furthermore, three repetitions are made, for a total of 324 measurements.

The sequential procedure on the instrument that must be carried out before performing each measure is the following: set intensity, set contrast, set polarizer, set auto light, set lateral resolution, register the value of brightness for each measure, execute the measure.

7.2 Measurement Process with Alicona IF-SensorR25

Once all the 324 measurements have been performed, each of the studiables is imported individually into MountainsMap software for processing and analysis through a specific Minidoc.

The Minidoc is defined as a powerful automation technique designed to optimize repetitive analysis tasks, acting as a saved, reusable procedure characterized by a set of sequential operations, eliminating the necessity of re-creating analyses from scratch each time.

Firstly, the geometric correction operation of Least Square (LS) Leveling is applied, with the intent of removing the global inclination from the surface under investigation.

The final corrected and leveled surface is obtained by subtracting from the measured surface a best-fit-plane, computed employing the least squares method, which means that the distances between the plane itself and the measured points are minimized [73].

A parameters table, as demonstrated in Table 6, is incorporated into the Minidoc to enable specific parameters to be extracted from each studiable.

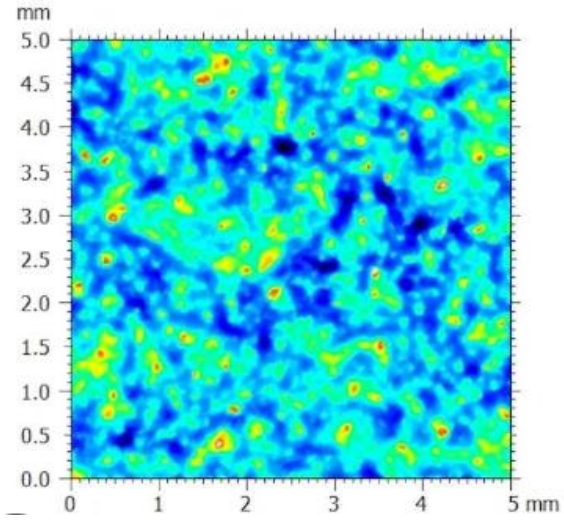

EUR 15178N - Waviness (S-F) [4]		
F: [Workflow] Leveled (LS-plane)		
S-filter (λc): Gaussian, 0.8 mm		
Amplitude parameters		
Sa	6.897	µm
Sq	8.655	µm
Sz	43.49	µm
Ssk	0.2466	
Sku	2.952	
Sp	28.92	µm
Sv	24.15	µm
St	53.07	µm

Table 6: Example of Parameters Table [74].

In this specific analysis, the areal surface texture parameters inserted in the parameters table that are useful to be studied are Sa, Sq and Sz.

Sa has been identified as the most commonly used parameter for surface roughness and has been defined as the average absolute deviation of height values from the mean plane. The drawback is that it cannot identify the spatial distribution, shape, or frequency of surface characteristics, and it has been demonstrated how completely different surfaces can have the same Sa values, as shown in Figure 25 below.

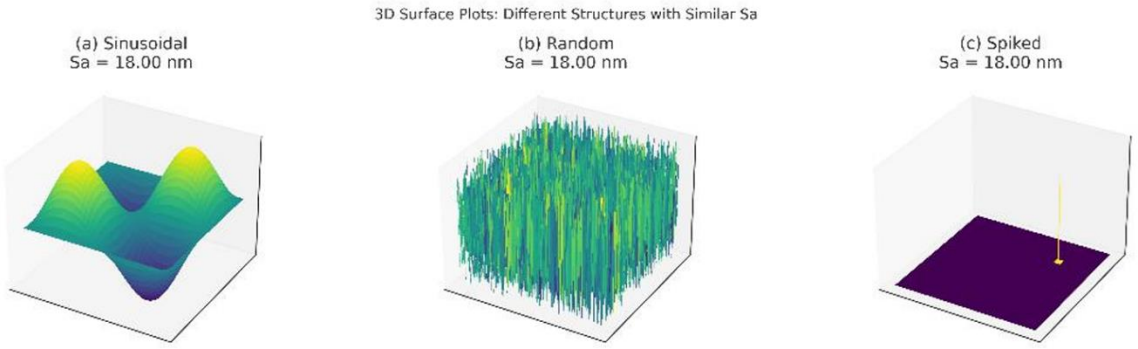

Figure 25: Completely different surfaces, but with identical Sa value [75].

Same logic is valid for Root Mean Square Height Sq parameter, since it is insensitive in differentiating peaks, valleys and the position of the various surface features, while it is useful for representing the standard deviation of the surface heights within a defined sampling area.

Sq is usually used for the evaluation of optical surfaces, while Sa is used for the specification of machined surfaces.

All these parameters can give incorrect results on their own; however, they can become important tools when combined with other parameters, such as Ssk, good in defining the symmetry of the height distribution by discriminating between peaks and valleys.

Sa and Sq are considered to be highly sensitive to lateral components, which means that they are affected by the lateral resolution of the measurement device, which is a major disadvantage in the evaluation of height dispersion.

When measurements are performed on an ideally flat surface, the value of Sq will not be null, due to the presence of Noise Floor of the instrument. In general, Sq, which squares the height values, will be more affected by spikes than Sa.

If Sq and Sa are linked by the following relation: [12]

$$Sq = \sqrt{\frac{\pi}{2}} \times Sa$$

then the surface is characterized by a random heigh distribution, otherwise the surface has a non-stochastic nature [83].

Unlike Sq and Sa which provide average-based information, the maximum heigh parameter Sz captures the extreme features of the surface.

It defines the maximum heigh of the surface by computing the sum of the largest peak height value and the largest pit depth value within the defined area and can be employed to identify isolated defects and analyze surfaces' worst conditions, due to its great sensitivity to outliers.

Overall, areal surface parameters are not only described by their mathematical formulas, but are also largely affected by the measurement conditions, instrument calibration, and data resolution.

7.3 Topography parameter sensitivity to measurement setup

After having collected the values of Sa, Sq and Sz for each of the 324 measurements, a Response Surface Design analysis can be performed on Minitab, with the objective of defining which of the different input factors has a statistically significant impact on the measured responses, in this case the roughness parameters, and which instead has a negligible influence.

This type of regression modeling is also able to investigate the possible interactions between the multiple factors.

The objective magnification has been treated as a block, rather than a factor in the experiment, in order to isolate its influence and avoid confounding effects. As a result, two different regression analyses were carried out for the 10x and 20x data sets.

To improve the evaluation of the accuracy of the Focus Variation technique employed in the measurement process, the response surface analysis has been repeated after calculating the difference topography between the Focus Variation (FV) and Atomic Force Microscopy (AFM) topographies.

The topography obtained using the FV working principle is the one to be evaluated and it is represented by the symbol Z_m, while the reference topography, denoted as Z_{ref}, is obtained using the AFM method.

AFM is a high-resolution method of characterizing surfaces, allowing the measurement of surface topography at the micro- and nanometer scale using a sharp tip mounted on a flexible cantilever, which is scanned over the object's surface.

The advantages of using the AFM method over other imaging techniques include its capacity to generate three-dimensional representations of surfaces with very high resolution, allowing the identification and depiction of small-scale features.

Then, instead of evaluating roughness parameters on the entire surface, a smaller calibrated area of 1020 × 1020 points have been extracted, to better study micro-geometries of the specimen.

The Iterative Closest Point alignment (ICP) has been performed, which consists in a widely used algorithm for aligning two-dimensional or three-dimensional point clouds.

It is an iterative procedure employed to minimize the distance and discrepancies between two different point clouds, which in this case are represented by the reference topography Z_{ref} and the measured topography Z_m.

To align the points of the two topographies, an optimal rigid transformation must be individuated.

Firstly, for every point of Z_m, the corresponding nearest point of Z_{ref} has been individuated. Then, the sum of square errors between the two-point clouds are minimized, through the computation of a transformation matrix composed of translation and rotation. The computed transformation is applied to the points of Z_m, until residual errors do not go above a defined threshold [76].

Since the results obtained highlighted for both magnification objectives a crucial role covered by Lateral Resolution, the response surface analysis has been replicated after inserting a block on Lateral Resolution.

This procedure is used to isolate the predominant effect of Lateral Resolution, which could cause the obscuration of the significance of the other factors.

By doing so, the variance generated by modifications in the dominant factor is isolated inside the block, making the model more sensitive to the importance covered by Contrast and Polarizer.

Chapter 8. Experimental Results

8.1 Experimental Results with Raw Data

As demonstrated by the results shown in Figure 26, representing the analysis performed on the Sq parameter with the 10x objective, the model explains almost the entire observed variability, with an R-sq value of 97.49%.

Lateral Resolution is the most influencing factor, characterized by a null value of P-Value and high value for F-Value.

Also Contrast and Polarizer have a great impact on Sq, while Intensity is statistically non relevant, meaning that lighting variations do not impact the measurement process.

Model Summary

S	R-sq	R-sq(adj)	R-sq(pred)
0,0347290	97,49%	97,22%	96,72%

Analysis of Variance

Source	DF	Adj SS	Adj MS	F-Value	P-Value
Model	16	6,80397	0,42525	352,58	0,000
Linear	5	6,40534	1,28107	1062,15	0,000
Contrast	1	0,05906	0,05906	48,97	0,000
intensity	1	0,00015	0,00015	0,12	0,724
Polarizer	1	0,06661	0,06661	55,23	0,000
Later resolution	2	6,27949	3,13975	2603,21	0,000
Square	2	0,00615	0,00308	2,55	0,082
Contrast*Contrast	1	0,00611	0,00611	5,07	0,026
intensity*intensity	1	0,00004	0,00004	0,03	0,858
2-Way Interaction	9	0,07796	0,00866	7,18	0,000
Contrast*intensity	1	0,00124	0,00124	1,03	0,312
Contrast*Polarizer	1	0,00606	0,00606	5,02	0,027
Contrast*Later resolution	2	0,02444	0,01222	10,13	0,000
intensity*Polarizer	1	0,00093	0,00093	0,77	0,382
intensity*Later resolution	2	0,00185	0,00093	0,77	0,466
Polarizer*Later resolution	2	0,04344	0,02172	18,01	0,000
Error	145	0,17489	0,00121		
Lack-of-Fit	37	0,01905	0,00051	0,36	1,000
Pure Error	108	0,15584	0,00144		
Total	161	6,97886			

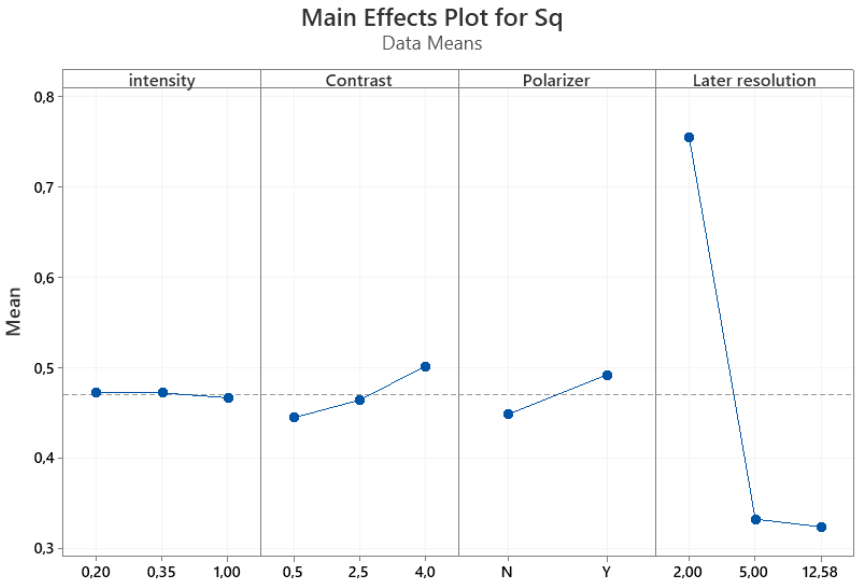

Figure 26: Results of analysis on Sq with 10x objective.

A very similar trend can be traced for the output of the analysis performed with 10x objective on Sa and Sz roughness parameters, as illustrated in Figures 27 and 28 below.

Model Summary

S	R-sq	R-sq(adj)	R-sq(pred)
0,0121435	99,50%	99,44%	99,36%

Analysis of Variance

Source	DF	Adj SS	Adj MS	F-Value	P-Value
Model	16	4,21637	0,26352	1787,01	0,000
Linear	5	4,00758	0,80152	5435,27	0,000
Contrast	1	0,01452	0,01452	98,49	0,000
intensity	1	0,00000	0,00000	0,00	0,952
Polarizer	1	0,06031	0,06031	408,95	0,000
Later resolution	2	3,93275	1,96638	13334,46	0,000
Square	2	0,00062	0,00031	2,12	0,124
Contrast*Contrast	1	0,00062	0,00062	4,23	0,042
intensity*intensity	1	0,00000	0,00000	0,01	0,930
2-Way Interaction	9	0,02585	0,00287	19,48	0,000
Contrast*intensity	1	0,00001	0,00001	0,09	0,759
Contrast*Polarizer	1	0,00084	0,00084	5,68	0,018
Contrast*Later resolution	2	0,00624	0,00312	21,14	0,000
intensity*Polarizer	1	0,00000	0,00000	0,01	0,928
intensity*Later resolution	2	0,00001	0,00000	0,02	0,979
Polarizer*Later resolution	2	0,01875	0,00938	63,59	0,000
Error	145	0,02138	0,00015		
Lack-of-Fit	37	0,00220	0,00006	0,33	1,000
Pure Error	108	0,01918	0,00018		
Total	161	4,23775			

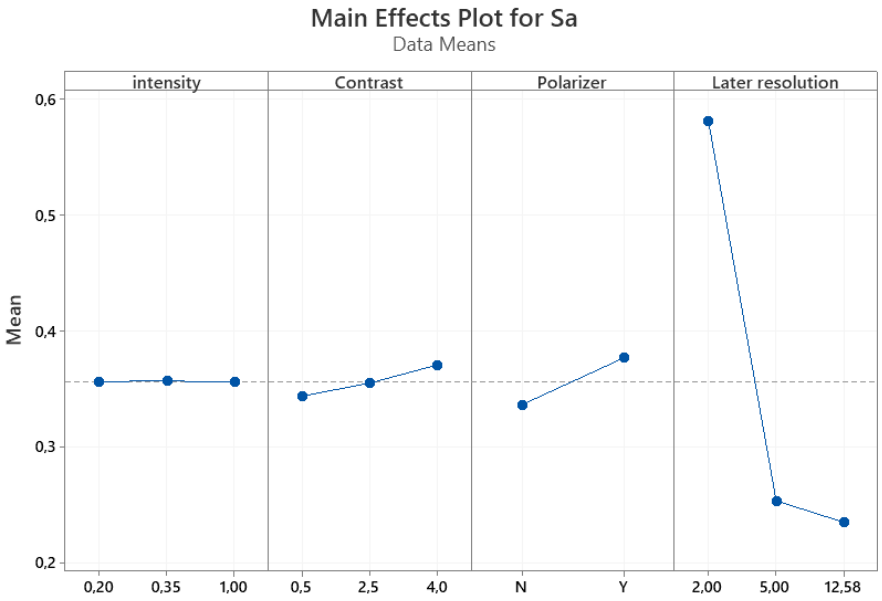

Figure 27: Results of analysis on Sa with 10x objective.

Model Summary

S	R-sq	R-sq(adj)	R-sq(pred)
0,0064729	99,83%	99,81%	99,79%

Analysis of Variance

Source	DF	Adj SS	Adj MS	F-Value	P-Value
Model	16	3,58751	0,22422	5351,42	0,000
Linear	5	3,36195	0,67239	16047,89	0,000
Contrast	1	0,00224	0,00224	53,46	0,000
intensity	1	0,00000	0,00000	0,01	0,924
Polarizer	1	0,01587	0,01587	378,76	0,000
Later resolution	2	3,34384	1,67192	39903,61	0,000
Square	2	0,00021	0,00011	2,55	0,082
Contrast*Contrast	1	0,00021	0,00021	5,06	0,026
intensity*intensity	1	0,00000	0,00000	0,03	0,864
2-Way Interaction	9	0,02770	0,00308	73,45	0,000
Contrast*intensity	1	0,00000	0,00000	0,00	0,972
Contrast*Polarizer	1	0,00052	0,00052	12,53	0,001
Contrast*Later resolution	2	0,00178	0,00089	21,23	0,000
intensity*Polarizer	1	0,00000	0,00000	0,03	0,852
intensity*Later resolution	2	0,00000	0,00000	0,03	0,969
Polarizer*Later resolution	2	0,02539	0,01270	303,00	0,000
Error	145	0,00608	0,00004		
Lack-of-Fit	37	0,00104	0,00003	0,60	0,960
Pure Error	108	0,00504	0,00005		
Total	161	3,59358			

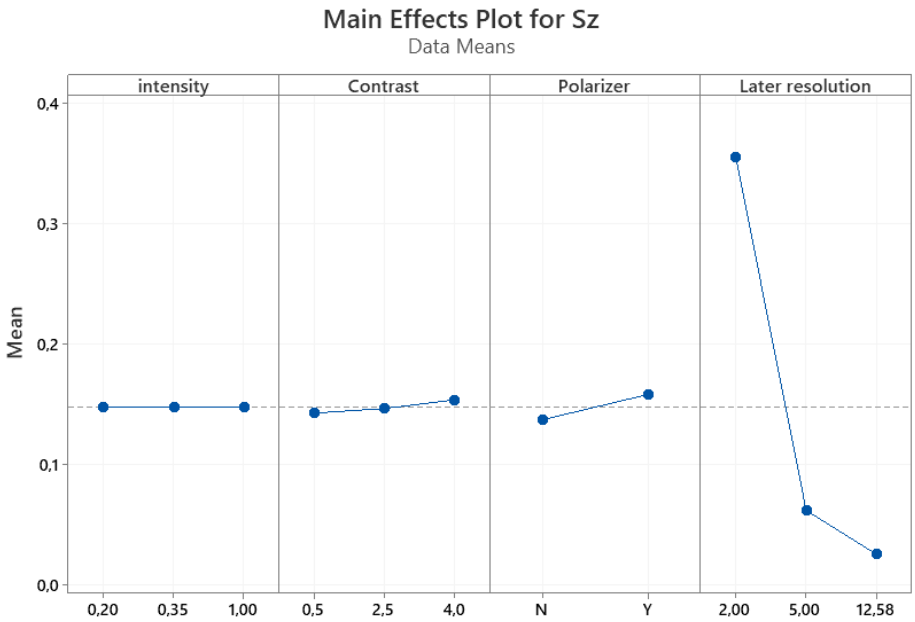

Figure 28: Results of analysis on Sz with 10x objective.

In all of the three cases, the Main Effects Plot graph exhibits an extremely steep curve for Lateral Resolution, reflecting its high relevance.

Great importance is also covered by the Polarizer, whose activation is fundamental for reducing the optical noises caused by undesired light reflections.

The analysis of the Interaction Plot graphs, illustrated in Figure 29, shows a similar behavior for the three parameters.

While Intensity is independent from the other factors, the accuracy of Sq, Sa, and Sz measurements is strictly dependent on the interaction between polarizer, contrast and lateral resolution.

Indeed, the activation of a polarizer and setting contrast to high values compensates for poor lateral resolution.

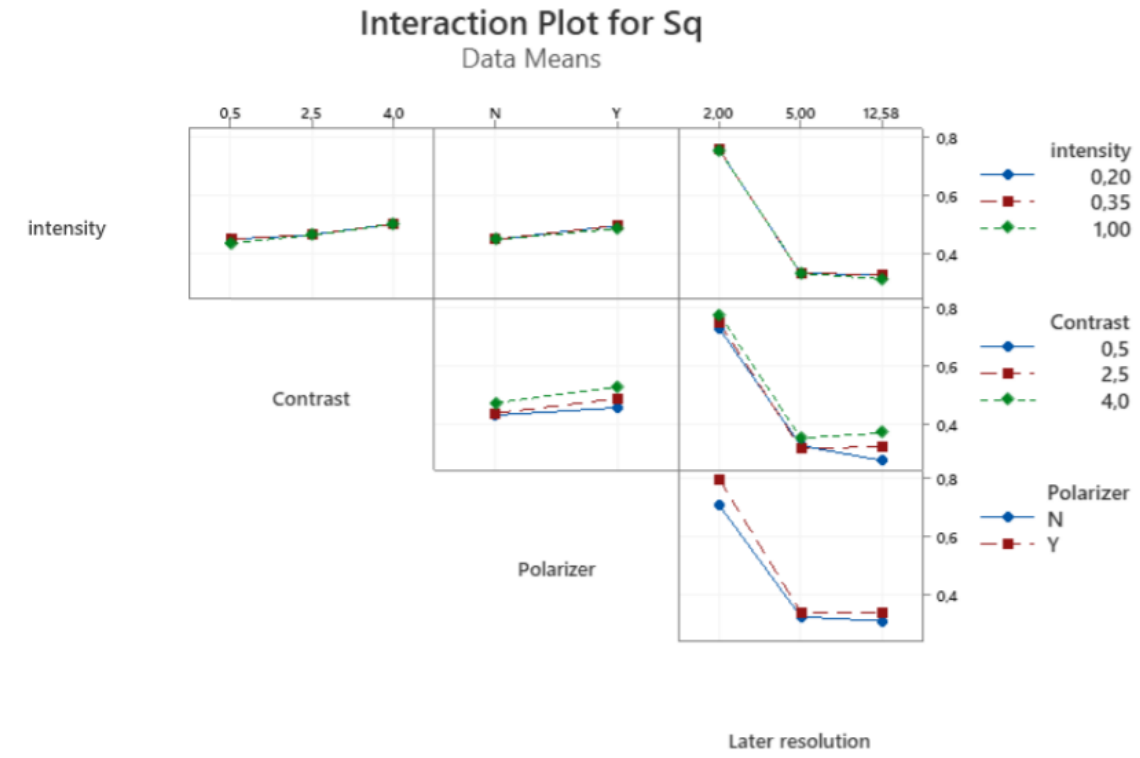
Interaction Plot for Sq
Data Means
0,5
2,5
4,0
N
Y
2,00
5,00
12,58
intensity
Contrast
Polarizer
0,8
0,6
0,4
intensity
0,20
0,35
1,00
Contrast
0,5
2,5
4,0
Polarizer
N
Y
Later resolution

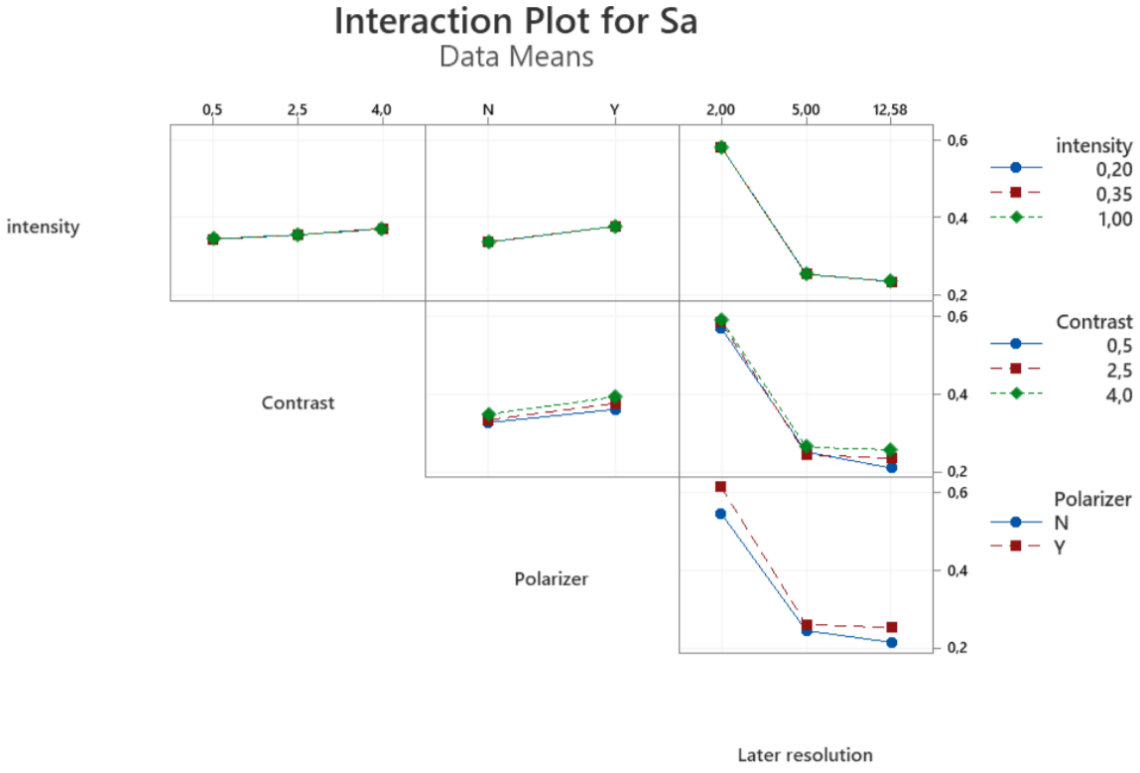
Interaction Plot for Sa
Data Means
0,5
2,5
4,0
N
Y
2,00
5,00
12,58
intensity
Contrast
Polarizer
0,6
0,4
0,2
intensity
0,20
0,35
1,00
Contrast
0,5
2,5
4,0
Polarizer
N
Y
Later resolution

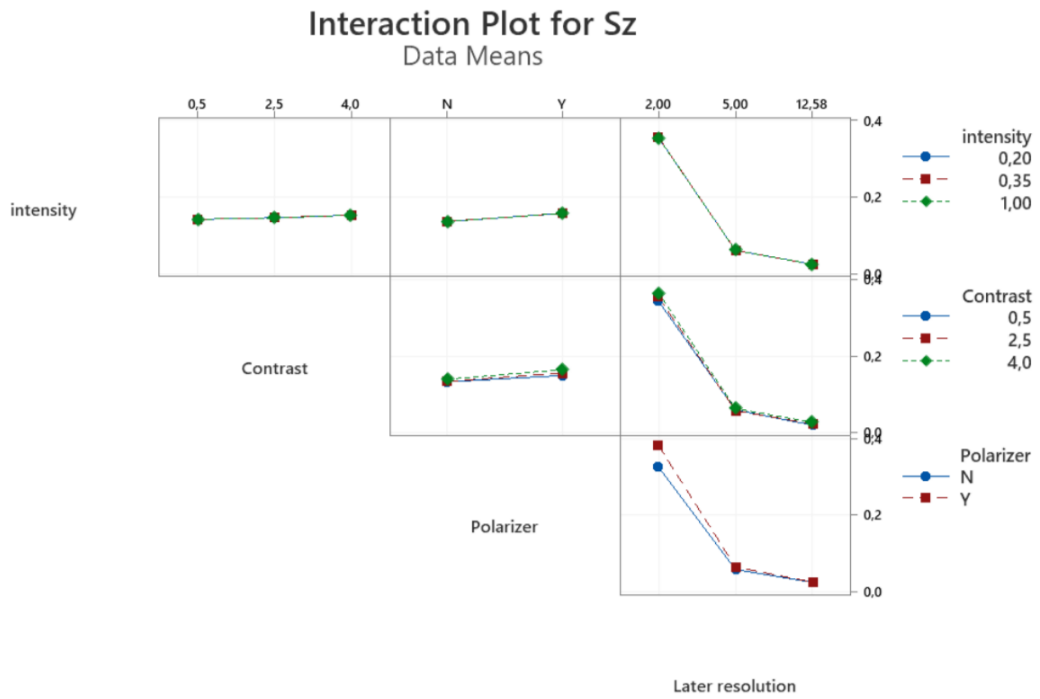

Figure 29: Interaction Plots graphs for Sq, Sa, Sz with 10x objective.

The exact same type of analysis has been replicated for the measures acquired with the 20x objective. The results on Sq, Sa, Sz are illustrated in Figures 30, 31, 32, and 33 below.

Model Summary

S	R-sq	R-sq(adj)	R-sq(pred)
0,0059059	99,41%	99,34%	99,26%

Analysis of Variance

Source	DF	Adj SS	Adj MS	F-Value	P-Value
Model	16	0,851320	0,053207	1525,44	0,000
Linear	5	0,811971	0,162394	4655,77	0,000
Contrast	1	0,004331	0,004331	124,17	0,000
intensity	1	0,000007	0,000007	0,19	0,666
Polarizer	1	0,001010	0,001010	28,96	0,000
Later resolution	2	0,806625	0,403313	11562,80	0,000
Square	2	0,000041	0,000020	0,59	0,558
Contrast*Contrast	1	0,000031	0,000031	0,90	0,344
intensity*intensity	1	0,000009	0,000009	0,27	0,605
2-Way Interaction	9	0,001346	0,000150	4,29	0,000
Contrast*intensity	1	0,000000	0,000000	0,00	0,946
Contrast*Polarizer	1	0,000026	0,000026	0,74	0,390
Contrast*Later resolution	2	0,000746	0,000373	10,69	0,000
intensity*Polarizer	1	0,000025	0,000025	0,72	0,399
intensity*Later resolution	2	0,000089	0,000045	1,28	0,282
Polarizer*Later resolution	2	0,000460	0,000230	6,60	0,002
Error	145	0,005058	0,000035		
Lack-of-Fit	37	0,002083	0,000056	2,04	0,002
Pure Error	108	0,002975	0,000028		
Total	161	0,856377			

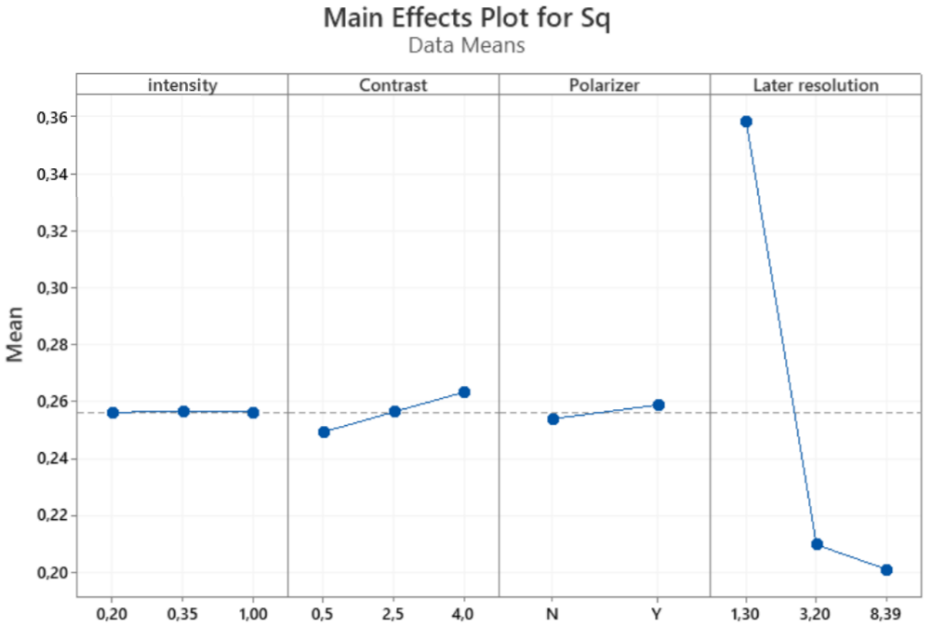

Figure 30: Results of analysis on Sq with 20x objective.

Model Summary

S	R-sq	R-sq(adj)	R-sq(pred)
0,0033832	99,71%	99,68%	99,64%

Analysis of Variance

Source	DF	Adj SS	Adj MS	F-Value	P-Value
Model	16	0,567757	0,035485	3100,24	0,000
Linear	5	0,543861	0,108772	9503,22	0,000
Contrast	1	0,001565	0,001565	136,71	0,000
intensity	1	0,000003	0,000003	0,30	0,587
Polarizer	1	0,001584	0,001584	138,37	0,000
Later resolution	2	0,540710	0,270355	23620,39	0,000
Square	2	0,000023	0,000012	1,02	0,364
Contrast*Contrast	1	0,000016	0,000016	1,39	0,240
intensity*intensity	1	0,000007	0,000007	0,64	0,424
2-Way Interaction	9	0,001763	0,000196	17,12	0,000
Contrast*intensity	1	0,000001	0,000001	0,12	0,730
Contrast*Polarizer	1	0,000003	0,000003	0,30	0,586
Contrast*Later resolution	2	0,001000	0,000500	43,69	0,000
intensity*Polarizer	1	0,000009	0,000009	0,80	0,373
intensity*Later resolution	2	0,000017	0,000009	0,74	0,477
Polarizer*Later resolution	2	0,000732	0,000366	31,99	0,000
Error	145	0,001660	0,000011		
Lack-of-Fit	37	0,001062	0,000029	5,18	0,000
Pure Error	108	0,000598	0,000006		
Total	161	0,569416			

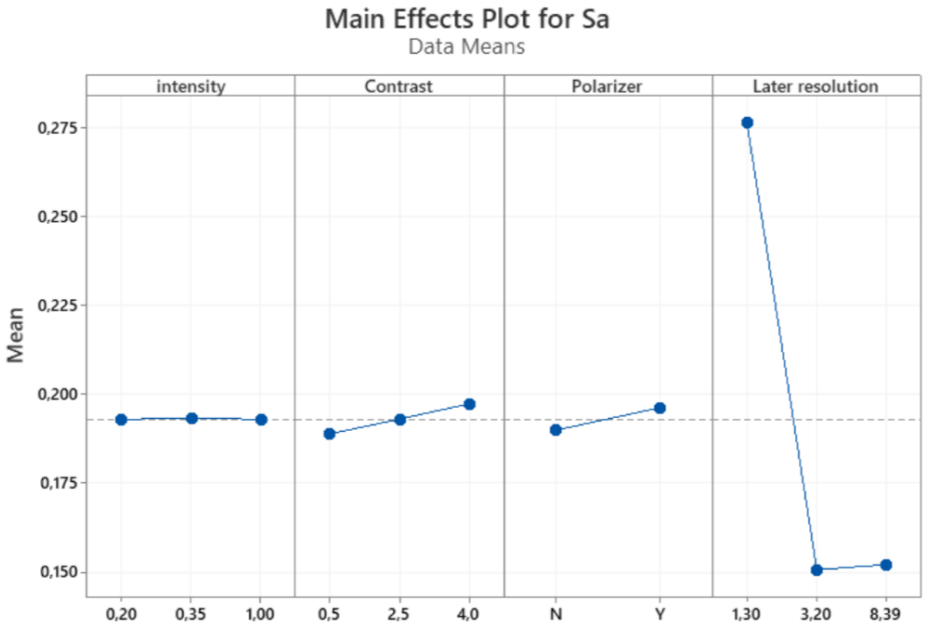

Figure 31: Results of analysis on Sa with 20x objective.

Model Summary

S	R-sq	R-sq(adj)	R-sq(pred)
0,0054118	99,73%	99,70%	99,66%

Analysis of Variance

Source	DF	Adj SS	Adj MS	F-Value	P-Value
Model	16	1,54259	0,096412	3291,86	0,000
Linear	5	1,44383	0,288767	9859,57	0,000
Contrast	1	0,00126	0,001259	42,97	0,000
intensity	1	0,00002	0,000023	0,78	0,378
Polarizer	1	0,00044	0,000438	14,95	0,000
Later resolution	2	1,44211	0,721056	24619,56	0,000
Square	2	0,00063	0,000315	10,77	0,000
Contrast*Contrast	1	0,00061	0,000611	20,86	0,000
intensity*intensity	1	0,00002	0,000020	0,67	0,413
2-Way Interaction	9	0,00284	0,000315	10,76	0,000
Contrast*intensity	1	0,00001	0,000008	0,27	0,603
Contrast*Polarizer	1	0,00002	0,000022	0,75	0,387
Contrast*Later resolution	2	0,00217	0,001086	37,09	0,000
intensity*Polarizer	1	0,00001	0,000006	0,22	0,639
intensity*Later resolution	2	0,00001	0,000003	0,10	0,909
Polarizer*Later resolution	2	0,00062	0,000310	10,60	0,000
Error	145	0,00425	0,000029		
Lack-of-Fit	37	0,00217	0,000059	3,04	0,000
Pure Error	108	0,00208	0,000019		
Total	161	1,54684			

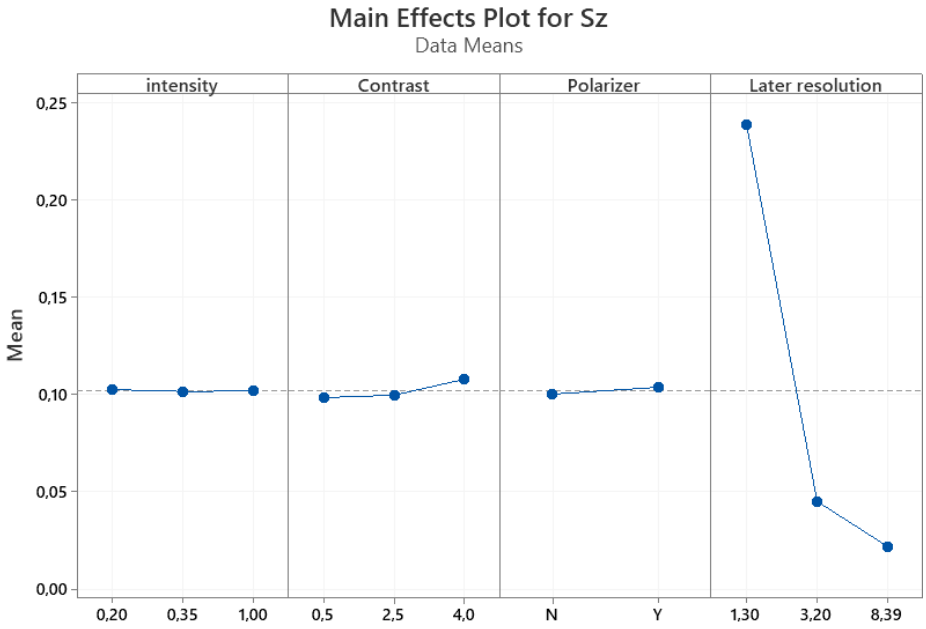

Figure 32: Results of analysis on Sz with 20x objective.

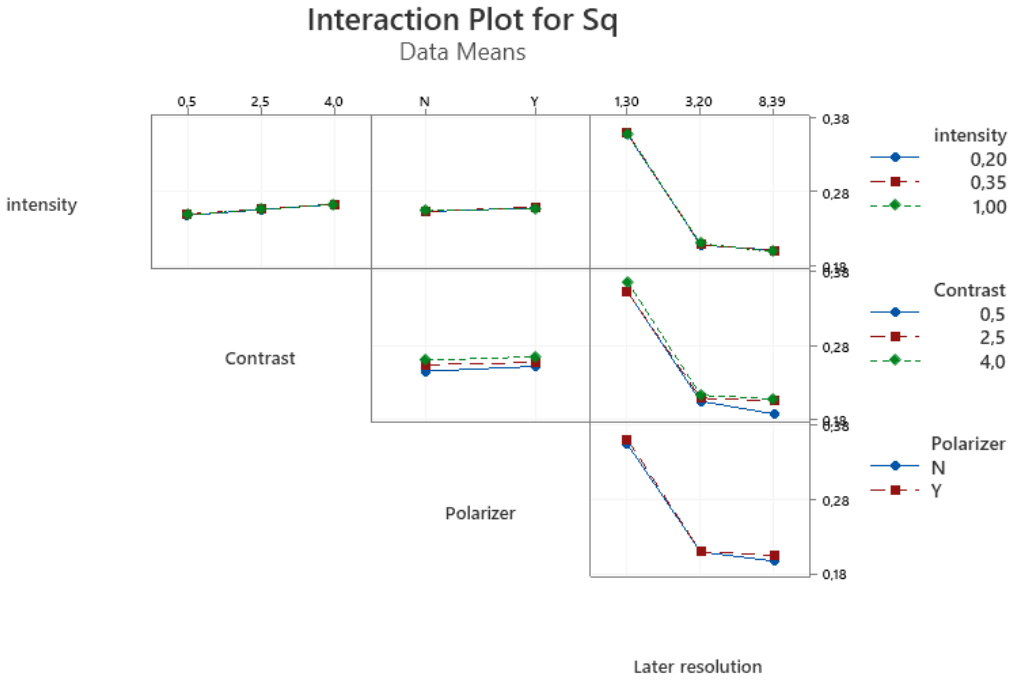

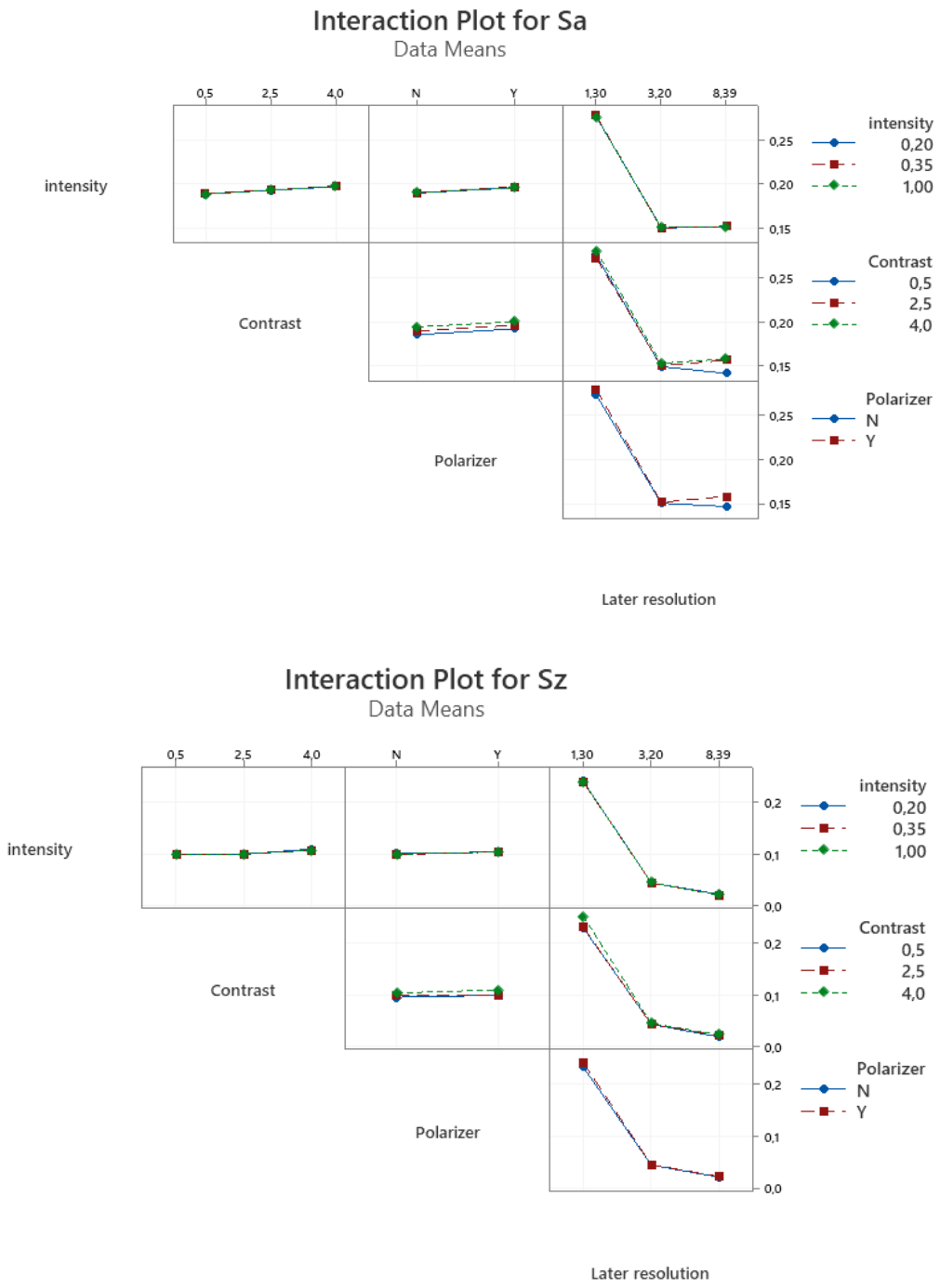

Figure 33: Interaction Plots graphs for Sq, Sa, Sz with 20x objective.

This model is even more precise with respect to the case of 10x objective, albeit with a more complex response surface as symbolized by the significant lack-of-fit, confirming that higher magnifications require a more accurate optimization of optical parameters to maintain measurement integrity.

In this case, the factor Contrast gains more relevance, even overcoming the role of lateral resolution.

8.2 Experimental Results with Difference Data

After having extracted the roughness parameters from each differentiated topography, the response surface design analysis is performed on Minitab, whose outputs are illustrated in Figures 34, 35, 36 for the 10x magnification objective, and Figure 37, 38, 39 for the 20x objective.

Model Summary

S	R-sq	R-sq(adj)	R-sq(pred)
0,0167612	99,47%	99,38%	99,27%

Analysis of Variance

Source	DF	Adj SS	Adj MS	F-Value	P-Value
Model	23	7,24050	0,314804	1120,54	0,000
Linear	6	0,00644	0,001074	3,82	0,001
Intensity	1	0,00283	0,002832	10,08	0,002
Contrast	1	0,00002	0,000023	0,08	0,775
Brightness / ms	1	0,00063	0,000625	2,23	0,138
Polarizer	1	0,00112	0,001119	3,98	0,048
Later resolution	2	0,00072	0,000360	1,28	0,281
Square	3	0,00444	0,001480	5,27	0,002
Intensity*Intensity	1	0,00066	0,000656	2,33	0,129
Contrast*Contrast	1	0,00175	0,001749	6,22	0,014
Brightness / ms*Brightness / ms	1	0,00063	0,000631	2,24	0,136
2-Way Interaction	14	0,09189	0,006564	23,36	0,000
Intensity*Contrast	1	0,00019	0,000185	0,66	0,418
Intensity*Brightness / ms	1	0,00283	0,002833	10,08	0,002
Intensity*Polarizer	1	0,00052	0,000520	1,85	0,176
Intensity*Later resolution	2	0,00589	0,002943	10,48	0,000
Contrast*Brightness / ms	1	0,00002	0,000025	0,09	0,766
Contrast*Polarizer	1	0,00292	0,002921	10,40	0,002
Contrast*Later resolution	2	0,00719	0,003593	12,79	0,000
Brightness / ms*Polarizer	1	0,00115	0,001154	4,11	0,045
Brightness / ms*Later resolution	2	0,00093	0,000466	1,66	0,194
Polarizer*Later resolution	2	0,05957	0,029787	106,03	0,000
Error	138	0,03877	0,000281		
Lack-of-Fit	30	0,03457	0,001152	29,65	0,000
Pure Error	108	0,00420	0,000039		
Total	161	7,27927			

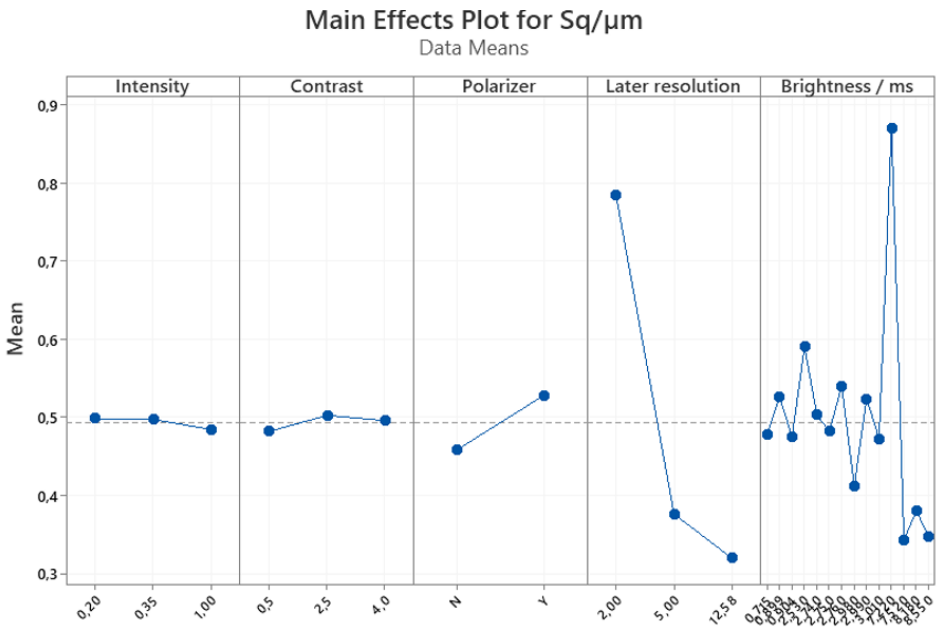

Figure 34: Results of differentiated topography analysis on Sq with 10x objective.

Model Summary

S	R-sq	R-sq(adj)	R-sq(pred)
0,0130762	99,48%	99,39%	99,29%

Analysis of Variance

Source	DF	Adj SS	Adj MS	F-Value	P-Value
Model	23	4,50950	0,196065	1146,67	0,000
Linear	6	0,00404	0,000674	3,94	0,001
Intensity	1	0,00139	0,001390	8,13	0,005
Contrast	1	0,00003	0,000032	0,19	0,665
Brightness / ms	1	0,00062	0,000616	3,60	0,060
Polarizer	1	0,00081	0,000811	4,74	0,031
Later resolution	2	0,00042	0,000212	1,24	0,292
Square	3	0,00344	0,001146	6,70	0,000
Intensity*Intensity	1	0,00010	0,000103	0,60	0,438
Contrast*Contrast	1	0,00127	0,001267	7,41	0,007
Brightness / ms*Brightness / ms	1	0,00062	0,000620	3,63	0,059
2-Way Interaction	14	0,05988	0,004277	25,01	0,000
Intensity*Contrast	1	0,00015	0,000153	0,90	0,345
Intensity*Brightness / ms	1	0,00139	0,001388	8,12	0,005
Intensity*Polarizer	1	0,00098	0,000978	5,72	0,018
Intensity*Later resolution	2	0,00363	0,001815	10,61	0,000
Contrast*Brightness / ms	1	0,00003	0,000034	0,20	0,657
Contrast*Polarizer	1	0,00137	0,001370	8,01	0,005
Contrast*Later resolution	2	0,00443	0,002213	12,94	0,000
Brightness / ms*Polarizer	1	0,00084	0,000835	4,88	0,029
Brightness / ms*Later resolution	2	0,00054	0,000268	1,57	0,213
Polarizer*Later resolution	2	0,03914	0,019570	114,45	0,000
Error	138	0,02360	0,000171		
Lack-of-Fit	30	0,02086	0,000695	27,40	0,000
Pure Error	108	0,00274	0,000025		
Total	161	4,53310			

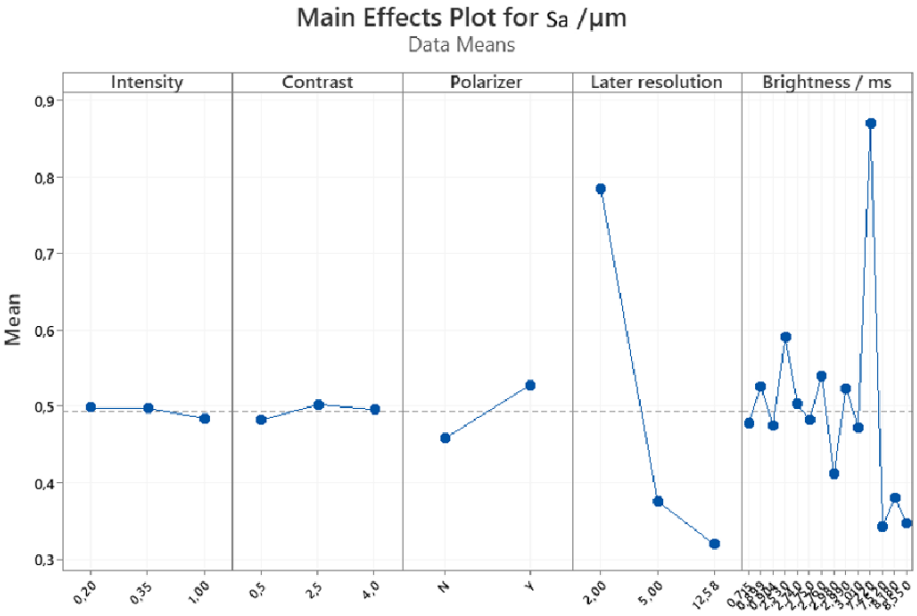

Figure 35: Results of differentiated topography analysis on Sa with 10x objective.

Model Summary

S	R-sq	R-sq(adj)	R-sq(pred)
0,367613	97,31%	96,86%	96,25%

Analysis of Variance

Source	DF	Adj SS	Adj MS	F-Value	P-Value
Model	23	674,605	29,3307	217,04	0,000
Linear	6	0,354	0,0590	0,44	0,853
Intensity	1	0,053	0,0532	0,39	0,531
Contrast	1	0,070	0,0702	0,52	0,472
Brightness / ms	1	0,163	0,1628	1,20	0,274
Polarizer	1	0,163	0,1630	1,21	0,274
Later resolution	2	0,154	0,0770	0,57	0,567
Square	3	0,235	0,0785	0,58	0,629
Intensity*Intensity	1	0,001	0,0008	0,01	0,939
Contrast*Contrast	1	0,002	0,0020	0,02	0,903
Brightness / ms*Brightness / ms	1	0,163	0,1626	1,20	0,275
2-Way Interaction	14	14,979	1,0700	7,92	0,000
Intensity*Contrast	1	0,335	0,3347	2,48	0,118
Intensity*Brightness / ms	1	0,053	0,0527	0,39	0,533
Intensity*Polarizer	1	1,453	1,4528	10,75	0,001
Intensity*Later resolution	2	2,218	1,1089	8,21	0,000
Contrast*Brightness / ms	1	0,070	0,0697	0,52	0,474
Contrast*Polarizer	1	0,282	0,2820	2,09	0,151
Contrast*Later resolution	2	2,536	1,2680	9,38	0,000
Brightness / ms*Polarizer	1	0,160	0,1599	1,18	0,279
Brightness / ms*Later resolution	2	0,195	0,0975	0,72	0,488
Polarizer*Later resolution	2	5,090	2,5449	18,83	0,000
Error	138	18,649	0,1351		
Lack-of-Fit	30	11,311	0,3770	5,55	0,000
Pure Error	108	7,338	0,0679		
Total	161	693,255			

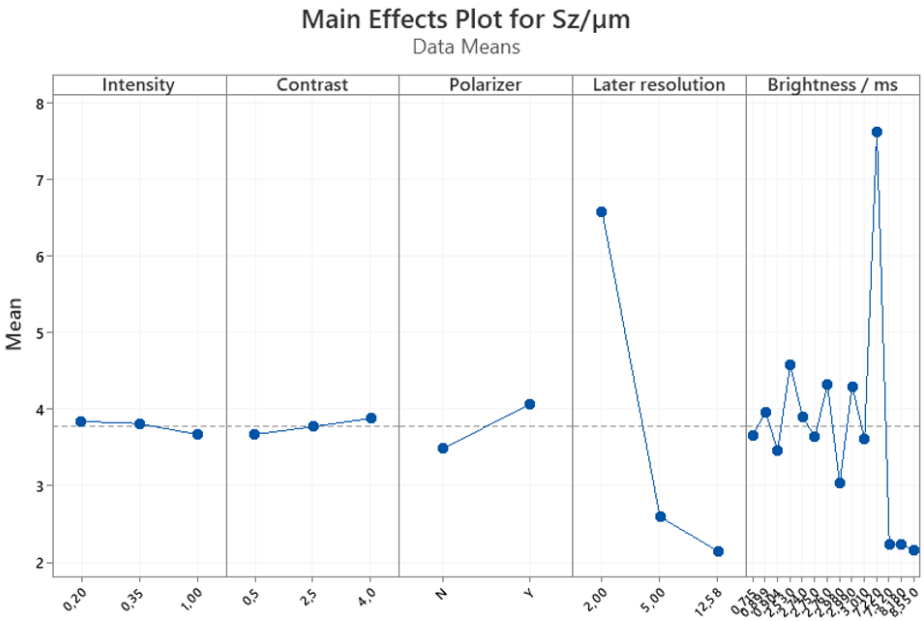

Figure 36: Results of differentiated topography analysis on Sz with 10x objective.

The results obtained show the overall reliability of the models, as all three models are characterized by high adjusted R-squared values, with the value gradually reducing for the Sz model, indicating its sensitivity to noises.

For Sq and Sa, a relevant role is covered by Intensity and Polarizer as independent factors. Although Lateral Resolution does not have a considerable impact as an independent linear factor, its significance arises when evaluating its interaction with other factors, such as Polarizer*Lateral resolution, Contrast*Lateral resolution, and Intensity*Lateral resolution. These interactions are indeed particularly impactful, suggesting that the impact of lateral resolution on FV accuracy is strictly linked to the lighting and filtering conditions.

On the other hand, no individual linear factors are registered to be significant for Sz. However, the interactions explained above are relevant even in this case.

As illustrated below, the results for Sq and Sa at 20x magnification objective exhibit a significant improvement in model accuracy and measurement precision compared to the 10x objective case.

Model Summary

S	R-sq	R-sq(adj)	R-sq(pred)
0.0030738	99.71%	99.66%	99.61%

Analysis of Variance

Source	DF	Adj SS	Adj MS	F-Value	P-Value
Model	23	0.451418	0.019627	2077.27	0.000
Linear	6	0.000391	0.000065	6.90	0.000
Intensity	1	0.000119	0.000119	12.55	0.001
Contrast	1	0.000003	0.000003	0.28	0.595
Brightness / ms	1	0.000002	0.000002	0.21	0.649
Polarizer	1	0.000003	0.000003	0.32	0.571
Later resolution	2	0.000236	0.000118	12.48	0.000
Square	3	0.000139	0.000046	4.89	0.003
Intensity*Intensity	1	0.000127	0.000127	13.42	0.000
Contrast*Contrast	1	0.000006	0.000006	0.60	0.440
Brightness / ms*Brightness / ms	1	0.000002	0.000002	0.21	0.649
2-Way Interaction	14	0.002881	0.000206	21.78	0.000
Intensity*Contrast	1	0.000208	0.000208	22.04	0.000
Intensity*Brightness / ms	1	0.000116	0.000116	12.32	0.001
Intensity*Polarizer	1	0.000222	0.000222	23.44	0.000
Intensity*Later resolution	2	0.000009	0.000005	0.48	0.619
Contrast*Brightness / ms	1	0.000003	0.000003	0.28	0.595
Contrast*Polarizer	1	0.000003	0.000003	0.31	0.580
Contrast*Later resolution	2	0.000169	0.000084	8.93	0.000
Brightness / ms*Polarizer	1	0.000003	0.000003	0.32	0.571
Brightness / ms*Later resolution	2	0.000292	0.000146	15.45	0.000
Polarizer*Later resolution	2	0.000541	0.000271	28.65	0.000
Error	138	0.001304	0.000009		
Lack-of-Fit	30	0.001134	0.000038	23.99	0.000
Pure Error	108	0.000170	0.000002		
Total	161	0.452722			

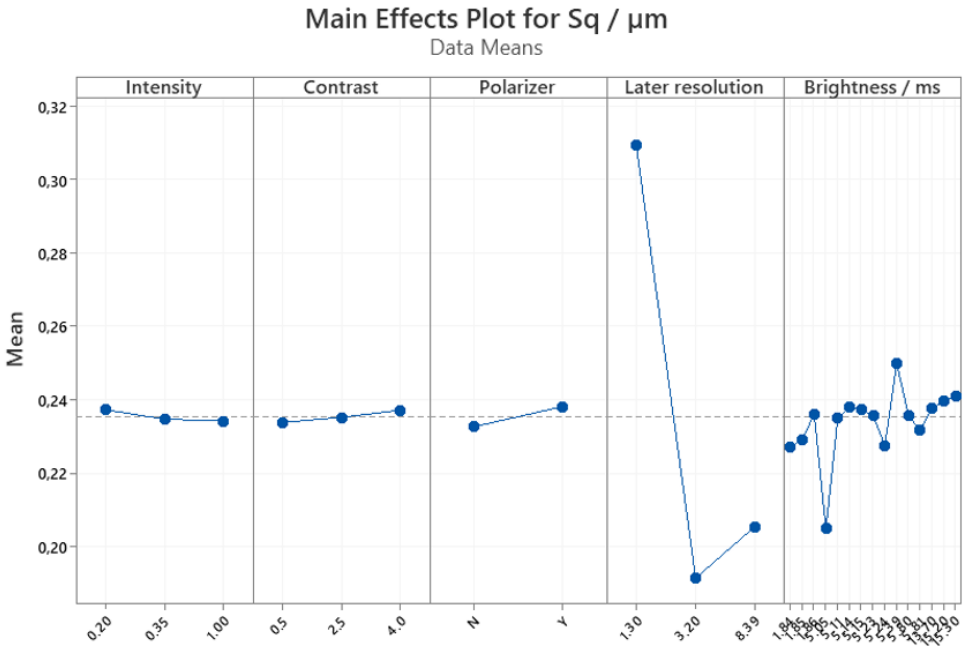

Figure 37: Results of differentiated topography analysis on Sq with 20x objective.

Model Summary

S	R-sq	R-sq(adj)	R-sq(pred)
0.0023653	99.73%	99.68%	99.63%

Analysis of Variance

Source	DF	Adj SS	Adj MS	F-Value	P-Value
Model	23	0.283980	0.012347	2206.99	0.000
Linear	6	0.000250	0.000042	7.44	0.000
Intensity	1	0.000068	0.000068	12.17	0.001
Contrast	1	0.000003	0.000003	0.53	0.469
Brightness / ms	1	0.000003	0.000003	0.52	0.471
Polarizer	1	0.000004	0.000004	0.63	0.427
Later resolution	2	0.000167	0.000083	14.92	0.000
Square	3	0.000082	0.000027	4.90	0.003
Intensity*Intensity	1	0.000079	0.000079	14.10	0.000
Contrast*Contrast	1	0.000005	0.000005	0.85	0.358
Brightness / ms*Brightness / ms	1	0.000003	0.000003	0.52	0.472
2-Way Interaction	14	0.002053	0.000147	26.22	0.000
Intensity*Contrast	1	0.000104	0.000104	18.59	0.000
Intensity*Brightness / ms	1	0.000067	0.000067	11.94	0.001
Intensity*Polarizer	1	0.000131	0.000131	23.40	0.000
Intensity*Later resolution	2	0.000006	0.000003	0.55	0.577
Contrast*Brightness / ms	1	0.000003	0.000003	0.52	0.470
Contrast*Polarizer	1	0.000003	0.000003	0.51	0.475
Contrast*Later resolution	2	0.000121	0.000061	10.84	0.000
Brightness / ms*Polarizer	1	0.000004	0.000004	0.63	0.428
Brightness / ms*Later resolution	2	0.000202	0.000101	18.07	0.000
Polarizer*Later resolution	2	0.000334	0.000167	29.89	0.000
Error	138	0.000772	0.000006		
Lack-of-Fit	30	0.000653	0.000022	19.69	0.000
Pure Error	108	0.000119	0.000001		
Total	161	0.284752			

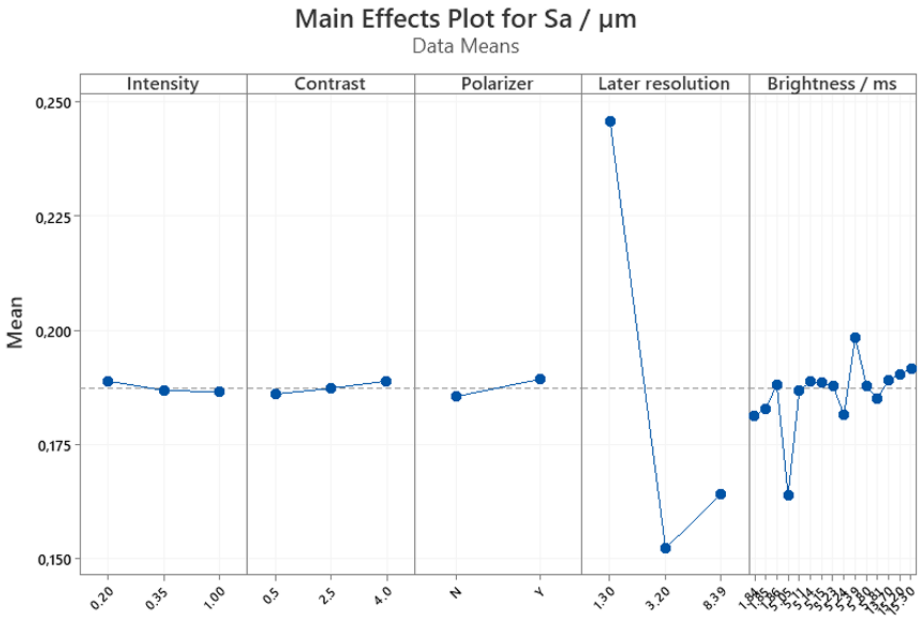

Figure 38: Results of differentiated topography analysis on Sa with 20x objective.

Model Summary

S	R-sq	R-sq(adj)	R-sq(pred)
0.0652619	98.68%	98.46%	98.20%

Analysis of Variance

Source	DF	Adj SS	Adj MS	F-Value	P-Value
Model	23	44.0055	1.91328	449.22	0.000
Linear	6	0.0390	0.00650	1.53	0.174
Intensity	1	0.0006	0.00060	0.14	0.708
Contrast	1	0.0002	0.00016	0.04	0.846
Brightness / ms	1	0.0000	0.00001	0.00	0.961
Polarizer	1	0.0000	0.00002	0.00	0.945
Later resolution	2	0.0328	0.01639	3.85	0.024
Square	3	0.0101	0.00335	0.79	0.503
Intensity*Intensity	1	0.0054	0.00543	1.27	0.261
Contrast*Contrast	1	0.0005	0.00046	0.11	0.742
Brightness / ms*Brightness / ms	1	0.0000	0.00001	0.00	0.962
2-Way Interaction	14	0.6143	0.04388	10.30	0.000
Intensity*Contrast	1	0.0133	0.01331	3.13	0.079
Intensity*Brightness / ms	1	0.0007	0.00069	0.16	0.688
Intensity*Polarizer	1	0.0000	0.00001	0.00	0.960
Intensity*Later resolution	2	0.3329	0.16647	39.08	0.000
Contrast*Brightness / ms	1	0.0002	0.00016	0.04	0.845
Contrast*Polarizer	1	0.0003	0.00033	0.08	0.782
Contrast*Later resolution	2	0.0098	0.00492	1.15	0.318
Brightness / ms*Polarizer	1	0.0000	0.00002	0.00	0.944
Brightness / ms*Later resolution	2	0.0412	0.02058	4.83	0.009
Polarizer*Later resolution	2	0.1085	0.05426	12.74	0.000
Error	138	0.5878	0.00426		
Lack-of-Fit	30	0.3913	0.01304	7.17	0.000
Pure Error	108	0.1965	0.00182		
Total	161	44.5933			

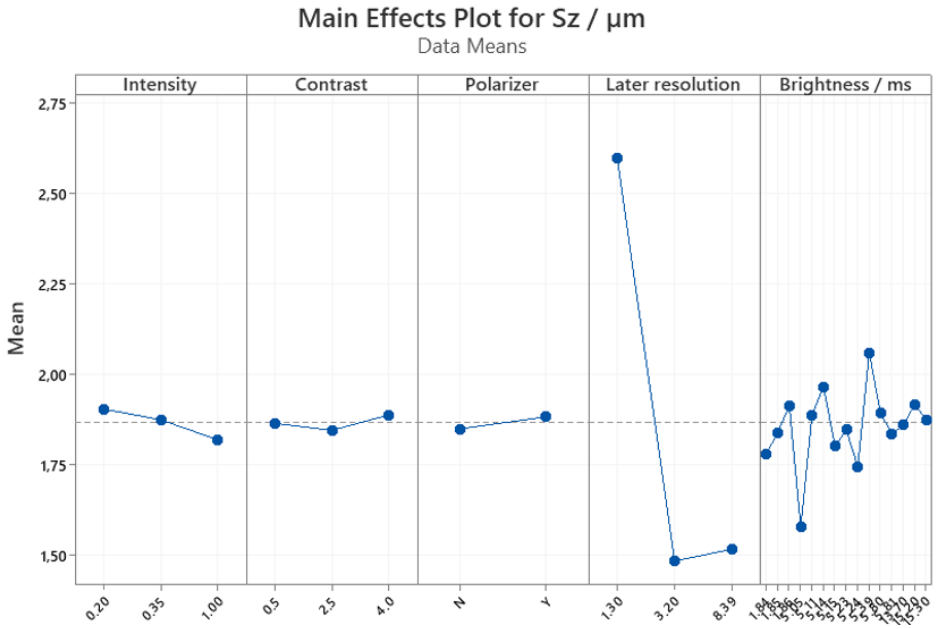

Figure 39: Results of differentiated topography analysis on Sz with 20x objective.

Different from the 10x analysis, Later Resolution is here a highly impactful linear factor for both Sq and Sa, indicating that at higher magnification, the spatial sampling frequency has a more direct and independent impact on the measurement error.

This analysis also reveals considerable effects from two-way interaction effects, namely those between Intensity and Contrast, Brightness, Polarizer, and those between Lateral Resolution and Contrast, Polarizer.

For Sz instead, Lateral Resolution remains the sole independent linear factor to have a significant importance, as well as its interaction with Intensity, Polarizer, and Brightness.

8.3 Experimental Results with Cropped Area Data

Once the values of Sq, Sa, and Sz parameters have been extracted from the measurement results performed on the cropped area, the same type of response surface design analysis has been replicated.

Figures 40, 41, and 42 below show the output of the analysis carried out for the 10x objective on Sq, Sa, Sz respectively.

Model Summary

S	R-sq	R-sq(adj)	R-sq(pred)
0,0176401	99,45%	99,36%	99,25%

Analysis of Variance

Source	DF	Adj SS	Adj MS	F-Value	P-Value
Model	23	7,79030	0,338709	1088,49	0,000
Linear	6	0,00781	0,001301	4,18	0,001
Contrast	1	0,00013	0,000128	0,41	0,522
Intensity	1	0,00271	0,002708	8,70	0,004
Brightness / ms	1	0,00111	0,001113	3,58	0,061
Polarizer	1	0,00108	0,001081	3,47	0,064
Later resolution	2	0,00098	0,000489	1,57	0,211
Square	3	0,00630	0,002099	6,75	0,000
Contrast*Contrast	1	0,00201	0,002012	6,47	0,012
Intensity*Intensity	1	0,00142	0,001423	4,57	0,034
Brightness / ms*Brightness / ms	1	0,00112	0,001121	3,60	0,060
2-Way Interaction	14	0,09097	0,006498	20,88	0,000
Contrast*Intensity	1	0,00075	0,000747	2,40	0,124
Contrast*Brightness / ms	1	0,00013	0,000133	0,43	0,514
Contrast*Polarizer	1	0,00378	0,003785	12,16	0,001
Contrast*Later resolution	2	0,00896	0,004480	14,40	0,000
Intensity*Brightness / ms	1	0,00271	0,002713	8,72	0,004
Intensity*Polarizer	1	0,00017	0,000167	0,54	0,465
Intensity*Later resolution	2	0,00603	0,003017	9,70	0,000
Brightness / ms*Polarizer	1	0,00112	0,001118	3,59	0,060
Brightness / ms*Later resolution	2	0,00125	0,000626	2,01	0,138
Polarizer*Later resolution	2	0,05768	0,028839	92,68	0,000
Error	138	0,04294	0,000311		
Lack-of-Fit	30	0,03876	0,001292	33,40	0,000
Pure Error	108	0,00418	0,000039		
Total	161	7,83324			

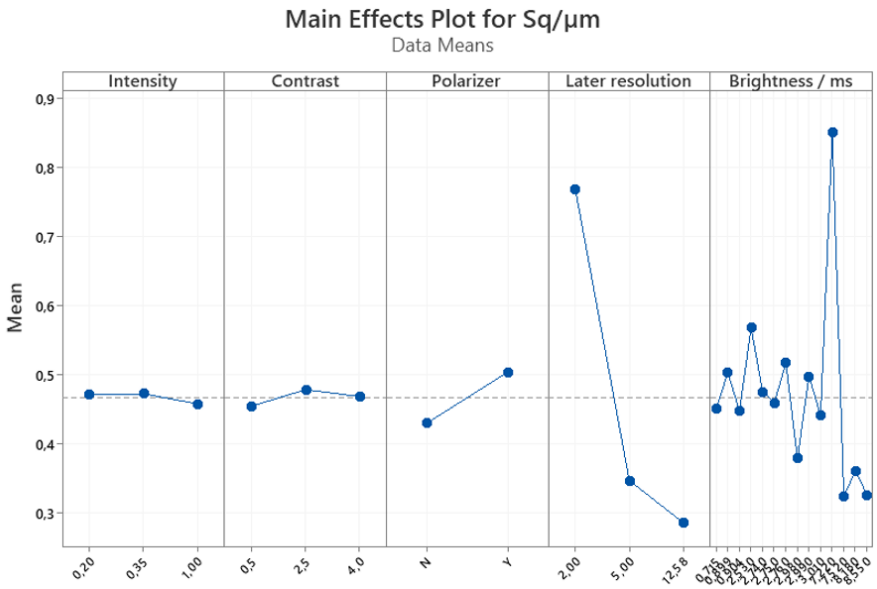

Figure 40: Results of cropped area analysis on Sq with 10x objective.

Model Summary

S	R-sq	R-sq(adj)	R-sq(pred)
0,0134727	99,49%	99,40%	99,30%

Analysis of Variance

Source	DF	Adj SS	Adj MS	F-Value	P-Value
Model	23	4,84948	0,210847	1161,61	0,000
Linear	6	0,00491	0,000819	4,51	0,000
Contrast	1	0,00011	0,000110	0,61	0,437
Intensity	1	0,00152	0,001521	8,38	0,004
Brightness / ms	1	0,00085	0,000854	4,71	0,032
Polarizer	1	0,00071	0,000713	3,93	0,050
Later resolution	2	0,00052	0,000260	1,43	0,243
Square	3	0,00417	0,001391	7,67	0,000
Contrast*Contrast	1	0,00135	0,001347	7,42	0,007
Intensity*Intensity	1	0,00051	0,000511	2,81	0,096
Brightness / ms*Brightness / ms	1	0,00086	0,000860	4,74	0,031
2-Way Interaction	14	0,05712	0,004080	22,48	0,000
Contrast*Intensity	1	0,00068	0,000685	3,77	0,054
Contrast*Brightness / ms	1	0,00011	0,000114	0,63	0,430
Contrast*Polarizer	1	0,00194	0,001940	10,69	0,001
Contrast*Later resolution	2	0,00507	0,002535	13,97	0,000
Intensity*Brightness / ms	1	0,00152	0,001522	8,38	0,004
Intensity*Polarizer	1	0,00032	0,000321	1,77	0,186
Intensity*Later resolution	2	0,00345	0,001723	9,49	0,000
Brightness / ms*Polarizer	1	0,00074	0,000737	4,06	0,046
Brightness / ms*Later resolution	2	0,00066	0,000330	1,82	0,166
Polarizer*Later resolution	2	0,03668	0,018339	101,03	0,000
Error	138	0,02505	0,000182		
Lack-of-Fit	30	0,02222	0,000741	28,26	0,000
Pure Error	108	0,00283	0,000026		
Total	161	4,87453			

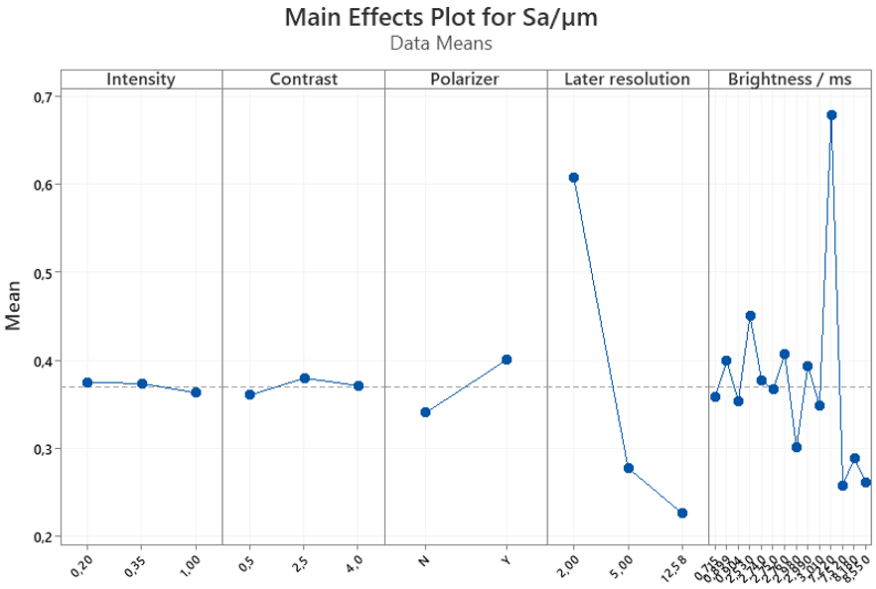

Figure 41: Results of cropped area analysis on Sa with 10x objective.

Model Summary

S	R-sq	R-sq(adj)	R-sq(pred)
0,365439	97,65%	97,26%	96,76%

Analysis of Variance

Source	DF	Adj SS	Adj MS	F-Value	P-Value
Model	23	766,217	33,3138	249,46	0,000
Linear	6	0,393	0,0655	0,49	0,814
Contrast	1	0,000	0,0001	0,00	0,984
Intensity	1	0,066	0,0659	0,49	0,484
Brightness / ms	1	0,003	0,0032	0,02	0,877
Polarizer	1	0,052	0,0525	0,39	0,532
Later resolution	2	0,241	0,1207	0,90	0,407
Square	3	0,141	0,0469	0,35	0,788
Contrast*Contrast	1	0,059	0,0594	0,44	0,506
Intensity*Intensity	1	0,067	0,0671	0,50	0,480
Brightness / ms*Brightness / ms	1	0,003	0,0032	0,02	0,877
2-Way Interaction	14	14,511	1,0365	7,76	0,000
Contrast*Intensity	1	0,213	0,2133	1,60	0,208
Contrast*Brightness / ms	1	0,000	0,0001	0,00	0,981
Contrast*Polarizer	1	0,556	0,5558	4,16	0,043
Contrast*Later resolution	2	2,465	1,2325	9,23	0,000
Intensity*Brightness / ms	1	0,065	0,0650	0,49	0,486
Intensity*Polarizer	1	0,942	0,9421	7,05	0,009
Intensity*Later resolution	2	2,135	1,0677	7,99	0,001
Brightness / ms*Polarizer	1	0,051	0,0506	0,38	0,539
Brightness / ms*Later resolution	2	0,280	0,1401	1,05	0,353
Polarizer*Later resolution	2	5,925	2,9624	22,18	0,000
Error	138	18,429	0,1335		
Lack-of-Fit	30	10,890	0,3630	5,20	0,000
Pure Error	108	7,539	0,0698		
Total	161	784,646			

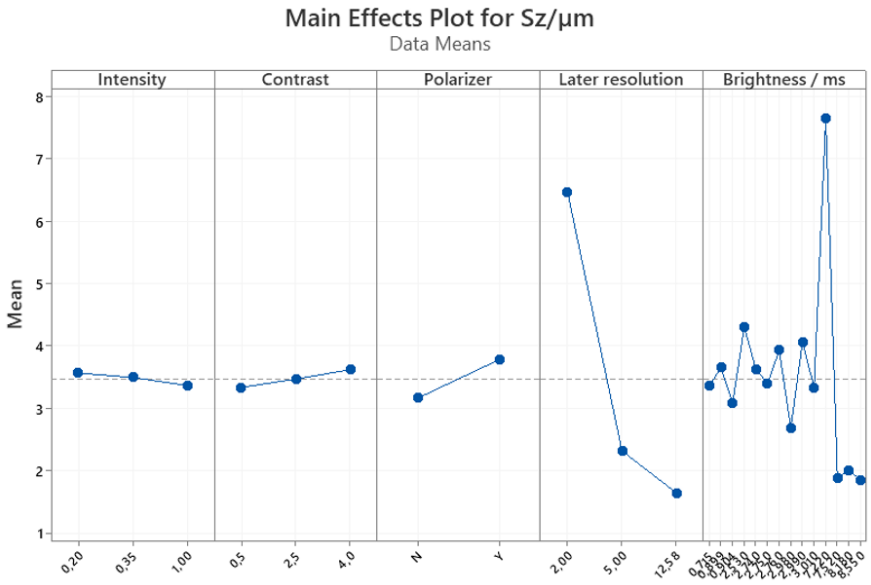

Figure 42: Results of cropped area analysis on Sz with 10x objective.

The results reported above indicate that also in this case, Lateral Resolution is the most influencing factor, meaning that a poorer value of Lateral Resolution generates greater impossibility in capturing surface's micro-geometries, leading to higher differences between the measured surface and the reference one.

Also, Polarizer and Contrast play a crucial role in the experiment, the first one especially on Sz and the second one on Sq and Sa.

Polarizer is capable of reducing the quantity of spikes and outliers, guaranteeing a better match between Z_{ref} and Z_m.

High values of Contrast instead, ensure a finer identification of local topographic features.

Coherently with previous raw data analyses, Intensity shows negligible statistical importance, due to its P-values greater than 0.05 threshold.

The exact same analysis can be performed for the case of measures carried out with 20x objective magnification.

The outputs, as shown in Figures 43, 44, 45, highlight the primary importance of Contrast with respect to the other factors, despite Lateral Resolution and Polarizer still keeping relevant importance.

Model Summary

S	R-sq	R-sq(adj)	R-sq(pred)
0.0027451	99.87%	99.85%	99.83%

Analysis of Variance

Source	DF	Adj SS	Adj MS	F-Value	P-Value
Model	23	0.813398	0.035365	4693.19	0.000
Linear	6	0.000449	0.000075	9.94	0.000
Intensity	1	0.000004	0.000004	0.58	0.446
Contrast	1	0.000002	0.000002	0.26	0.612
Brightness / ms	1	0.000006	0.000006	0.75	0.389
Polarizer	1	0.000003	0.000003	0.36	0.548
Later resolution	2	0.000366	0.000183	24.29	0.000
Square	3	0.000103	0.000034	4.54	0.005
Intensity*Intensity	1	0.000065	0.000065	8.57	0.004
Contrast*Contrast	1	0.000000	0.000000	0.00	0.954
Brightness / ms*Brightness / ms	1	0.000006	0.000006	0.75	0.389
2-Way Interaction	14	0.005035	0.000360	47.73	0.000
Intensity*Contrast	1	0.000005	0.000005	0.65	0.421
Intensity*Brightness / ms	1	0.000005	0.000005	0.66	0.419
Intensity*Polarizer	1	0.000022	0.000022	2.93	0.089
Intensity*Later resolution	2	0.000139	0.000070	9.22	0.000
Contrast*Brightness / ms	1	0.000002	0.000002	0.26	0.611
Contrast*Polarizer	1	0.000001	0.000001	0.15	0.701
Contrast*Later resolution	2	0.000163	0.000082	10.84	0.000
Brightness / ms*Polarizer	1	0.000003	0.000003	0.36	0.548
Brightness / ms*Later resolution	2	0.000477	0.000238	31.62	0.000
Polarizer*Later resolution	2	0.000342	0.000171	22.69	0.000
Error	138	0.001040	0.000008		
Lack-of-Fit	30	0.000727	0.000024	8.38	0.000
Pure Error	108	0.000312	0.000003		
Total	161	0.814438			

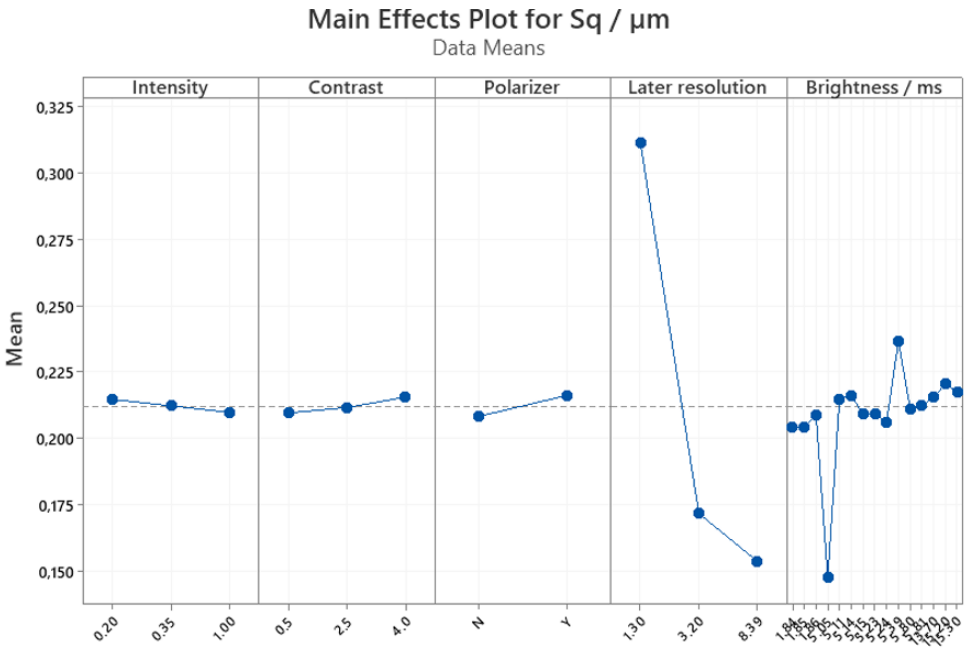

Figure 43: Results of cropped area analysis on Sq with 20x objective.

Model Summary

S	R-sq	R-sq(adj)	R-sq(pred)
0.0023278	99.85%	99.83%	99.80%

Analysis of Variance

Source	DF	Adj SS	Adj MS	F-Value	P-Value
Model	23	0.513937	0.022345	4123.58	0.000
Linear	6	0.000401	0.000067	12.33	0.000
Intensity	1	0.000005	0.000005	0.84	0.361
Contrast	1	0.000001	0.000001	0.15	0.700
Brightness / ms	1	0.000003	0.000003	0.63	0.431
Polarizer	1	0.000001	0.000001	0.25	0.620
Later resolution	2	0.000328	0.000164	30.23	0.000
Square	3	0.000084	0.000028	5.18	0.002
Intensity*Intensity	1	0.000050	0.000050	9.15	0.003
Contrast*Contrast	1	0.000000	0.000000	0.01	0.916
Brightness / ms*Brightness / ms	1	0.000003	0.000003	0.63	0.430
2-Way Interaction	14	0.003583	0.000256	47.23	0.000
Intensity*Contrast	1	0.000006	0.000006	1.03	0.313
Intensity*Brightness / ms	1	0.000005	0.000005	0.93	0.337
Intensity*Polarizer	1	0.000018	0.000018	3.41	0.067
Intensity*Later resolution	2	0.000043	0.000021	3.95	0.021
Contrast*Brightness / ms	1	0.000001	0.000001	0.15	0.699
Contrast*Polarizer	1	0.000000	0.000000	0.06	0.808
Contrast*Later resolution	2	0.000093	0.000046	8.55	0.000
Brightness / ms*Polarizer	1	0.000001	0.000001	0.25	0.620
Brightness / ms*Later resolution	2	0.000404	0.000202	37.30	0.000
Polarizer*Later resolution	2	0.000225	0.000112	20.73	0.000
Error	138	0.000748	0.000005		
Lack-of-Fit	30	0.000531	0.000018	8.84	0.000
Pure Error	108	0.000216	0.000002		
Total	161	0.514685			

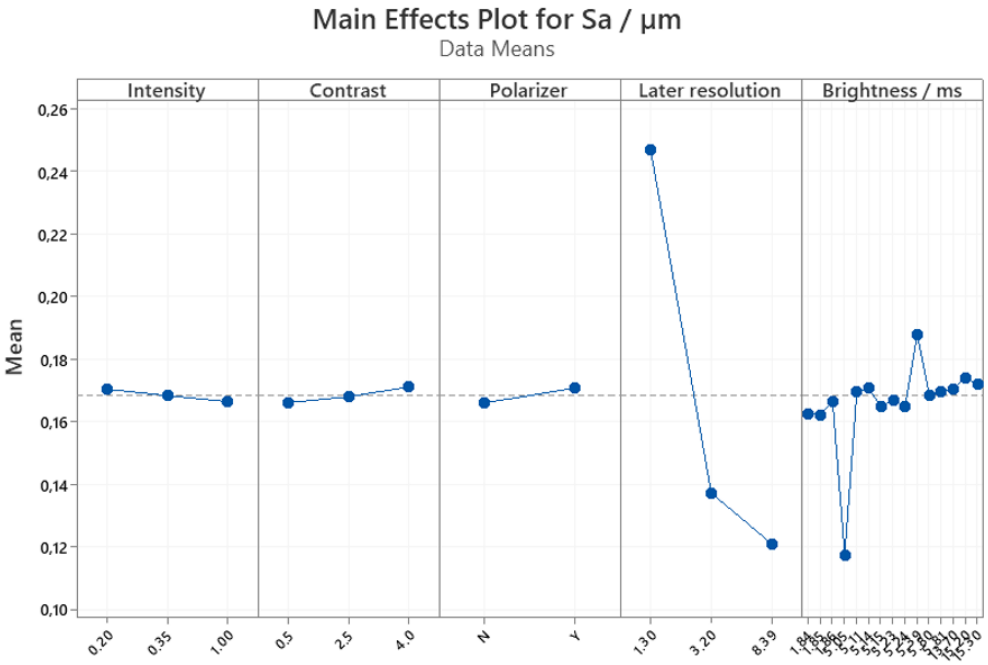

Figure 44: Results of cropped area analysis on Sa with 20x objective.

Model Summary

S	R-sq	R-sq(adj)	R-sq(pred)
0.0778731	99.01%	98.85%	98.62%

Analysis of Variance

Source	DF	Adj SS	Adj MS	F-Value	P-Value
Model	23	83.8382	3.64514	601.09	0.000
Linear	6	0.0598	0.00996	1.64	0.140
Intensity	1	0.0055	0.00549	0.90	0.343
Contrast	1	0.0000	0.00001	0.00	0.971
Brightness / ms	1	0.0001	0.00005	0.01	0.926
Polarizer	1	0.0000	0.00001	0.00	0.968
Later resolution	2	0.0486	0.02432	4.01	0.020
Square	3	0.0042	0.00140	0.23	0.874
Intensity*Intensity	1	0.0026	0.00263	0.43	0.511
Contrast*Contrast	1	0.0000	0.00003	0.01	0.941
Brightness / ms*Brightness / ms	1	0.0001	0.00005	0.01	0.926
2-Way Interaction	14	0.7729	0.05521	9.10	0.000
Intensity*Contrast	1	0.0026	0.00265	0.44	0.510
Intensity*Brightness / ms	1	0.0058	0.00576	0.95	0.332
Intensity*Polarizer	1	0.0584	0.05842	9.63	0.002
Intensity*Later resolution	2	0.2067	0.10333	17.04	0.000
Contrast*Brightness / ms	1	0.0000	0.00001	0.00	0.971
Contrast*Polarizer	1	0.0000	0.00003	0.01	0.942
Contrast*Later resolution	2	0.0237	0.01187	1.96	0.145
Brightness / ms*Polarizer	1	0.0000	0.00001	0.00	0.968
Brightness / ms*Later resolution	2	0.0546	0.02731	4.50	0.013
Polarizer*Later resolution	2	0.0393	0.01963	3.24	0.042
Error	138	0.8369	0.00606		
Lack-of-Fit	30	0.6476	0.02159	12.32	0.000
Pure Error	108	0.1892	0.00175		
Total	161	84.6751			

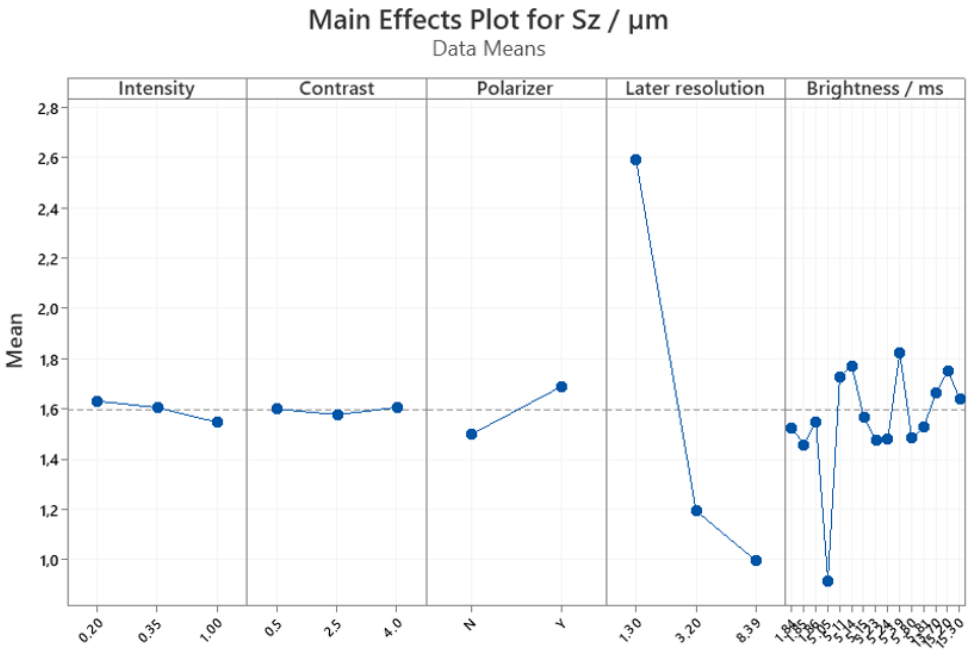

Figure 45: Results of cropped area analysis on Sz with 20x objective.

The results of the new analysis obtained after inserting a block on Lateral Resolution, are illustrated below, in Figures 46, 47, 48 for the case of 10x magnification objective, and Figures 49, 50, 51 for the 20x objective.

Model Summary

S	R-sq	R-sq(adj)	R-sq(pred)
0,0283572	98,50%	98,35%	98,17%

Analysis of Variance

Source	DF	Adj SS	Adj MS	F-Value	P-Value
Model	15	7,71584	0,51439	639,68	0,000
Blocks	2	6,66793	3,33396	4146,03	0,000
Linear	4	0,00682	0,00171	2,12	0,081
Contrast	1	0,00206	0,00206	2,56	0,112
Brightness / ms	1	0,00000	0,00000	0,00	0,996
Intensity	1	0,00295	0,00295	3,67	0,057
Polarizer	1	0,00141	0,00141	1,76	0,187
Square	3	0,01168	0,00389	4,84	0,003
Contrast*Contrast	1	0,00970	0,00970	12,06	0,001
Brightness / ms*Brightness / ms	1	0,00000	0,00000	0,00	0,994
Intensity*Intensity	1	0,00166	0,00166	2,06	0,153
2-Way Interaction	6	0,01651	0,00275	3,42	0,003
Contrast*Brightness / ms	1	0,00204	0,00204	2,54	0,113
Contrast*Intensity	1	0,00077	0,00077	0,95	0,331
Contrast*Polarizer	1	0,00260	0,00260	3,23	0,074
Brightness / ms*Intensity	1	0,00295	0,00295	3,67	0,057
Brightness / ms*Polarizer	1	0,00145	0,00145	1,80	0,181
Intensity*Polarizer	1	0,00002	0,00002	0,02	0,876
Error	146	0,11740	0,00080		
Lack-of-Fit	38	0,11322	0,00298	77,01	0,000
Pure Error	108	0,00418	0,00004		
Total	161	7,83324			

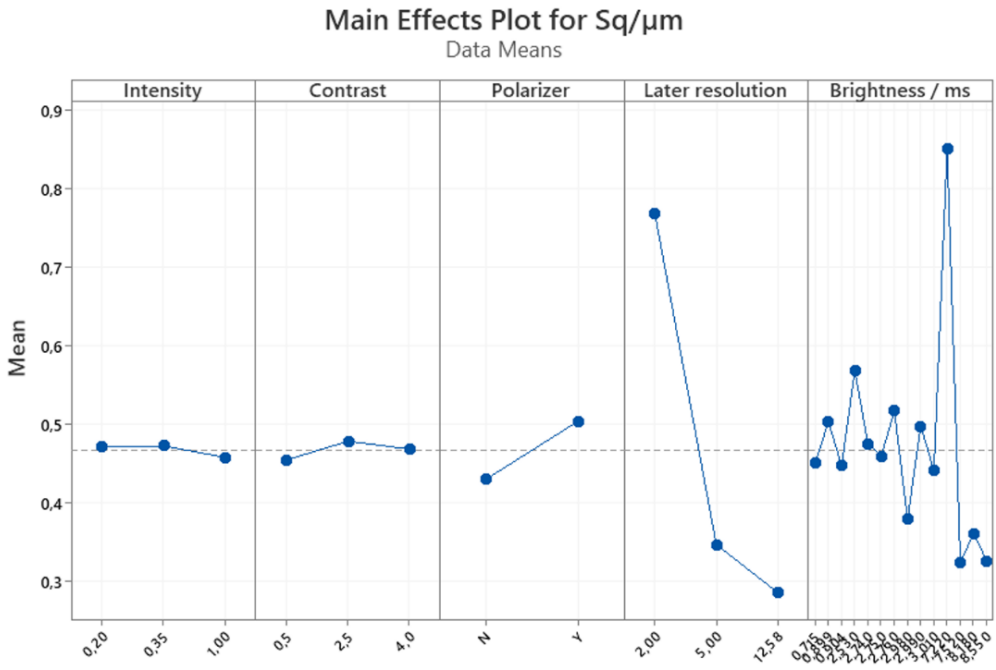

Figure 46: Results of cropped area analysis on Sq with 10x objective and blocks.

Model Summary

S	R-sq	R-sq(adj)	R-sq(pred)
0,0221577	98,53%	98,38%	98,21%

Analysis of Variance

Source	DF	Adj SS	Adj MS	F-Value	P-Value
Model	15	4,80285	0,32019	652,17	0,000
Blocks	2	4,14041	2,07020	4216,61	0,000
Linear	4	0,00444	0,00111	2,26	0,065
Contrast	1	0,00111	0,00111	2,26	0,135
Brightness / ms	1	0,00002	0,00002	0,05	0,825
Intensity	1	0,00169	0,00169	3,43	0,066
Polarizer	1	0,00087	0,00087	1,77	0,185
Square	3	0,00723	0,00241	4,91	0,003
Contrast*Contrast	1	0,00601	0,00601	12,24	0,001
Brightness / ms*Brightness / ms	1	0,00002	0,00002	0,05	0,824
Intensity*Intensity	1	0,00058	0,00058	1,19	0,277
2-Way Interaction	6	0,01049	0,00175	3,56	0,003
Contrast*Brightness / ms	1	0,00110	0,00110	2,23	0,137
Contrast*Intensity	1	0,00068	0,00068	1,38	0,242
Contrast*Polarizer	1	0,00120	0,00120	2,44	0,120
Brightness / ms*Intensity	1	0,00169	0,00169	3,44	0,066
Brightness / ms*Polarizer	1	0,00090	0,00090	1,83	0,179
Intensity*Polarizer	1	0,00010	0,00010	0,21	0,646
Error	146	0,07168	0,00049		
Lack-of-Fit	38	0,06885	0,00181	69,14	0,000
Pure Error	108	0,00283	0,00003		
Total	161	4,87453			

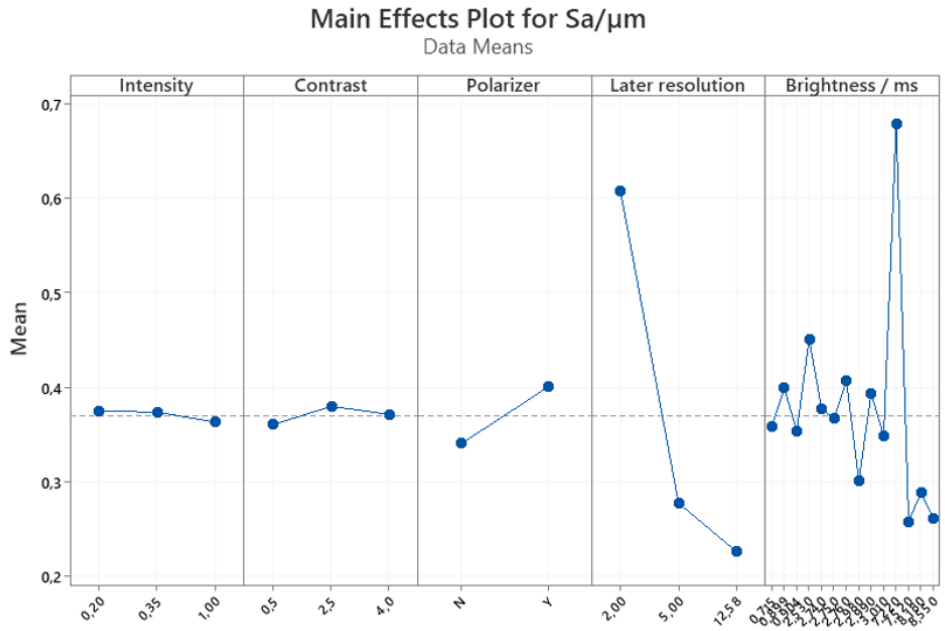

Figure 47: Results of cropped area analysis on Sa with 10x objective and blocks.

Model Summary

S	R-sq	R-sq(adj)	R-sq(pred)
0,444849	96,32%	95,94%	95,48%

Analysis of Variance

Source	DF	Adj SS	Adj MS	F-Value	P-Value
Model	15	755,754	50,384	254,60	0,000
Blocks	2	652,343	326,171	1648,24	0,000
Linear	4	0,822	0,205	1,04	0,390
Contrast	1	0,628	0,628	3,17	0,077
Brightness / ms	1	0,637	0,637	3,22	0,075
Intensity	1	0,052	0,052	0,26	0,608
Polarizer	1	0,021	0,021	0,11	0,744
Square	3	0,715	0,238	1,21	0,310
Contrast*Contrast	1	0,219	0,219	1,11	0,294
Brightness / ms*Brightness / ms	1	0,637	0,637	3,22	0,075
Intensity*Intensity	1	0,063	0,063	0,32	0,574
2-Way Interaction	6	4,048	0,675	3,41	0,004
Contrast*Brightness / ms	1	0,626	0,626	3,16	0,077
Contrast*Intensity	1	0,267	0,267	1,35	0,247
Contrast*Polarizer	1	0,452	0,452	2,28	0,133
Brightness / ms*Intensity	1	0,051	0,051	0,26	0,612
Brightness / ms*Polarizer	1	0,020	0,020	0,10	0,750
Intensity*Polarizer	1	1,050	1,050	5,31	0,023
Error	146	28,892	0,198		
Lack-of-Fit	38	21,353	0,562	8,05	0,000
Pure Error	108	7,539	0,070		
Total	161	784,646			

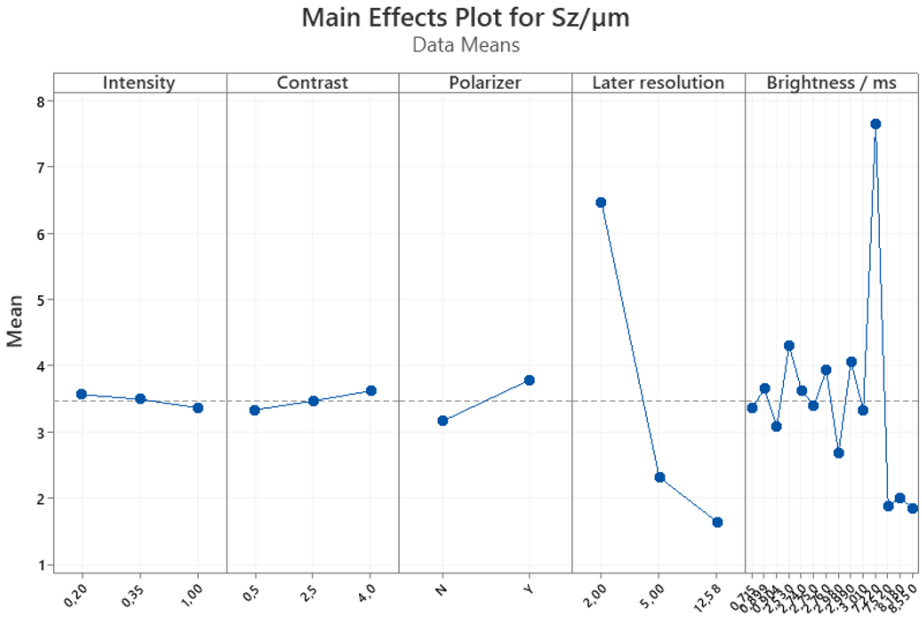

Figure 48: Results of cropped area analysis on Sz with 10x objective and blocks.

Model Summary

S	R-sq	R-sq(adj)	R-sq(pred)
0,0064032	99,26%	99,19%	99,10%

Analysis of Variance

Source	DF	Adj SS	Adj MS	F-Value	P-Value
Model	15	0,808452	0,053897	1314,52	0,000
Blocks	2	0,789036	0,394518	9622,13	0,000
Linear	4	0,000041	0,000010	0,25	0,908
Contrast	1	0,000004	0,000004	0,10	0,749
Intensity	1	0,000005	0,000005	0,13	0,721
Brightness / ms	1	0,000008	0,000008	0,20	0,656
Polarizer	1	0,000006	0,000006	0,15	0,695
Square	3	0,000085	0,000028	0,69	0,559
Contrast*Contrast	1	0,000003	0,000003	0,08	0,778
Intensity*Intensity	1	0,000076	0,000076	1,86	0,175
Brightness / ms*Brightness / ms	1	0,000008	0,000008	0,20	0,656
2-Way Interaction	6	0,000089	0,000015	0,36	0,902
Contrast*Intensity	1	0,000007	0,000007	0,17	0,682
Contrast*Brightness / ms	1	0,000004	0,000004	0,10	0,749
Contrast*Polarizer	1	0,000003	0,000003	0,07	0,785
Intensity*Brightness / ms	1	0,000006	0,000006	0,14	0,705
Intensity*Polarizer	1	0,000026	0,000026	0,63	0,428
Brightness / ms*Polarizer	1	0,000006	0,000006	0,15	0,695
Error	146	0,005986	0,000041		
Lack-of-Fit	38	0,005674	0,000149	51,60	0,000
Pure Error	108	0,000312	0,000003		
Total	161	0,814438			

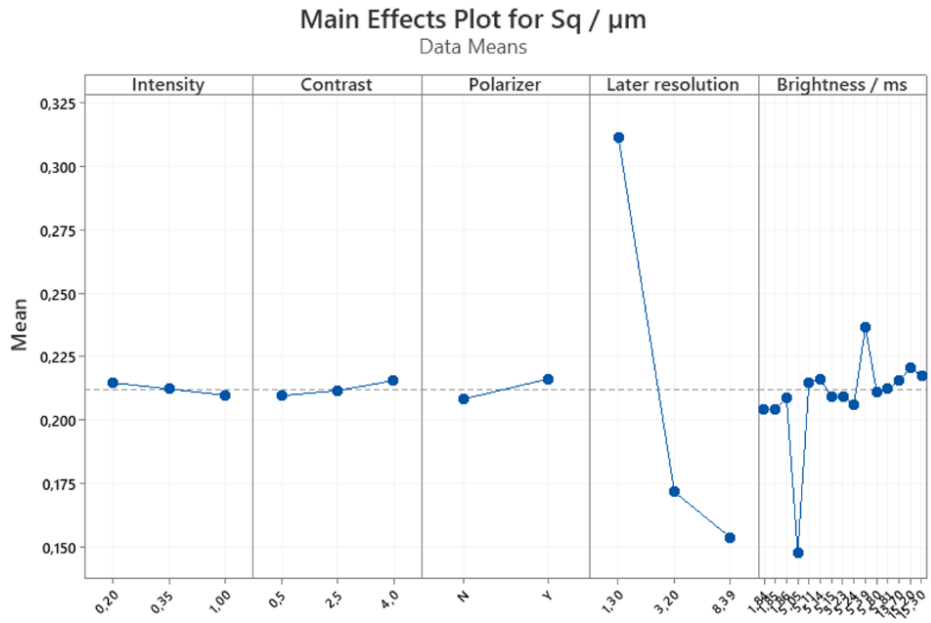

Figure 49: Results of cropped area analysis on Sq with 20x objective and blocks.

Model Summary

S	R-sq	R-sq(adj)	R-sq(pred)
0,0054024	99,17%	99,09%	98,98%

Analysis of Variance

Source	DF	Adj SS	Adj MS	F-Value	P-Value
Model	15	0,510424	0,034028	1165,91	0,000
Blocks	2	0,498864	0,249432	8546,32	0,000
Linear	4	0,000037	0,000009	0,31	0,868
Contrast	1	0,000002	0,000002	0,05	0,820
Intensity	1	0,000005	0,000005	0,17	0,679
Brightness / ms	1	0,000004	0,000004	0,15	0,700
Polarizer	1	0,000003	0,000003	0,09	0,769
Square	3	0,000074	0,000025	0,84	0,472
Contrast*Contrast	1	0,000000	0,000000	0,01	0,915
Intensity*Intensity	1	0,000056	0,000056	1,90	0,170
Brightness / ms*Brightness / ms	1	0,000004	0,000004	0,15	0,700
2-Way Interaction	6	0,000070	0,000012	0,40	0,880
Contrast*Intensity	1	0,000007	0,000007	0,23	0,635
Contrast*Brightness / ms	1	0,000002	0,000002	0,05	0,820
Contrast*Polarizer	1	0,000001	0,000001	0,03	0,866
Intensity*Brightness / ms	1	0,000006	0,000006	0,19	0,663
Intensity*Polarizer	1	0,000020	0,000020	0,70	0,405
Brightness / ms*Polarizer	1	0,000003	0,000003	0,09	0,769
Error	146	0,004261	0,000029		
Lack-of-Fit	38	0,004045	0,000106	53,13	0,000
Pure Error	108	0,000216	0,000002		
Total	161	0,514685			

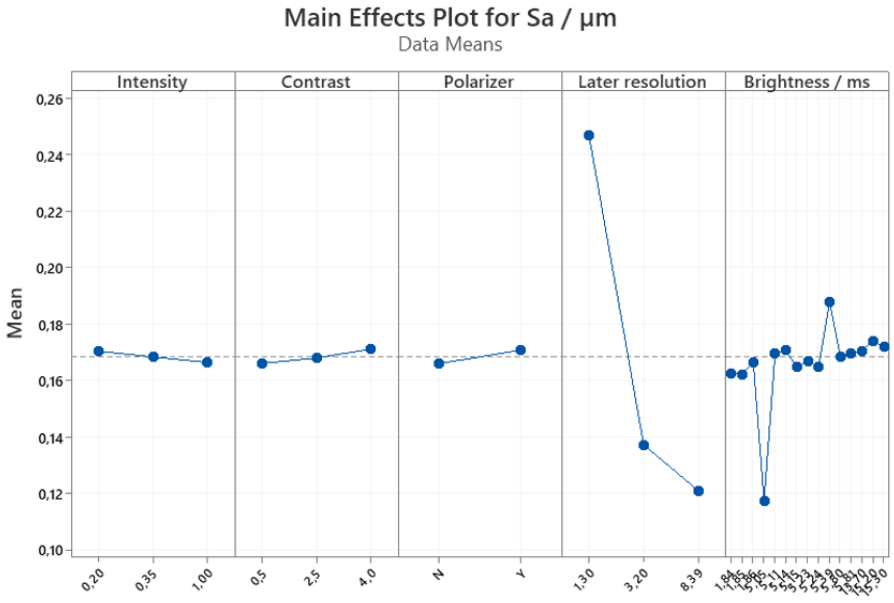

Figure 50: Results of cropped area analysis on Sa with 20x objective and blocks.

Model Summary

S	R-sq	R-sq(adj)	R-sq(pred)
0,0981872	98,34%	98,17%	97,93%

Analysis of Variance

Source	DF	Adj SS	Adj MS	F-Value	P-Value
Model	15	83,2676	5,5512	575,80	0,000
Blocks	2	79,7463	39,8732	4135,91	0,000
Linear	4	0,0145	0,0036	0,38	0,826
Contrast	1	0,0000	0,0000	0,00	0,996
Intensity	1	0,0057	0,0057	0,59	0,445
Brightness / ms	1	0,0001	0,0001	0,01	0,922
Polarizer	1	0,0001	0,0001	0,01	0,940
Square	3	0,0037	0,0012	0,13	0,943
Contrast*Contrast	1	0,0000	0,0000	0,00	0,980
Intensity*Intensity	1	0,0031	0,0031	0,32	0,571
Brightness / ms*Brightness / ms	1	0,0001	0,0001	0,01	0,922
2-Way Interaction	6	0,2022	0,0337	3,50	0,003
Contrast*Intensity	1	0,0029	0,0029	0,30	0,586
Contrast*Brightness / ms	1	0,0000	0,0000	0,00	0,996
Contrast*Polarizer	1	0,0000	0,0000	0,00	0,982
Intensity*Brightness / ms	1	0,0059	0,0059	0,62	0,434
Intensity*Polarizer	1	0,0595	0,0595	6,17	0,014
Brightness / ms*Polarizer	1	0,0001	0,0001	0,01	0,940
Error	146	1,4075	0,0096		
Lack-of-Fit	38	1,2183	0,0321	18,30	0,000
Pure Error	108	0,1892	0,0018		
Total	161	84,6751			

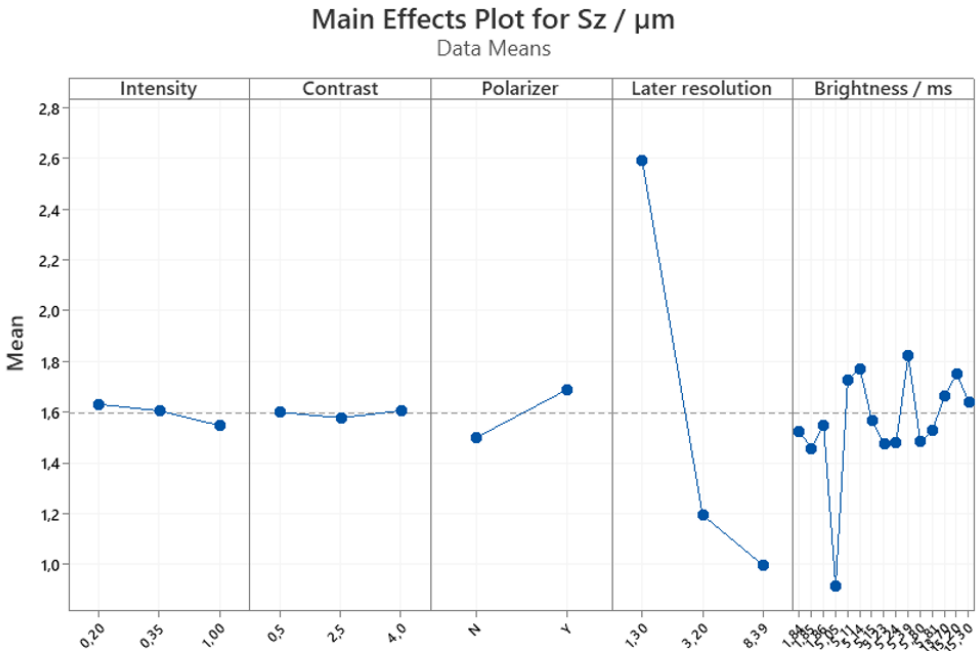

Figure 51: Results of cropped area analysis on Sz with 20x objective and blocks.

This strategy highlights the importance of Contrast and Polarizer for 10x magnification objective analysis, as their null P-values and increased values of F-values well represent.

In case of measurements performed with 20x objective magnification, Contrast is found to be the most impactful factor, confirming the theory according to which the optical signal quality has greater importance than physical resolution at higher magnifications.

The robustness of the models towards illumination changes is underlined by the non-relevance of the factor Intensity even in the case of analysis performed with blocks.

In both cases the models are particularly precise, as illustrated by the extremely high values of R-sq (adjusted), and able to explain all the variability left after removing the one associated with Lateral Resolution.

Even when blocks are inserted into the analysis, the positive impact of high values of contrast and polarizer to counterbalance poor resolution is still present, meaning that this is not just a random coincidence, but rather a proven feature of the Alicona.

Chapter 9. Conclusions

This thesis focused on the early stage of development and implementation of a Digital-Metrological Twin (D-MT) for a Focus Variation Coordinate Measurement System, which attempts to address a major problem that exists in surface metrology, which is how to ensure traceable, accurate, and precise measurements of complex three-dimensional surface topography.

The main objective of this thesis is the development of a Digital Twin, that targets the simulation of a specimen's measurement process and prediction of a physical system's performance, with a specific attention on measurement uncertainty and surface topography analysis.

The increasing importance covered by surface texture has been examined in the initial phase of the work, by describing how surface topography, which was at first considered a secondary outcome of the process, became then an important feature to be examined.

For this purpose, traditional contact-based methods, such as Coordinate Measuring Machines (CMMs), revealed important physical and operational limitations, due to the negative effects produced by the tactile probe on the product’s surface, especially when dealing with complex geometries.

To overcome these limitations, surface metrology has moved forward with advancements in optical surface measurement devices, especially with the incorporation of Focus Variation principles, which facilitate precise non-contact surface texture analysis.

Nevertheless, these devices also pose new sources of uncertainty and complexity, mainly related to the interaction between light and surface properties.

This thesis offers a study on traceability, calibration, measurement uncertainty, and physical sources of error.

The study focuses on the limitations of conventional calibration methods with regard to adequately describing traceable measurements carried out with highly developed optical devices, while conventional traceability chains exist for two-dimensional measurements.

Metrological Characteristics (MCs) have then been explained, offering a solution to overcome the previously highlighted limitations. However, they do not consider a relevant feature for the evaluation of measurement results: the interaction between parameters.

To overcome the limitations that exist with conventional calibration, a Digital-Metrological Twin (D-MT) construction process was carried out.

The D-MT offers the possibility of simulating the process of a measurement and the results that a physical device produces by replicating a measurement system in a virtual environment.

This approach facilitates the determination of measurement uncertainty for geometries with complex shapes and materials with different properties, without having to rely on physical measurements.

The experimental part of this thesis has played a crucial role in validating these concepts. In this regard, a series of measurements was carried out using a specific type of instrument, namely, the Alicona IF-SensorR25.

Within this context, different data processing approaches were also employed for processing the obtained measurements, which included raw data processing, differentiated topography, and cropped area evaluation.

The aim was to identify which factors related to the instruments, under different circumstances, play a significant role in influencing the surface roughness parameters, Sq, Sa, and Sz.

The outputs underlined the strong dependency of measurement results to instrument settings and data processing strategies, clearly indicating that uncertainty is not only related to the instruments but also to different algorithms employed for processing the data.

Nevertheless, several challenges remain open for future research, including the development of precise models related to optical interactions, employing machine learning algorithms for predicting uncertainty, and standardizing digital twin methodologies with international metrological standards. Also, further studies to investigate dependance on surface geometrical and optical characteristics are needed towards a more general application framework.

References

[1] G. Barbato, A. Germak, G. Genta, "Measurements for Decision Making", Società Editrice Esculapio, Bologna, 2013.

[2] JCGM 200:2012, International vocabulary of metrology – Basic and general concepts and associated terms (VIM), 3rd edition, 2008.

[3] R.K. Leacha, C.L. Giusca, H. Haitjema, C. Evans, X. Jiang, Calibration and verification of areal surface texture measuring instruments, CIRP Annals Manufacturing Technology.

[4] "Metrology – in short" 3rd edition, 2008, EURAMET project 1011

[5] R. Leach, M. Ferrucci, H. Haitjema, Manufacturing Metrology Team, Faculty of Engineering, University of Nottingham, Nottingham, UK, Research and Development, Materialise NV, Leuven, Belgium, Mechanical Engineering Department, KU Leuven, Leuven, Belgium, Dimensional Metrology.

[6] The National Physical Laboratory, https://www.npl.co.uk

[7] Istituto Nazionale di Ricerca Metrologica, https://www.inrim.it

[8] M. Cable, Isa Technician Series, Calibration a Technician's Guide.

[9] R. Leach, Characterisation of Areal Surface Texture, 2013.

[10] R. Leach, H. Haitjema, R. Su, A. Thompson, Metrological characteristics for the calibration of surface topography measuring instruments: a review, 2021.

[11] R. Leach, Optical Measurement of Surface Topography, 2011.

[12] JCGM 100:2008, Evaluation of measurement data - Guide to the expression of uncertainty in measurement.

[13] P. M. Harris, R. K. Leach, C. Giusca, National Physical Laboratory, Hampton Road, Teddington TW11 0LW, UK, Uncertainty evaluation for the calculation of a surface texture parameter in the profile case.

[14] R. Leach, Dimensional & Optical Metrology Team Centre for Basic, Thermal and Length Metrology National Physical Laboratory United Kingdom TW11 0LW, Calibration, traceability and uncertainty issues in surface texture metrology Version 2.

[15] Iso/iec guide 98-3:2008 uncertainty of measurement– part 3: Guide to the expression of uncertainty in measurement.

[16] S. Bell, Centre for Basic, Thermal and Length Metrology National Physical Laboratory, A Beginner's Guide to Uncertainty of Measurement.

[17] J. G. Salsbury, Test Uncertainty: Guide to the evaluation of measurement uncertainty in the conformity assessment of measuring instruments, 2nd Edition; May 20, 2022.

[18] L. De Chiffre, P. Lonardo, H. Trumpold, D. A. Lucca, G. Goch, C. A. Brown, J. Raja, H. N. Hansen, Technical University of Denmark, University of Genova, Technical University Chemnitz, Oklahoma State University, Bremen University, Worcester Polytechnic Institute, University of North Carolina-Charlotte, Quantitative Characterisation of Surface Texture.

[19] L. Blunt, T. Hobson, School of Engineering, University of Huddersfield, UK, Advanced Techniques for Assessment Surface Topography.

[20] H. Haitjema, Mitutoyo Research Center Europe. Uncertainty in measurement of surface topography

[21] G. Belforte, B. Bona, E. Canuto, F. Donati, F. Ferraris, I. Gorini, S. Morei, M. Pesino, S. Sartori, R. Levi, Coordinate Measuring Machines and Machine Tools Selfcalibration and Error Correction.

[22] A. Gaska, W. Harmatys, P. Gaska, M. Gruza, K. Gromczak, K. Ostrowska, Laboratory of Coordinate Metrology, Cracow University of Technology, Virtual CMM-based model for uncertainty estimation of coordinate measurements performed in industrial conditions.

[23] J. G. Salsbury, Guide to the evaluation of measurement uncertainty in the conformity assessment of measuring instruments 2nd Edition, Test Uncertainty.

[24] S. Lou, S. B. Brown, W. Sun, W. Zeng, X. Jiang, P. J. Scott, EPSRC Future Metrology Hub, University of Huddersfield, National Physical Laboratory, Engineering, Materials and

Electrical Science, An investigation of the mechanical filtering effect of tactile CMM in the measurement of additively manufactured parts.

[25] W. Sun, J. D. Claverley, Engineering Measurement Division, National Physical Laboratory, UK, Verification of an optical micro-CMM using the focus variation technique: Aspects of probing errors.

[26] S. Darukumalli, T. Santoso, W. P. Syam, F. Helmli. R. Leach, Manufacturing Metrology Team, University of Nottingham, Alicona Imaging GmbH, Dr. Auner Straße, 2019, On-machine optical surface topography measurement sensor based on focus variation.

[27] H. Schwenke, U. Neuschaefer-Rube, T. Pfeifer, H. Kunzmann, Physikalisch-Technische Bundesanstalt, Braunschweig, RWTH Aachen, Germany, Optical Methods for Dimensional Metrology in Production Engineering.

[28] S. Yalcinkaya, B. Yildiz, M. Borak, Marmara University Faculty of Technology, Optical 3D scanner technology.

[29] https://measuremetrology.com

[30] https://www.sipconinstrument.com

[31] T. Brajlih, T. Tasic, I. Drstvensek, B. Valentan, M. Hadzistevic, V. Pogacar, J. Balic, B. Acko, University of Maribor, Faculty of Mechanical Engineering, Slovenia, University of Novi Sad, Faculty of Technical Sciences, Serbia, 2011, Possibilities of Using Three-Dimensional Optical Scanning in Complex Geometrical Inspection.

[32] https://vitrek.com

[33] W. Pastorius, Triangulation Sensors An Overview.

[34] https://www.micro-epsilon.com

[35] https://www.azosensors.com

[36] N. Vilar, R. Artigas, C. Bermudez, A. Thompson, L. Newton, R. Leach, M. Duocastella, G. Carles, Sensofar Tech S.L., Parc Audiovisual de Catalunya, Advanced Manufacturing Building, Jubilee Campus, University of Nottingham, Department of Applied Physics,

University of Barcelona, 2022, Optical system for the measurement of the surface topography of additively manufactured parts.

[37] https://www.alicona.com

[38] G. Maculotti, G. Genta, D. Quagliotti, H. N. Hansen, M. Galetto, Department of Management and Production Engineering, Politecnico di Torino, Department of Mechanical Engineering, Technical University of Denmark, 2023, Comparison of methods for management of measurement errors in surface topography measurements.

[39] R. Danzl, F. Helmli, S. Scherer, Alicona, Grambach, Austria, Focus Variation – a Robust Technology for High Resolution Optical 3D Surface Metrology.

[40] A. F. Merchant, K. A. Bartels, A. C. Bovik, K. R. Diller, Confocal Microscopy.

[41] https://www.zygo.com

[42] P. de Groot, Zygo Corporation, Coherence Scanning Interferometry.

[43] M. Tarabini, Politecnico di Milano, Red Hot Steel: Challenges of 3D Optical Metrology in Open-Die Forging.

[44] S. Shan, F. Zhao, Z. Li, L. Luo, X. Li, Tsinghua Shenzhen International Graduate School, Tsinghua University, 2025, A Comprehensive Review of Optical Metrology and Perception Technologies.

[45] J. Sładek, P. M. Błaszczyk, M. Kupiec, R. Sitnik, Cracow University of Technology, Laboratory of Coordinate Metrology, Warsaw University of Technology, Institute of Micromechanics and Photonics, State Higher Vocational School, Institute of Engineering, Staszica, 2010, The hybrid contact–optical coordinate measuring system.

[46] X. J. Jiang, F. Gao, H. Martin, J. Williamson, D. Li, University of Huddersfield, Huddersfield, United Kingdom, On-Machine Metrology for Hybrid Machining.

[47] R. Danzl, T. Lankmair, A. Calvez, F. Helmi, Alicona, R&D Department, Austria, Alicona SARL, France, 2017, Robot solutions for automated 3D surface measurement in production.

[48] T. Santoso, W. P. Syam, S. Darukumalli, R. Leach, Manufacturing Metrology Team, Faculty of Engineering, University of Nottingham, UK, 2022, Development of a compact focus variation microscopy sensor for on-machine surface topography measurement.

[49] S. Catalucci, A. Thompson, S. Piano, D. T. Branson, R. Leach, 2022, Optical metrology for digital manufacturing: a review.

[50] H. Schwenke, W. Knapp, H. Haitjema, A. Weckenmann, R. Schmitte, F. Delbressine, Geometric error measurement and compensation of machines, CIRP Annals-Manufacturing Technology, 2008.

[51] ISO 9283:1998, Manipulating industrial robots – performance criteria and related test methods

[52] A. Y. Elatta, L. P. Gen, F. L. Zhi, Y. Daoyuan, L. Fei, Department of Mechanical, Faculty of Engineering, Huazhong University of Science and Technology, China, 2004, An Overview of Robotic Calibration

[53] L. Wang, X. Wu, Y. Gao, X. Chen, B. Wang, Key Laboratory of Intelligent Manufacturing Quality Big Data Tracing and Analysis of Zhejiang, College of Mechanical and Electrical Engineering, China Jiliang University, Sensitivity Analysis of Performance Tests for Six-Degree-of-Freedom Serial Industrial Robots.

[54] A. M. Madni, C. C. Madni, S. D. Lucero, Intelligent Systems Technology, Inc., Los Angeles, USA, Leveraging Digital Twin Technology in Model-Based Systems Engineering.

[55] A. Egidi, A. Balsamo, D. Corona, Monte Carlo method for evaluating the uncertainty of roundness measurements on a CMM – a Python implementation, INRIM, Istituto Nazionale di Ricerca Metrologica, 2021.

[56] M. Trenk, M. Franke, Dr. H. Schwenke, ASPE Summer Topical Meeting on Uncertainty Analysis in Measurement and Design. State College, Pennsylvania, USA, 2004, The “Virtual CMM” a software tool for uncertainty evaluation – practical application in an accredited calibration lab.

[57] I. Poroskun, C. Rothleitner, D. Heißelmann, Physikalisch-Technische Bundesanstalt (PTB), 2022, Structure of digital metrological twins as software for uncertainty estimation.

[58] B. V. Dorp, H. Haitjema, F. Delbressine, R. Bergmans, P. Schellekens, Eindhoven University of Technology, Virtual CMM using Monte Carlo Methods based on Frequency Content of the Error Signal.

[59] J. Sładek, A. Gaska, Laboratory of Coordinate Metrology, Cracow University of Technology, Evaluation of coordinate measurement uncertainty with use of virtual machine model based on Monte Carlo method.

[60] S. Schmelter, I. Fortmeier, D. Heißelmann, Physikalisch-Technische Bundesanstalt (PTB), Germany, Metrology for Virtual Measuring Instruments Illustrated by Three Applications.

[61] G. Kok, M. v. Dijk, Van Swinden Laboratorium, Thijsseweg, Measurement Uncertainty Evaluation: Differences Between Virtual Experiments and the Standardized Approach.

[62] S. M. Stojadinovic, V. D. Majstorovic,N. M. Durakbasa, Dusan Stanic University of Belgrade, Faculty of Mechanical Engineering, Contribution to the development of a digital twin based on CMM to support the inspection process.

[63] G. Maculotti, M. Marschall, J. Flores, G. Genta, G. Kok, P. Puerto, B. A. Chekh, M. Galetto, M. v. Dijk, S. Schmelter, Department of Management and Production Engineering, Politecnico di Torino, Physikalisch-Technische Bundesanstalt, Van Swinden Laboratory, Mechanical Engineering Unit, TEKNIKER, IDEKO, Basque Research and Technology Alliance (BRTA), 2024, AShared Metrological Framework for Trustworthy Virtual Experiments and Digital Twins.

[64] M. Liu, S. Fang, H. Dong, C. Xu, State Key Laboratory of Fluid Power and Mechatronic System, College of Mechanical Engineering, Zhejiang University, Hangzhou, Review of digital twin about concepts, technologies, and industrial applications.

[65] L. Wright, S. Davidson, Data Science Department, National Physical Laboratory, Teddington, United Kingdom, 2024, Digital twins for metrology; metrology for digital twins.

[66] J. Zhou, S. Zhang, M. Gu, 1 University of Oulu, Heibei University, Beijing aerospace smart manufacturing technology development Co., Revisiting Digital Twins: Origins, Fundamentals and Practices.

[67] E. H. Glaessgen, D. S. Stargel, 2012, The digital twin paradigm for future NASA and U.S. air force vehicles.

[68] A. M. Madni, C. C. Madni, S. D. Lucero, Intelligent Systems Technology, Inc., Los Angeles, Research and Engineering, Office of the USD, Washington, DC, 2019, Leveraging Digital Twin Technology in Model-Based Systems Engineering.

[69] J. Ríos, G. Staudter, M. Weber, R. Anderl, A. Bernard, Department of Computer Integrated Design (DiK), Technische Universität Darmstadt, Department of Mechanical Engineering, Universidad Politécnica de Madrid, Laboratory for Digital Sciences of Nantes (LS2N), Ecole Centrale de Nantes, 2020, Uncertainty of data and the digital twin: a review.

[70] J. Ríos, G. Staudter, M. Weber, R. Anderl, Department of Computer Integrated Design (DiK), Technische Universität Darmstadt, Department of Mechanical Engineering, Universidad Politécnica de Madrid, 2020, Enabling the digital twin: a review of the modelling of measurement uncertainty on data transfer standards and its relationship with data from tests.

[71] https://www.alicona.com

[72] https://www.zeppelinmet.com

[73] https://www.digitalsurf.com

[74] https://imagescience.hu

[75] V. Alar, A. Razumic, B. Runje, I. Stojanovic, M. Kurtela, B. Štrbac, Faculty of Mechanical Engineering and Naval Architecture, University of Zagreb, Department of Polytechnics, Dr. Franjo Tudman Defense and Security University, Faculty of Technical Sciences, University of Novi Sad, 2025, Application of Areal Topography Parameters in Surface Characterization.

[76] https://learnopencv.com

[77] https://www.vaisala.com

[78] https://hexagon.com

[79] Z. Duan, N. Wang, J. Fu, W. Zhao, B. Duan, J. Zhao, School of Mechanical Engineering, Shenyang University of Technology, Shenyang, College of Aerospace Engineering, Nanjing

University of Aeronautics and Astronautics, Nanjing, Development Planning Department, China Academy of Launch Vehicle Technology, Beijing, High Precision Edge Detection Algorithm for Mechanical Parts.

[80] Muralikrishnan, Balasubramanian, Raja, Jayaraman, Springer Science & Business Media, 2008, Computational Surface and Roundness Metrology.

[81] https://www.alfatest.it

[82] https://www.sensofar.com

[83] https://evidentscientific.com